Master’s Thesis

Contact Modelling of Rack and Pinion in an Electric Power Steering System

under the supervision of

Senior Scientists Privatdoz. Dr. Eray Arslan

E325 - Institute of Mechanics and Mechatronics

submitted to the Faculty of Mechanical and Industrial Engineering
of Technische Universität Wien
for the degree of Diplom-Ingenieur (Dipl.-Ing.)

by

Aksel Cicyasvili, BSc
[redacted]

This study is financially supported by the research project titled “Analyse des Druckstückklapperns in Lenksystemen”, a joint project between Vienna University of Technology and BMW Munich.

Statutory Declaration

This thesis is the result of my own work and includes nothing that is the outcome of work done in collaboration except as specified in the text.

It is not substantially the same as any that I have submitted, or, is being con- currently submitted for a degree or diploma or other qualification at Technische Universität Wien or any other University or similar institution except as specified in the text. I further state that no substantial part of my thesis has already been submitted, or, is being concurrently submitted for any such degree, diploma or other qualification at Technische Universität Wien or any other University or similar institution except as specified in the text.

Vienna, April 2025 ....

(Aksel Cicyasvili, BSc.)

Acknowledgments

Here I would like to thank everyone who helped me with my studies and made this thesis possible.

First, I would like to thank Senior Scientist Dr. Eray Arslan for granting me the opportunity to partake in this research topic and always supporting me through the whole process while also contributing with his esteemed supervision.

Furthermore, I would like to thank the Institute of Mechanics and Mechatronics and the whole research group Technical Dynamics and Vehicle Systems (E325-01) together with Univ.Prof. Dipl.-Ing. Dr.techn. Johannes Edelmann for their valuable contributions to this thesis, and for the use of institute equipment and spaces.

I would like to also thank Mr. Markus Bullinger and Mr. Lukas Durand from BMW Munich for their research on which this thesis is based on, and I would like to appreciate their exciting and rewarding contributions to this work.

A thank you goes to every student and lecturer, whom I had the opportunity to meet and collaborate on different occasions and supported me through this journey. Special thank you goes to my closest friends whom I started and finished studying together, who were always by my side and made this thesis possible.

Finally, the greatest thank you goes to my family, especially my parents and by brother, who always trusted and supported me in my studies.

Abstract

This thesis investigates and presents the results of the contact modelling of a crossed helical rack and pinion pair in an electric power steering system. The main objectives of this thesis are to design a crossed helical rack and pinion system with a high contact ratio, and simulate to contact behaviour together with bearing forces using a finite element modelling simulation.

First, this thesis presents detailed calculations for the geometric modelling of the rack and pinion and their contact ratio using different methods based on the works of pioneer scientist and engineers in this respective field. The calculations are based on input parameters provided by BMW, and then used as a basis for 3D design using computer aided engineering and gear calculation software. A 3D finite element model of the rack and pinion contact is developed, and a quasi-static implicit dynamic analysis is performed. Three different cases are investigated and their results are compared. The cases differentiate in various contact models in terms of hard contact, and in mesh densities, where their impact on the contact behaviour is explored. The bearing behaviour of the pinion and the contact line behaviour on the tooth flank of the rack were simulated and analysed.

The results of the simulations for both bearing reactions and contact behaviour showed consistent results with the theoretical predictions and with the expected outcomes. The bearing reactions and the distribution of the forces along the contact lines vary with different parameters, and the most accurate model will be used as a reference for future work involving a multibody analysis of this steering system.

Kurzfassung

Diese Arbeit untersucht und präsentiert die Ergebnisse der Kontaktmodellierung eines schrägverzahnten Zahnstangen-Ritzel-Paares in einer elektrischen Servolenkung. Ziel ist die Konstruktion eines Zahnstangen-Ritzel-Systems mit hohem Überdeckungsgrad sowie die Simulation des Kontaktverhaltens und der Lagerkräfte mittels Finite-Elemente-Analyse.

Zunächst werden detaillierte Berechnungen zur geometrischen Modellierung von Zahnstange und Ritzel sowie zur Bestimmung des Überdeckungsgrads vorgestellt. Diese stützen sich auf Methoden, die auf den Arbeiten von Pionieren in diesem Fachgebiet basieren. Die Berechnungen beruhen auf Eingabeparametern, die von BMW bereitgestellt wurden, und bilden die Grundlage für die 3D-Konstruktion mittels CAD- und Getriebeberechnungssoftware. Darauf aufbauend wird ein 3D-Finite-Elemente-Modell des Zahnstangen-Ritzel-Kontakts entwickelt und eine quasistatische, implizite dynamische Analyse durchgeführt.

Drei verschiedene Szenarien werden untersucht und deren Ergebnisse miteinander verglichen. Diese unterscheiden sich hinsichtlich der Kontaktmodellierung (harter Kontakt) und der Vernetzungsdichten, um deren Einfluss auf das Kontaktverhalten zu analysieren. Das Lagerverhalten des Ritzels sowie das Kontaktlinienverhalten an der Zahnflanke der Zahnstange werden simuliert und ausgewertet.

Die Simulationsergebnisse der Lagerreaktionen und des Kontaktverhaltens zeigen gute Übereinstimmung mit theoretischen Vorhersagen und den erwarteten Resultaten. Sowohl die Lagerreaktionen als auch die Kraftverteilung entlang der Kontaktlinien variieren in Abhängigkeit von den Parametern. Das genaueste Modell dient als Referenz für zukünftige Arbeiten im Rahmen einer Mehrkörperanalyse des Lenksystems.

Table of Contents

List of Figures

List of Tables

Abbreviations

BC	Boundary Condition
BMW	Bayerische Motoren Werke AG
CAD	Computer Aided Design
CAE	Computer Aided Engineering
CFORCE	Contact Force
CNORMF	Normal Contact Force
CSTRESS	Contact Pressure
CTF	Connector Total Forces
CTM	Connector Total Moments
CU	Connector Relative Displacement
CUR	Connector Relative Rotation
DOF	Degrees of Freedom
EPS	Electric Power Steering
FEM	Finite Element Method
MBD	Multibody Dynamics
NLGEOM	Nonlinear Geometry
RF	Reaction Forces
RM	Reaction Moments
STP	Standard For The Exchange of Product Data
TF	Total Forces
UR	Rotational Displacement
UT	Translational Displacement

VR Rotational Velocity

VT Translational Velocity

Index for Geometric Modelling

$m_{n,i}$	Normal Module of Pinion ($i = 1$), Rack ($i = 2$)
$m_{t,i}$	Transverse Module of Pinion ($i = 1$), Rack ($i = 2$)
$\alpha_{n,i}$	Normal Pressure Angle on Pinion ($i = 1$), Rack ($i = 2$)
$\alpha_{t,i}$	Transverse Pressure Angle of Pinion ($i = 1$), Rack ($i = 2$)
λ	Skew (Crossed Shaft) Angle
z_1	Pinion Teeth Number
β_i	Helix Angle on Pinion ($i = 1$), Rack ($i = 2$)
$\beta_{b,i}$	Base Helix Angle on Pinion ($i = 1$), Rack ($i = 2$)
b_i	Width of Pinion ($i = 1$), Rack ($i = 2$)
d_2	Diameter of Rack
$C_{\beta,1}$	Flank Line Crowning of Pinion
r_k	Tip Rounding of Pinion
h_k	Tip Chamfer Length of Rack
δ_{hk}	Tip Chamfer Angle of Rack
$p_{n,i}$	Normal Pitch of Pinion ($i = 1$), Rack ($i = 2$)
$p_{t,i}$	Transverse Pitch of Pinion ($i = 1$), Rack ($i = 2$)
r_1	Pitch Circle Radius of Pinion
d_1	Pitch Circle Diameter of Pinion
r_{b1}	Base Circle Radius of Pinion
d_{b1}	Base Circle Diameter of Pinion
$x_{min,1}$	Minimum Profile Shift of Pinion
κ	Tooth Profile Height Factor of Pinion
$x_{selected,1}$	Selected Profile Shift of Pinion
k	Tooth Tip Alteration of Pinion
k^*	Tooth Tip Alteration Factor Pinion
c	Tip Clearance for Pinion and Rack
c_p	Tip Clearance Factor for Pinion and Rack
$h_{a,i}$	Addendum of Pinion ($i = 1$), Rack ($i = 2$)

$h_{f,i}$	Deddendum of Pinion ($i = 1$), Rack ($i = 2$)
h_i	Tooth Height of Pinion ($i = 1$), Rack ($i = 2$)
$d_{a,1}$	Tip Circle Diameter of Pinion
d_{f1}	Root Circle Diameter of Pinion
$r_{a,1}$	Tip Circle Radius of Pinion
r_{f1}	Root Circle Radius of Pinion
γ_1	Transverse Pressure Angle at the Tip of the Tooth
$r_{a,1.max}$	Maximum Tip Circle Radius of Pinion
a	Distance Between Pinion and Rack Axis
AS	Contact Line from Deddendum Begin Until Rack Teeth
SE	Contact Line from Pitch Point Until Pinion Base Circle
AE	Contact Line
$\varepsilon_{\gamma,1}$	Total Contact Ratio Based on Niemann and Winter
$g_{\alpha,2}$	Total Contact Line Between Pinion and Rack Based on ISO 21771
$\varepsilon_{\alpha,2}$	Transverse Contact Ratio Based on ISO 21771
$\varepsilon_{\alpha,K}$	Transverse Contact Ratio Based on Method of Krause
$\varepsilon_{\beta,K}$	Overlap Contact Ratio Based on Method of Krause
$A_{n,1}E_{n,1}$	Total Contact Line Between Pinion and Rack Based on Method of Krause
$\varepsilon_{\beta,2}$	Overlap Contact Ratio Based on Method of Krause
$\varepsilon_{\gamma,2}$	Total Contact Ratio Based on Method of Krause
$\varepsilon_{\gamma,3.1,2}$	Total Contact Ratio Based on KISSSOFT Calculations With ($i = 2$), and Without ($i = 1$) Modifications

Index for Finite Element Modelling

α_R	Mass Proportional Rayleigh Damping Coefficient
β_R	Stiffness Proportional Rayleigh Damping Coefficient
ω_i	i^{th} Natural Frequency
ζ_i	Critical Damping for the i^{th} Natural Frequency
x_1, y_1, z_1	First Datum System CSYS-1 (Global Datum System)
x_2, y_2, z_2	Second Datum System CSYS-2 (Pinion Datum System)
RP_1	Reference Point 1on the Rack

RP_2	Reference Point 2 on the Pinion
$RP_{1,Coupling}$	Coupling Vector of RP_1
$RP_{2,Coupling}$	Coupling Vector of RP_2
$u_{i,j,c}$	Kinematical Coupling of the Translation in the *i* Axis Based on CSYS-j
$\varphi_{i,j,c}$	Kinematical Coupling of the Rotation in the *i* Axis Based on CSYS-j
$C_{R,i,j}$	Rotational Damping Matrix Component of the Connector Based on CSYS-2
$BC_{1,i}$	Initial Boundary Condition Vector of RP-1 in CSYS-1 (Rack)
$BC_{2,i}$	Initial Boundary Condition Vector of RP-2 in CSYS-2 (Pinion)
$u_{i,j,i}$	Initial Displacement Boundary Condition of the Translation in the *i* Axis Based on CSYS-j
$\varphi_{i,j,i}$	Initial Displacement Boundary Condition of the Rotation in the *i* Axis Based on CSYS-j
$v_{i,j,i}$	Initial Velocity Boundary Condition of the Translation in the *i* Axis Based on CSYS-j
$\omega_{i,j,i}$	Initial Velocity Boundary Condition of the Rotation in the *i* Axis Based on CSYS-j
$a_{i,j,i}$	Initial Acceleration Boundary Condition of the Translation in the *i* Axis Based on CSYS-j
$\dot{\omega}_{i,j,i}$	Initial Acceleration Boundary Condition of the Rotation in the *i* Axis Based on CSYS-j
$BC_{1,step}$	Boundary Condition Vector of RP_1 in CSYS-1 for Step-1 (Rack)
$BC_{2,step}$	Boundary Condition Vector of RP_2 in CSYS-2 for Step-1 (Pinion)
$BC_{3,step}$	Boundary Condition Vector of RP_1 in CSYS-1 for Step-1 (Rack)
$BC_{Hinge,step}$	Applied Boundary Condition Vector of the Hinge Connector in CSYS-2
$u_{i,j,step}$	Displacement Boundary Condition of the Translation in the *i* Axis Based on CSYS-j for Step-1
$\varphi_{i,j,step}$	Displacement Boundary Condition of the Rotation in the *i* Axis Based on CSYS-j for Step-1
$v_{i,j,step}$	Velocity Boundary Condition of the Translation in the *i* Axis Based on CSYS-j for Step-1

$\omega_{i,j,step}$	Velocity Boundary Condition of the Rotation in the *i* Axis Based on CSYS-j for Step-1
$a_{i,j,step}$	Acceleration Boundary Condition of the Translation in the *i* Axis Based on CSYS-j for Step-1
$\dot{\omega}_{i,j,step}$	Acceleration Boundary Condition of the Rotation in the *i* Axis Based on CSYS-j for Step-1

Chapter 1

1 Introduction

1.1 Motivation

Rack and pinion systems are notable machine elements for power and force/torque transmissions, that are being used in various fields. The automotive industry is one of the fields where rack and pinion mechanisms are used for this purpose, as steering systems. **Figure 1** (Hnátík & Kroft, 2017)[1] shows the components of a conventional steering system with rack and pinion in automobiles, where the driver inputs rotate the steering shaft to which a pinion is connected. The pinion contacts the steering rack with a given shaft angle (acting as a crossed gear system) and moves the rack and the tie rods along its axis to turn the wheels on both sides. Although rack and pinion steering gears offer various advantages such as direct power transmission, high level of rigidity, and ease of manufacture (Suryanvanshi, Sathe, & Takey, 2017)[2] they also pose some challenges in terms of torque ripples, noise and vibrations (Harrer & Pfeffer, 2017)[3] therefore it is essential to design and analyse these systems meticulously. A correct and precise understanding of the contact force distribution on the contact surfaces and

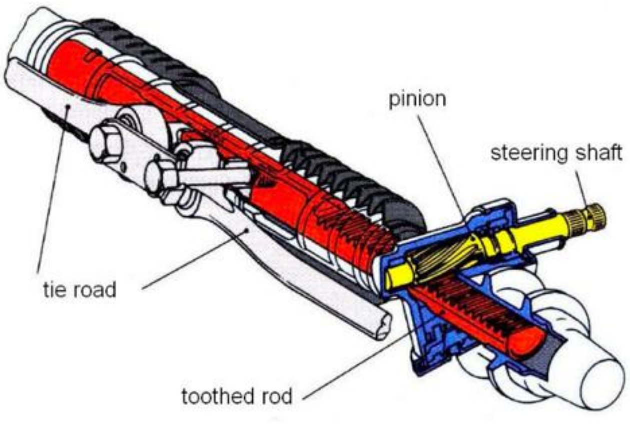

Figure 1*: The basic concept of a rack steering mechanism (Hnátík & Kroft, 2017)*

system behaviour is essential to achieve an excellent driving feel (Harrer & Pfeffer, 2017)[4] as steering systems are one of the most critical feedback systems in terms of vehicle manoeuvrability for the driver (Fankem, Weiskircher, & Müller, 2014)[5]. This is especially important for the design of automobiles now, as providing superb comfort for the passengers is a significant consideration (Chandler, 1924)[6] especially for premium brands such as Bayerische Motoren Werke (BMW). **Figure 2** (Automotive Systems and Accessories, 2018)

1 See page 569.

2 See page 79.

3 See page 17.

4 See page 169.

5 See page 8469.

6 See page 338.

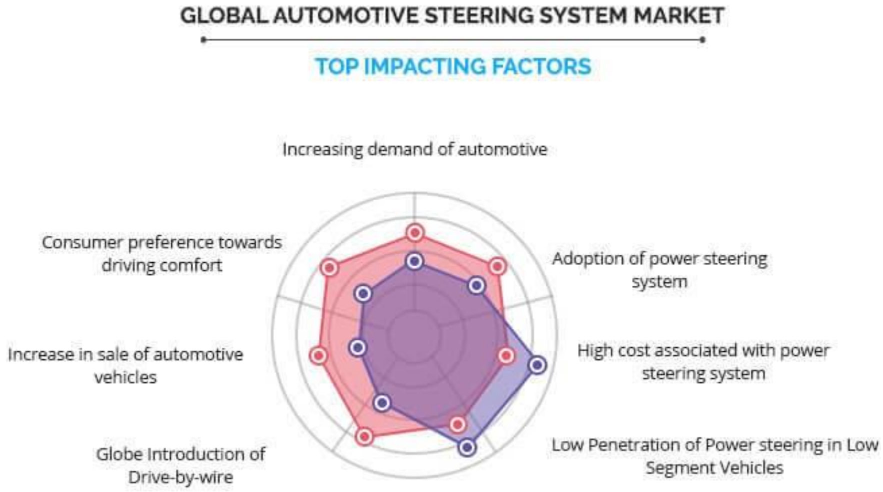

Figure 2: *Top impacting factors in automobile market according to Automotive Systems and Accessories (Automotive Systems and Accessories, 2018)*

presents a study by Allied Market Research regarding the change of top impacting factors of steering systems in the automotive market and argues a significant demand increase for driving comfort of consumers. Comfort regarding steering gear includes, not only ease of steering, but also aspects such as sound, vibrations, reliability, and continuous power transfer.

A dynamic contact and stiffness analysis between the pinion and rack is crucial to investigate the geometries, power transmission and force distribution among the tooth flanks and consequently investigate the reaction behaviour of the pinion. This reaction also includes the total forces and moments that act on the pinion and the relative displacement and velocities of the constrained system. A high total contact ratio between the pinion and rack is necessary. Total contact ratio is defined as the sum of the transverse contact ratio and overlap contact ratio where transverse contact ratio defines the on the average engaging teeth in a gear pair (Wittel, Muhs, Jannasch, & Voßiek, 2015)[7], and overlap ratio defines the face advance contact of helical teeth (Vullo, 2020)[8]. For a smooth gear operation, a higher contact ratio (more than 1) is recommended (Wittel, Muhs, Jannasch, & Voßiek, 2015)[9] which results with more- and longer teeth engagement and leads to less noise, greater loading capacity and more durability (Vullo, 2020)[10]. The total contact ratio is a theoretical factor that is dependent on the tooth geometry and material constraints of the designed system (exact calculations will be presented in chapter three). It can be raised by increasing the common contact areas of the tooth, or by extending the tooth engagement along the tooth width in helical gears. In practice, spur gears have a total contact ratio (transverse contact ratio) between 1.2 and 2 and helical gears can have a total contact ratio (transverse and overlap ratio) from 2 to 5. Some limiting factors against reaching higher total contact ratios are increased friction and wear, higher axial forces (with increasing helix angle) and difficulty of manufacturing.

7 See page 748, original language in German.

8 See page 315.

9 See page 763, original language in German.

10 See page 575.

1.2 Methods

The aim of this thesis is to model the contact between the pinion and the rack and analyse their interactions using Finite Element Method (FEM) by designing and optimizing a pinion and rack system that focuses on having a high total contact ratio. As a future work and research, the force, moment, and contact analysis will be later implemented in a Multibody Dynamics (MBD) simulation. In order to conduct a broad analysis of the rack and pinion system, the FEM is employed to study the contact forces, moments, relative displacements of the deformable contact bodies. While FEM is extremely resourceful with respect to these aspects, it lacks the features to model the dynamics of the whole system. The FEM results will therefore be combined in the future works with an MBD simulation, allowing the behaviour and dynamics of the steering system to be represented more accurately and extensively.

FEM is a numerical method where approximate solutions are obtained without altering the properties of the model such as shape, boundary conditions (BC), and loads (Bhavikatti, 2005)[11]. This method was initially designed to be used in complex engineering problems involving structural analysis but evolved to solve a wider range of problems such as dynamics, thermal analyses, wave propagation, acoustic studies, biomedical and biomaterial studies,

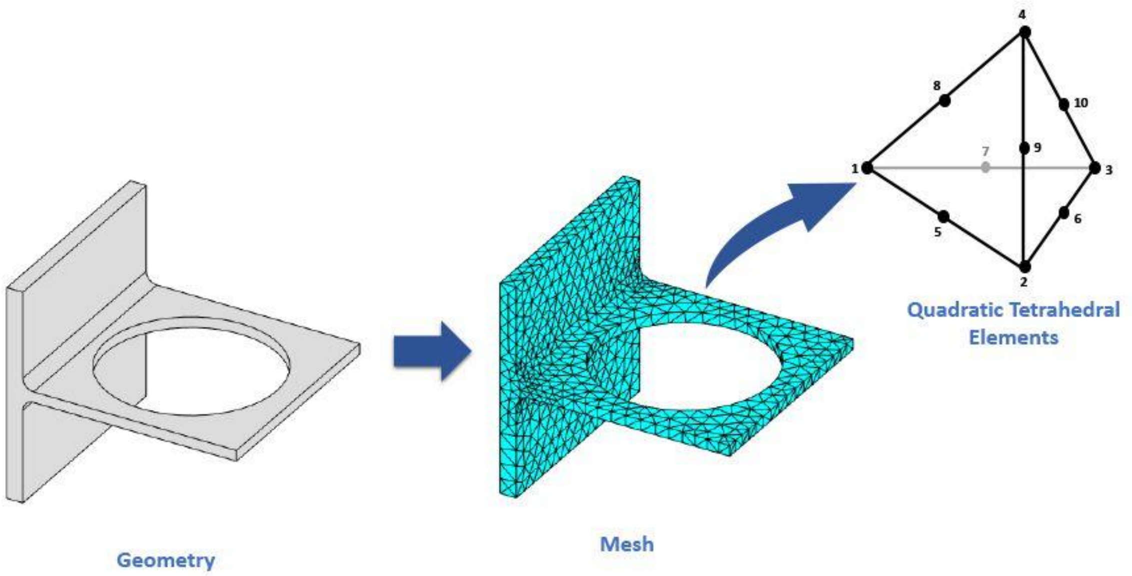

Figure 3: *Geometrical discretization example for FEM (Mathworks, n.d.)*

fracture mechanics and problems of discontinuum mechanics (Okerke & Keates, 2018)[12]. The FEM uses subdivided geometrical elements such as triangles, squares, tetrahedra and hexahedra as a groundwork to formulate basis functions that are non-zero over a small number of elements (Szabó & Babuška, 2011)[13]. These elements are interconnected at nodes and the accuracy of the solution is dependent on the number of these nodes, size of the geometrical shapes, the use of linear/non-linear equations and, therefore, dependent on the mesh quality. **Figure 3** (Mathworks, n.d.) shows a geometrical discretization example of quadratic tetrahedral elements, where black dots represent the nodes to which mesh elements are connected. On one hand we can argue that FEM is an ideal method for this thesis, as detailed analysis of stress, contact forces/contact path and deformation behaviour can be obtained with

11 See page 1.

12 See page 17.

13 See page 6.

high flexibility and high accuracy. FEM allows the user to change the material properties, the loading conditions, the contact conditions and analysis settings which makes it relatively uncomplicated to do simulations using different system properties to research various cases. On the other hand, FEM poses several challenges and limitations such as stiffness/equilibrium problem, meshing distortions because of size or difficult geometry, mesh shape errors and discontinuity cases where extreme deformations and material loss can prevent reaching the correct solution (Okerke & Keates, 2018)[14]. This means that, the accuracy of the results of a FEM simulation is heavily dependent on the user inputs, solver settings and correct modelling of the system.

As a future work connected to this thesis an MBD analysis is planned. MBD is considered as a computational method that has been especially getting popular among vehicle ride and handling dynamical analysis in recent years (Rahnejat, 2000)[15] and deals with how multiple solid bodies and their interactions act in a system under the influence of given parameters and loads (Larsson, 2001)[16] In comparison to FEM, MBD does not offer intricate analysis of stress, contact, strain, etc. between parts or assemblies, but it offers results regarding the dynamics (displacement, velocity, acceleration, time behaviour, etc.) of the system. An MBD analysis program often provides a number of tools and elements that allow model flexibility and elastic connection between bodies (Blundell & Harty, 2004)[17]. These links could be for example different kinds of joints, which have various kinematic constraints and therefore areas of applications. An advantage of MBD simulation is the availability of linking Computer Aided Design (CAD) and Computer Aided Engineering (CAE) methods to create virtual prototypes (Blundell & Harty, 2004)[18] and make it possible to combine and compare results effortlessly. In this thesis, FEM will be used to define the contact with given parameters, and later this definition will be implemented in MBD to analyse the complete steering system as a future work. **Figure 4** (Vienna University of Technology, 2023) is a represented MBD model of the steering system, where all components of the steering system are available not just the pinion and rack contrary to the FEM model.

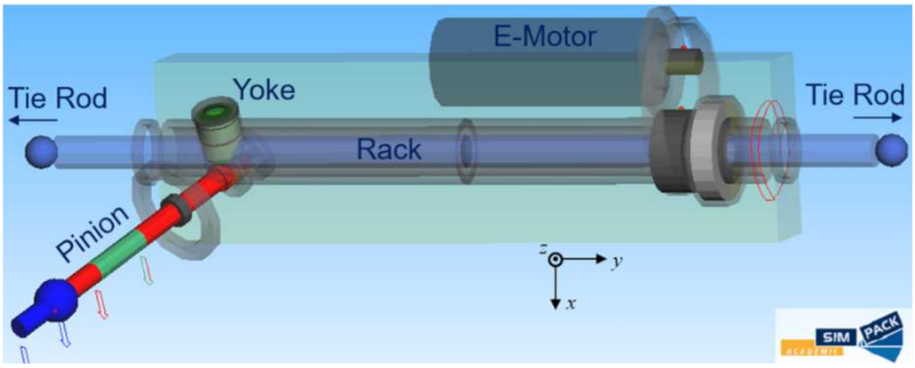

Figure 4: *The MBD simulation model of the steering system (Vienna University of Technology, 2023)*

The design of this system requires parameters, and specific geometric properties of rack and pinion system to obtain total contact ratio. The main objective here is not to create the most

14 See page 17-18.

15 See page 151.

16 See page 4.

17 See page 77.

18 See page 75.

realistic assembly, but to create a practical and affordable model to ensure compatibility with the MBD model using Simulia Simpack, which is a software that is tailored to model dynamic road, track and power systems (Dassault Systems, 2025). The geometrical calculations for the system will be done on the match calculations of engineering software Mathcad (Mathcad, 2025) and will be based on International Standards Organisation (ISO) norms and industry methods. The geometric design model will be then created using CAD software SolidWorks (Dassault Systems, 2025) and with a modular calculation program for the design of machine elements KISSSOFT (KISSSOFT, 2025). KISSSOFT export of the pinion module will be used for the assembly of the complete model. The next section is focused on meeting the objectives of creating an analysis model of the rack and pinion in the general-purpose CAE software ABAQUS (Dassault Systems, 2025) without causing the model to become far too detailed and unsolvable but simultaneously be compatible with the MBD model. This process involves the import of Standard For The Exchange of Product Data (STP) files of assemblies of both the rack, and pinion to CAE and implementing simulation properties. Additionally, the model will require contact parameters such as the coefficient of friction, general contact stiffness, damping, loading, BC, interactions, and meshing properties. For the use of simulation, a quasi-static analysis will be used. After all the necessary initial simulation conditions are determined a mesh convergence and a contact improvement analysis will be done to compare and eventually improve the results. Although the scope of this thesis encompasses until the results and evaluation of the FEM analysis, this project will continue using the results by dealing with the MBD modelling. Our industrial partner BMW has provided an existing MBD model that consists of rack, pinion, forces, and subroutines. This model will be examined, studied, and refined. In terms of examination, same/equivalent parameters will be compared, the results will be investigated, and parametric analysis will be performed for different loading conditions. Expected result of this thesis is to accurately calculate the reaction moments, reaction forces and the relative motion of the rack and pinion system together with a contact analysis on the rack teeth using a model with a desired contact ratio using FEM simulation. Similar results are aimed to be achieved with an MBD analysis in the subsequent research following this thesis.

2 Thesis Structure

This thesis is structured in five chapters.

- **Chapter 1:** The first chapter provides an introduction overview of the thesis. This chapter includes the problem statement and motivation that argues the background and importance of this thesis and description of the methods that are used to achieve the results.

- **Chapter 2:** The second chapter deals with the state of the art. In this chapter the thesis presents a comprehensive review of the existing research, experiments and literature related to the goal and methodologies. The outcomes and limitations of the proposed research methods are given in this chapter.

- **Chapter 3:** The third chapter focuses on system construction and modelling. In this chapter the calculation and the design/analysis process of the system through CAD, CAE will be discussed and supported with theoretical explanations. Detailed presentation of the research and simulation conditions are provided.

- **Chapter 4:** The fourth chapter is dedicated for the presentation of the results of the FEM analysis. System performance, evaluation and comparison of the results for different cases are presented.

- **Chapter 5:** The final chapter concludes the thesis and summarizes key findings and the interpretation of the significance of this thesis. General overview of this study and possible contributions are discussed.

Chapter 2

3 State of the Art

There are numerous ways to design, model and analyse the contact phenomenon between a rack and pinion. Different geometries, modifications, testing methods and applied models have an impact on the results. Therefore, analysing the existing literature is essential to decide how the contact analysis should be carried out and to understand expected outcomes. In this chapter, the existing literature regarding rack and pinion contact, FEM analysis and MBD simulation will be discussed, and the outcomes and limitations will be shown.

Kohnadaker et al. investigate in their research the strength of a rack and pinion system in a jack-up rig (Khondaker, MD, & Ibriju, 2020)[19]. In terms of their research, the developed model consists of a spur pinion with 7 teeth, a pressure angle of 25° and a pitch radius of 177.8 mm, which were developed using an Excel spreadsheet (Khondaker, MD, & Ibriju, 2020)[20]. Their goal for this research was to accurately analyse the contact and the resulting contact stress occurring on the rack and pinion at different rotation angles (10° rotation) (Khondaker, MD, & Ibriju, 2020)[21]. For the non-linear FEM analysis in ABAQUS, the complete rack and pinion was modelled instead of only investigating the interacting tooth pair using hex dominated meshing and a hard surface to surface contact (Khondaker, MD, & Ibriju, 2020)[22]. According to their results, maximum stress occurs in two positions, one being the contact point of rack and pinion and the other one being at the pinion root and the total maximum stress is dependent on the positioning of the contact line between them (Khondaker, MD, & Ibriju, 2020)[23].

Marano et al. explored the modelling and simulation results of a steering gear using MBD while also considering manufacturing errors (Marano, Pellicano, Pallara, & Piantoni, 2018)[24]. In their study, the crossed helical rack and pinion steering system was tested in terms of rack yoke clearance, rack displacement force, and rack rolling to assess the functional performance of the system (Marano, Pellicano, Pallara, & Piantoni, 2018)[25]. In terms of MBD simulation, Marano et al. used the software FunctionBay RecurDyn and created an arrangement that compensated the slight misalignments of rack axis and centre distance variation caused by the manufacturing errors by supporting the rack with a flexible bush and by a yoke at both ends (Marano, Pellicano, Pallara, & Piantoni, 2018)[26]. **Figure 5** (Marano, Pellicano, Pallara, & Piantoni, 2018)[27] shows the multibody model they used for their stidy and **Table 1** (Marano, Pellicano, Pallara, & Piantoni, 2018)[28] shows the multi body constraints of the system.

19 See page 42.
20 See page 42.
21 See page 42.
22 See page 44.
23 See page 45.
24 See page 178.
25 See page 183-184.
26 See page 184.
27 See page 184.
28 See page 185.

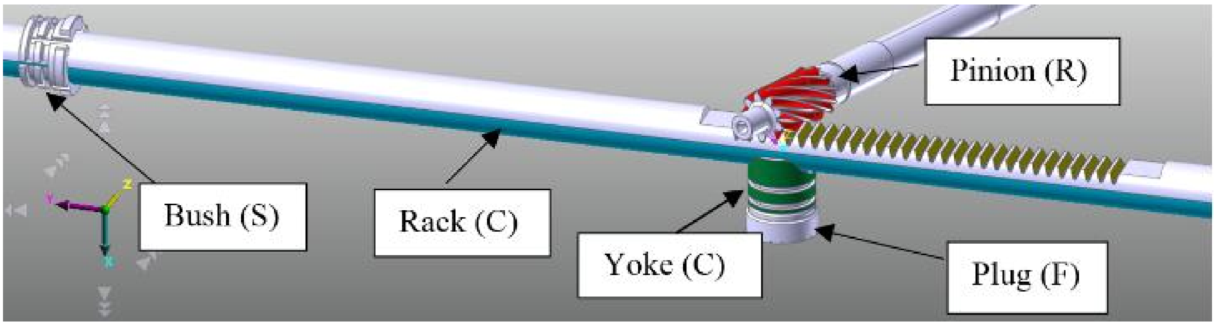

Figure 5: *Multi body model of the steering gear (Marano et al., 2018)*

Reference body	*Action body*	*Joint*
Ground	Pinion	Revolute R
Ground	Bush	Bushing (S)
Bush	Rack	Cylindrical (C)
Ground	Yoke	Cylindrical (C)
Ground	Plug	Fixed (F)
Liner	Yoke	Fixed (F)

Table 1: *Constraints of the multi body system (Marano et al., 2018)*

The surfaces in the contact zones are represented using triangular patches and boundary zones are approximated to triangular patches while the normal contact force uses a penetration function with nonlinear properties and equipped with damping and a spring (Marano, Pellicano, Pallara, & Piantoni, 2018)[29]. The contact discretisation is shown in **Figure 6** (Marano, Pellicano, Pallara, & Piantoni, 2018)[30]. The simulation results show a very stable interaction between the pinion and rack, and distance variation and rack roll variations are negligible (Marano, Pellicano, Pallara, & Piantoni, 2018)[31].

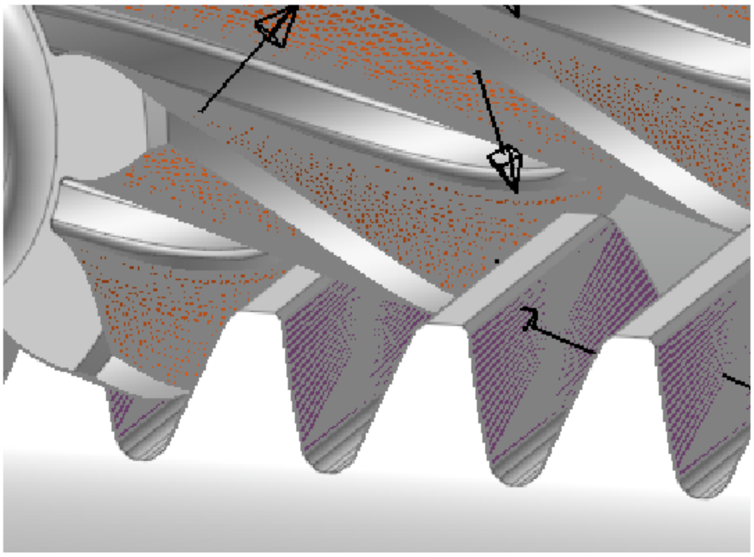

Figure 6: *Contact discretization of the rack (purple) and the pinion (orange) (Marano et al., 2018)*

29 See page 185.

30 See page 184.

31 See page 187.

Zhen et al. extensively investigated the stresses of pure rolling of rack and pinion using different geometries (Zhen, Ming, & Alfonso, 2019)[32]. In their paper, they present the geometric design parameters and calculations for pure rolling rack mechanisms and the simulations and meshing of tooth contact analysis together with the evaluation of the mechanical behaviour of the system in terms of contact and bending stresses (Zhen, Ming, & Alfonso, 2019)[33]. Four different rack-pinion tooth geometries were tested: convex-to-convex, convex-to-concave, convex-to-plane and involute geometries were the compared designs in this article (Zhen, Ming, & Alfonso, 2019)[34]. The FEM analysis in ABAQUS of the stress and contact analysis states that, the case with involute geometries represents the highest contact ratio among all cases (Zhen, Ming, & Alfonso, 2019)[35]. Larger active tooth surfaces of the rack that have been selected as the master surface while the pinion tooth surfaces are selected as slave surfaces and a linear hexahedral meshing have been used for the analysis (Zhen, Ming, & Alfonso, 2019)[36]. **Figure 7** (Zhen, Ming, & Alfonso, 2019)[37] represents the contact and stress lines on the different cases of racks with illustration a) convex-to-convex, b) convex-to-concave, c) convex-to-plane and d) involute geometries. The results indicate that, the involute geometry displays the highest bending stress due to an existing point contact (Zhen, Ming, & Alfonso, 2019)[38] and yields the lowest von Misses stress as the helical involute geometry with

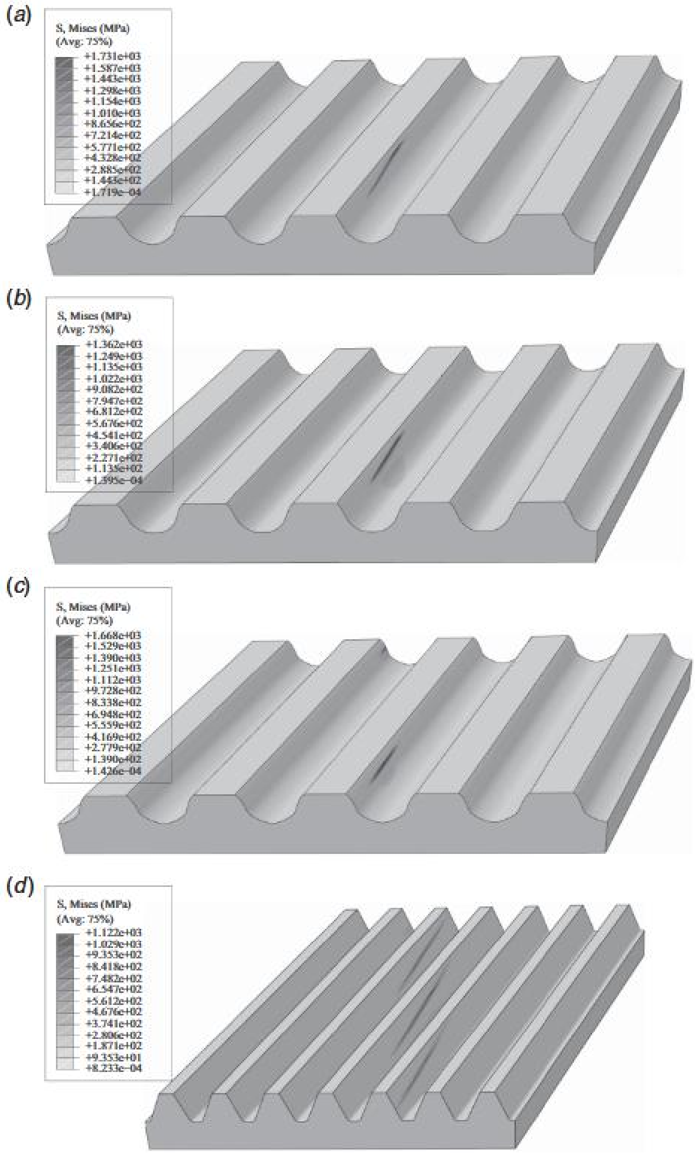

Figure 7: *Contact stress lines of a) convex-to-convex, b) convex-to-concave, c) convex-to-plane, d) involute geometries (Zhen et al., 2019)*

32 See page 1.

33 See page 1.

34 See page 2.

35 See page 7.

36 See page 7.

37 See page 8.

38 See page 9.

modifications lead to greater contact ellipses compared to non-involute geometries (Zhen, Ming, & Alfonso, 2019)[39].

Moreover, Yanjun et al., delved into establishing a dynamic model for rack and pinion transmission mechanism and solved the model by acquiring the natural frequencies of the system using a FEM (Ansys) analysis (Yanjun, Lihu, Jiayu, & Yanchun, 2014)[40]. Through obtaining the natural frequencies and comparing with the mesh frequencies, they investigated whether pinion rotational speed is reasonable and lower than the natural frequency thus avoiding resonance (Yanjun, Lihu, Jiayu, & Yanchun, 2014)[41] . To achieve good contact results, they have divided the rack and pinion in to four separate meshing zones where the densest and highest quality mesh can be found in the contact area and they the applied necessary boundary conditions (Yanjun, Lihu, Jiayu, & Yanchun, 2014)[42]. After natural frequencies are found, a transient dynamic analysis was conducted to calculate mechanical properties such as contact stress and bending stress. This was achieved by rotating the pinion and applying a horizontal force to the rack, allowing the system to act as a pinion-driven system (Yanjun, Lihu, Jiayu, & Yanchun, 2014)[43]. They conclude their investigation by reporting that maximum stresses in the rack occurs at dedendum and contact points, where for the pinion in the out-meshing contacts such as the tip (Yanjun, Lihu, Jiayu, & Yanchun, 2014)[44].

In his paper Khalifa presents a study of the stress distribution, strains and elastic deformations in the contact area of three different types of rack and pinion systems: single gear, double gear and herringbone gear (double helical gear without space between teeth) (Khalifa, 2021)[45]. He argued that, as opposed to single gears which have their left-hand helix teeth and right-hand helix not in contact, herringbone gears lack the necessary space to prevent this situation and therefore a contact can be observed (Khalifa, 2021)[46]. It was consequently important to do a contact stress analysis for these helical gear types using FEM (Ansys) with Lagrange multiplier technique (Khalifa, 2021)[47]. The pinion teeth were selected to be the contact surface and the rack teeth were selected to be the target surface where the two bodies possess similar stiffness values (Khalifa, 2021)[48]. The results for his paper suggest that, the stress and wear performances of all systems are very much dependent on the E-Modul and the highest stresses were observed in the single helical rack and pinion system whereas the double helical and herringbone experiments performed significantly better stress distribution and effectively lowering the total stress (Khalifa, 2021)[49]. Furthermore, he concluded that the elastic deformation is a crucial aspect to consider in terms of safe and efficient use (Khalifa, 2021)[50].

In the current state, we can investigate diverse studies regarding the contact problem and contact analysis between a rack and pinion or between a gear pair that is simulated using a FEM or MBD simulation software. Although each of these studies present important results for their fields, the main goal for this thesis is to carry out a dynamic analysis for the purpose of

39 See page 8.
40 See page 662.
41 See page 663.
42 See page 663.
43 See page 664.
44 See page 664.
45 See page 956.
46 See page 956.
47 See page 956.
48 See page 957.
49 See page 964.
50 See page 964.

analysing the bearing reactions and the contact behaviours based on different types of simulation conditions. In that sense, two papers are the most relevant for this thesis. The first one being "Geometric Design, Meshing Simulation, and Stress Analysis of Pure Rolling Rack and Pinion Mechanisms" (Zhen, Ming, & Alfonso, 2019) where a crossed axis rack pinion system is investigated using different geometries. The second being "Modelling and simulation of rack-pinion steering systems with manufacturing errors for performance prediction" (Marano, et al., 2018), where a MBD simulation of a crossed helical rack and pinion system was analysed.

However, there is a lack of studies that fully complement this thesis fully regarding in terms of a dynamic contact analysis of the rack and pinion as well as the bearing reactions of the pinion.

Chapter 3

4 Geometric Design and Modelling

4.1 Basic Definitions

4.1.1 Gear Types

Gears can be designed, arranged, and manufactured in various ways that would complement their purpose or adapt to the environment. At the most basic level, gears can be classified based on their teeth orientation and the relative positioning of the axes of the gear wheels, or the pinion and the rack. **Figure 8** (Ever-Power, 2024) shows different gear types, and their orientations. Three most relevant gear types (cylindrical spur gear, cylindrical helical gear and crossed helical gear) will be explained in this chapter, to provide a basic understanding of the used formulas and the contact behaviour.

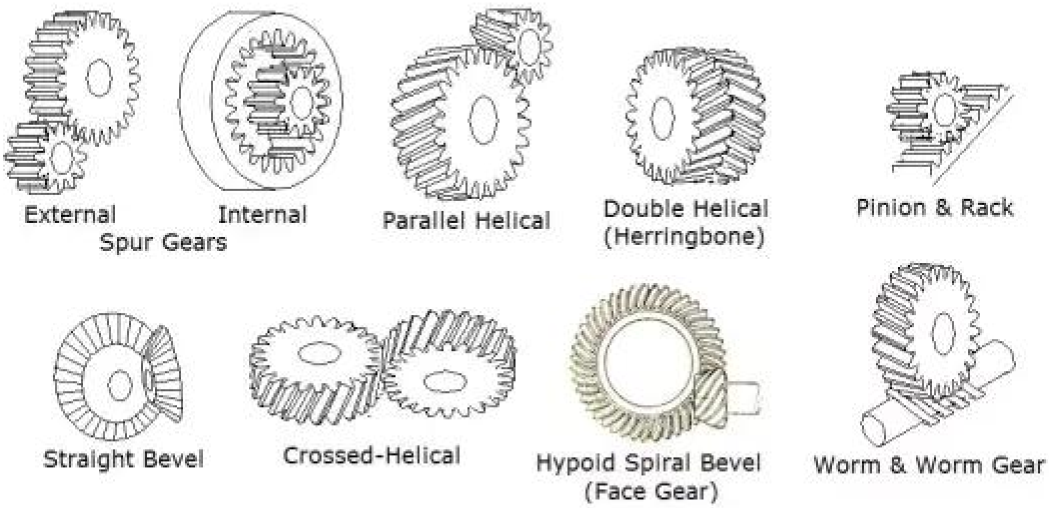

Figure 8: *Different types of gears (Ever-Power, 2024)*

- **Cylindrical Spur Gears:** Spur gears are the most basic type of gears with their tooth profile parallel to the axis of the gear and for racks, the tooth profile is directly perpendicular to the axis of the rack along the length. Therefore, the axes of the gear pair are parallel, while for racks they are perpendicular. A cylindrical spur gear pair offers a higher amount of efficiency compared to other types of gears, typically ranging between 98% to 99% (Vullo, 2020)[51]. The contact between the teeth is a line contact (Wittel, Muhs, Jannasch, & Voßiek, 2015)[52]. They are commonly being used in basic steering gears where the pinion axis is perpendicular to the rack axis along its length as shown in **Figure 9** (Hlaing, Win, & Thein, 2017)[53].

51 See page 13.

52 See page 718, original language in German.

53 See page 861.

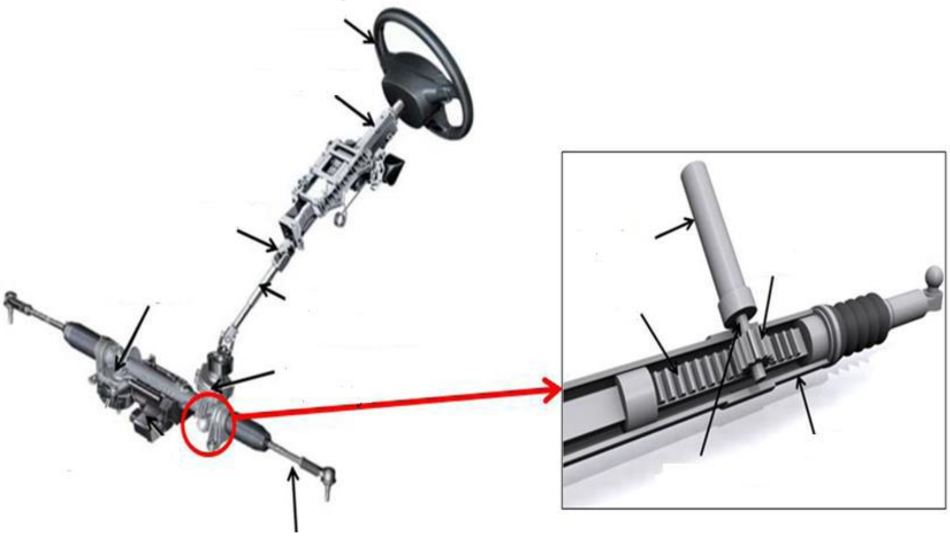

Figure 9: A representation of a steering gear without skew angle (Hlaing, Win, & Thein, 2017)

- **Cylindrical Helical Gears**: *"Helical gears have the same use of the spur gears, but their teeth have helical or screw shape; therefore, transverse profiles of teeth are the same in the various transverse sections, but change in the angular position along the longitudinal direction from end to end."* (Vullo, 2020)[54]. This shape is defined by a helical angle and provides advantages against spur gears such as smoother operation because of better tooth engagement due to existing overlap contact ratio, and improved load resistance (Wittel, Muhs, Jannasch, & Voßiek, 2015)[55]. However, they are susceptible to axial forces, which create additional stress, and are they are prone to higher friction losses because of greater contact ratio leading to lower efficiency and more space requirement compared to straight teeth (Wittel, Muhs, Jannasch, & Voßiek, 2015)[56]. Like spur gears, a line contact exists on the flanks of the teeth and can be seen in **Figure 10** (Princeton Edu, n.d.) below. These gears are used in manual transmissions of automobiles because of their advantages and for steering gears.

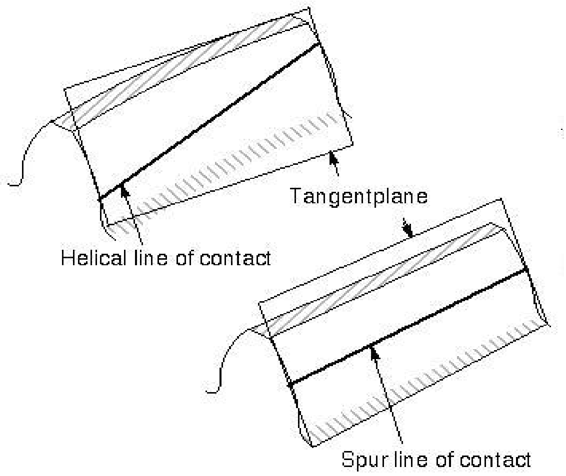

Figure 10: Contact lines on straight and helical tooth (Princeton Edu, n.d.)

54 See page 8.

55 See page 760, original language in German.

56 See page 8, original language in German.

- **Crossed Helical (Screw) Gears:** Crossed helical gears, or a rack and pinion pair share similar properties with helical gears, except for relative positioning of their axes. As opposed to the cylindrical helical gears, they possess a shaft (skew) angle that defines the rotation of the pinion from the driven gear or rack. This allows the use of two different helical angles for the driver and driven gear, and their sum is defined as the skew angle. A crucial property of these gears is that they are only suitable for transmitting low powers, as the interaction between the teeth generates a point contact rather than a line contact due to the existing tangent plane between the gear pair (Abdulaal & Abdulah, 2024)[57]. According to Niemann and Winter, a line contact is possible to achieve if the sum of the helical angles is 0°, meaning they have the same angle in opposite directions (Niemann & Winter, 1986)[58]. A representation of the theoretical contact phenomenon comparison can be seen in **Figure 11** (Litvin, Gonzalez-Perez, Fuentes, Vecchiato, & Sep, 2005) below: a) contact lines of a helical gear pair with parallel axes, b) contact points of helical gears with crossed axes. This system with a rack is the examined case in this thesis, as the crossed axis placement of the rack and pinion is the most prominent method of steering in automobiles where the driver is not seated in the middle of the automobile. The details are discussed in more detail in the Modelling and Calculation sections.

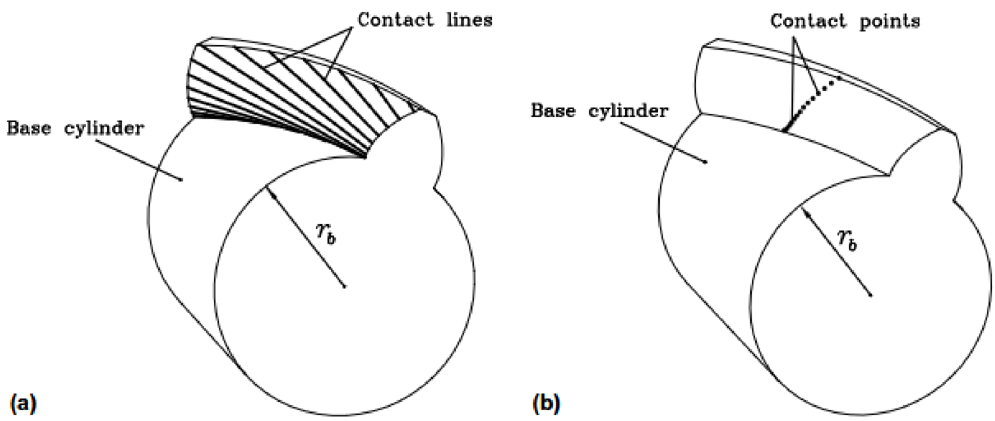

Figure 11: *Contact phenomena in a) helical gear pair with parallel axes, b) helical gears with crossed axes (Litvin, Gonzalez-Perez, Fuentes, Vecchiato, & Sep, 2005)*

4.1.2 Gear Terminology

- **Tooth Geometry:**

All the following information is taken from the standard norms for gear geometry "ISO 21771: Gears – Cylindrical involute gears and gear pairs – Concepts and geometry" (International Standards Organisation, 2007) **unless stated otherwise.**

- **Module (m_n):** The normal module is a parametrical unit that describes the size of the gear or the rack and can be described as the pitch of the rack divided by π.
- **Teeth Number (z):** The teeth number is an integer that describes the number of teeth on the gear. Teeth number is infinite for racks.

57 See page 3.

58 See page 3original language in German.

- **Transverse Module (m_t):** The transverse module is a parameter for helical gears and racks which is the module that is perpendicular to the axis of the gear or to the rack axis along the length.
- **Normal Pressure Angle ($\alpha_{n,}$):** The normal pressure angle is the angle of inclination at the reference cylinder and referred to as the pressure angle for basic rack profile.
- **Transverse Pressure Angle (α_t):** The transverse pressure angle is the acute angle between the tangents to the involute at their point of intersection with the reference circle and the radius and is a relevant parameter for helical gears.
- **Helix Angle (β):** The helix angle is the angle between a tangent to a reference helix and the reference cylinder envelope line thorough the tangent contact point. The lead angle and helix angle are always in total 90°.
- **Base Helix Angle (β_b):** Helix angle on the base cylinder.
- **Flank Direction:** Direction of the helix.
- **Addendum (h_a):** The radial difference between the addendum circle (tip circle diameter) and the pitch circle (Vullo, 2020)[59].
- **Dedendum (h_f):** The radial difference between the dedendum circle (root circle diameter) and the pitch circle (Vullo, 2020)[60].
- **Tooth Depth (h):** Tooth depth is the teeth difference between the tip and root radius.
- **Transverse Tooth Thickness (s_t):** The length of the circular arc of diameter between two involute helicoids of a tooth. Also called tooth width.
- **Space Width (e_t):** The length of the circular arc of diameter between two involute helicoids of a space. Also called tooth space.
- **Tip Alteration Coefficient (k^*):** A modification to the addendum can be described by tip alteration, where tip alteration coefficient times module determines the tip alteration.
- **Tooth Profile Height Factor (κ):** Is a tool-based parameter that is used to determine the minimum profile shift to avoid undercut (Wittel, Muhs, Jannasch, & Voßiek, 2015)[61]

Gear tooth geometries can be also seen for spur gears in **Figure 12** (Chaturvedi, Acar, & Sandu, 2022)[62] and for helical geometries in **Figure 13** (Akinnuli, Ogdengbe, & Oladosu, 2019)[63] Also, the basic rack profile (International Standards Organisation, 2007)[64] and its parameters are given in **Figure 14** and **Figure 15**.

59 See page 24.
60 See page 24.
61 See page 751, original language in German.
62 See page 3.
63 See page 959.
64 See page 13.

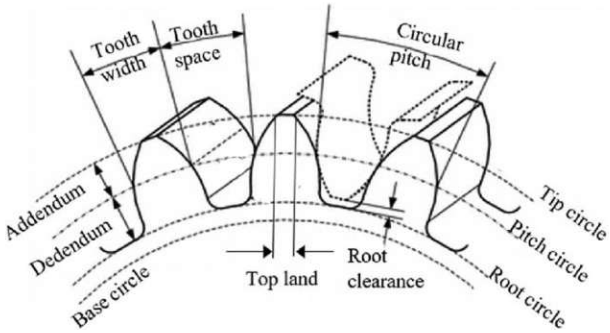

Figure 12: *Gear tooth geometries for straight gears (Chaturvedi, Acar, & Sandu, 2022)*

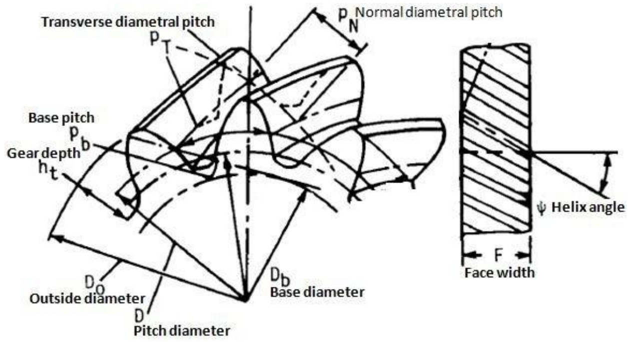

Figure 13: *Gear tooth geometries for helical gears (Akinnuli, Ogdengbe, & Oladosu, 2019)*

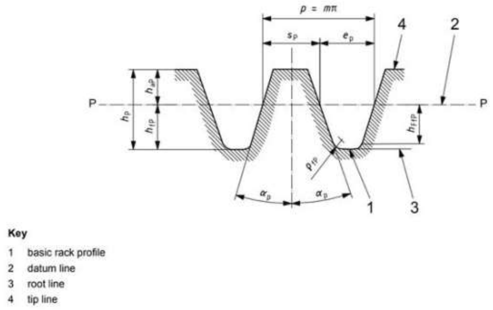

Figure 15: *Basic rack tooth profile according to ISO 53 (International Standards Organisation, 2007)*

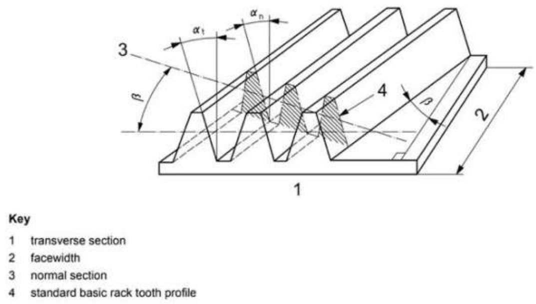

Figure 14: *Basic rack profile according to ISO 53 (International Standards Organisation, 2007)*

- **Gear Pair and Contact Geometry**
  - **Pitch Circle Diameter (d):** Pitch circle diameter or reference diameter is the reference surface for cylindrical gears and can be described as the intersection of the reference cylinder with a transverse plane section. Pitch diameter is a plane for the rack, instead of a circle.
  - **Base Circle Diameter (d_b):** The base circle is the intersection of the base cylinder and the transverse section, where the involute formation of the teeth starts.
  - **Root Circle Diameter (d_f):** Root cylinder forms the bottom of the tooth space, and root circle diameter is the diameter where the tooth starts.
  - **Tip Circle Diameter (d_a):** Tip cylinder forms the tips of the tooth system, and tip circle diameter is the diameter where the tooth ends.
  - **Facewidth (b):** Length of the toothed part of the cylindrical gear measured in the axial direction.
  - **Active Facewidth (b_w):** Useable face widths of the gear pair.
  - **Normal Pitch ($p_{n,}$):** The normal pitch is the length of the helix arc between two successive equal-handed tooth flanks on the reference cylinder in the normal section.
  - **Transverse Pitch (p_t):** The transverse pitch is the length of the helix arc between two successive equal-handed tooth flanks.

- **Axial Pitch (p_x):** The portion of a generation line of a cylinder concentric with the gear axis between two successive equal-handed tooth flanks of a helical gear.
- **Contact Ratio:**
    - **Path of Contact (g_α):** Path of contact or lines of action are the planes of action where the transverse section of mating gears or rack and pinion pairs intersect. The starting point is the tip circle of the driven gear and the end point is the tip circle of the driving gear. **Figure 16** (Princeton Edu, n.d.) represents the path of action where the pitch point moves along and defines the contact.
    - **Transverse Contact Ratio (ε_α):** Ratio of the length of path of contact to the transverse normal base pitch.
    - **Overlap Ratio (ε_β):** The ratio of the facewidth to the axial pitch.
    - **Total Contact Ratio (ε_γ):** Sum of the transverse and overlap ratios.

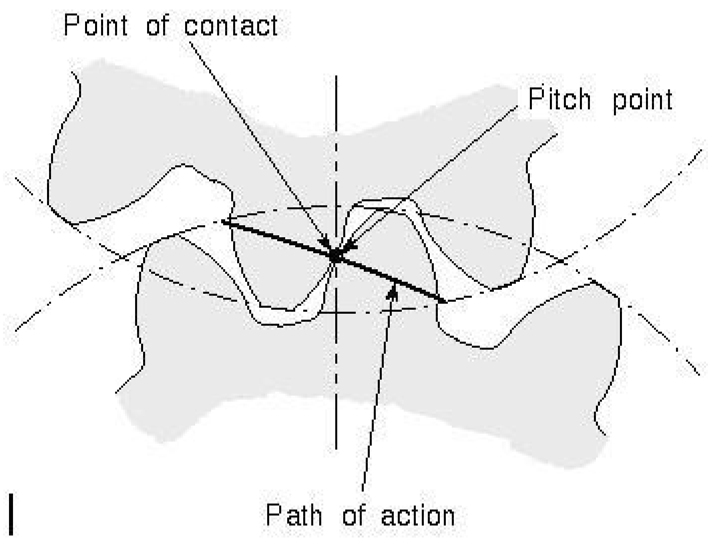

Figure 16: *Contact line in the transverse section (Princeton Edu, n.d.)*

- **Profile Shift (x):** The displacement of the basic datum line from the reference cylinder in involute gear teeth. Positive profile shifts increase the tooth thickness on the reference cylinder and negative profile shift decreases.
- **Centre Distance (a):** Working distance between the gear axes of two gears on the line of centres.
- **Tip Clearance (c):** The distance by which the tip circle of a gear is separated from the root circle of the mating gear or rack.

Basic gear pair geometry of spur gears is represented in **Figure 17** (Peršin, 2013)[65].

65 See page 11.

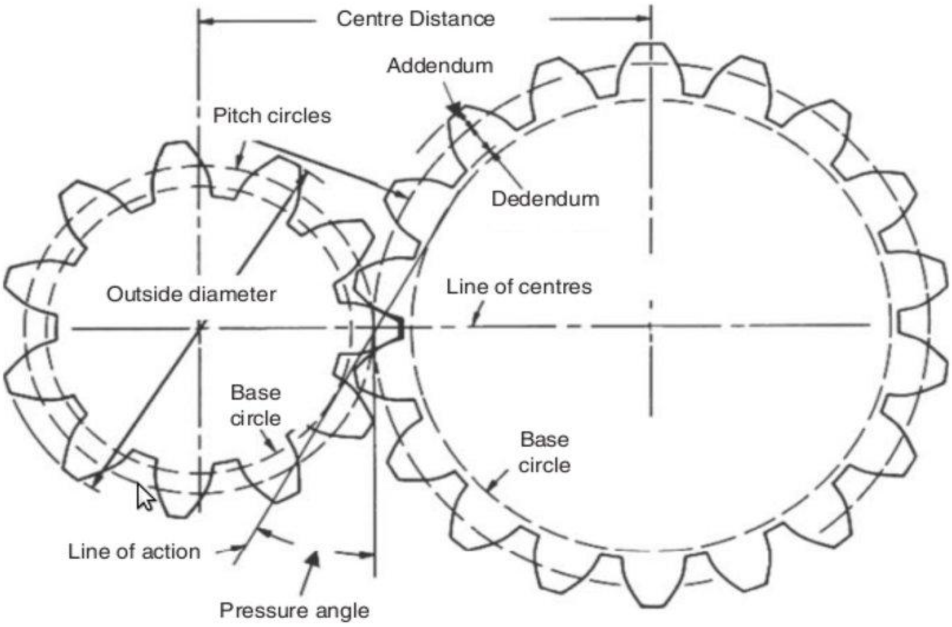

Figure 17: *Spur gear pairing geometry and definitions (Peršin, 2013)*

4.2 Involute Geometry

The involute profile is one of the most widely used tooth geometry in modern gear design, described as an almost generalised curve that satisfies the first fundamental law of gearing. According to this law, the geometries of the gear tooth pair must ensure a constant transmission ratio, which is achieved when mating profiles engage in a conjugated action. *"Conjugacy is a specific property of a gear and a mating pinion tooth flanks (tooth profiles) that roll over one another- "* (Radzevich & Storchak, 2022)[66]. A constant transmission ratio assures a smoother operation, while geometric accuracy contributes to a near vibration and noise excitation free movement (Radzevich & Storchak, 2022)[67]. As stated in the book by Vullo, "*The basic law of conjugated action between two mating profiles states that as the profiles rotate, the common normal to the profiles at the point of contact must always intersect the line of centers at the same point, called the pitch point."* (Vullo, 2020)[68]. The second fundamental law of gearing states that for smooth and uniform rotary transmission between a gear pair, the perpendicular lines originating from the tooth flanks at all contact points must intersect with the axis of the gear pair (Radzevich & Storchak, 2022)[69]. An involute geometry inherently satisfies the above-mentioned laws of gearing.

66 See page 11.

67 See page 3.

68 See page 15.

69 See page 21.

The involute curve is generated by a point on a straight line that rolls along the circumference of a circle, known as the base circle (Wittel, Muhs, Jannasch, & Voßiek, 2015)[70]. Alternatively, it can also be described as the trajectory of the endpoint of a straight line that remains tangent to the base circle as it unwinds. The curve is created by drawing straight lines of varying lengths that have a basic ratio tangent to the base circle and then combining the ends of those lines into a smooth curve. **Figure 18** (Vullo, 2020)[71] illustrates the construction of arcs of the base circle and corresponding involute curves, showing the alignment of the curve as the tangent point moves along the circle based again on a ratio. A more detailed explanation of the implementation of this geometry is provided in the CAD Modelling section.

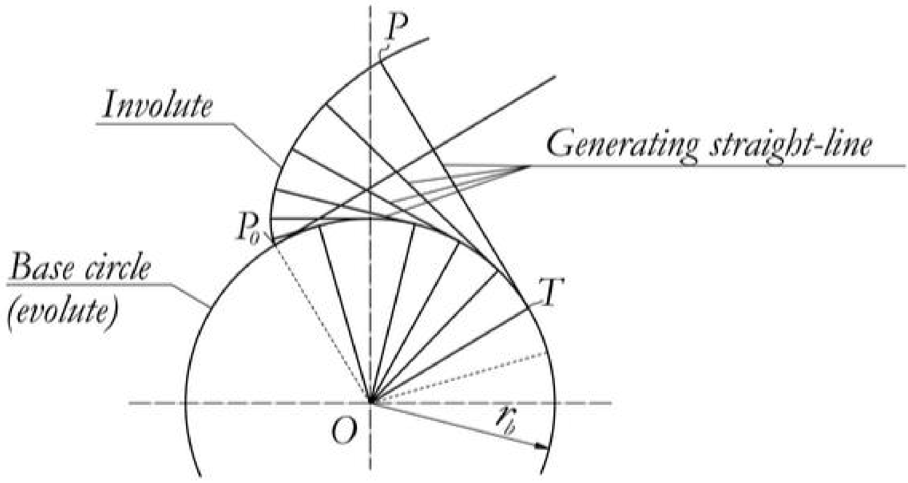

Figure 18: *Involute geometry (Vullo, 2020)*

The involute curve has several advantages that make it ideal for gear design (Vullo, 2020)[72].

1. **Independent of Centre Distance Variations:** The conjugate action between involute profiles remains unaffected by small changes in the centre distance between gears.
2. **Accurate Power Transmission:** The involute profile guarantees high-grade accuracy, ensuring constant velocity ratios without friction dependency.
3. **Straight-Sided Basic Rack Profile:** The basic rack profile for involute geometries has straight sides, simplifying design and production.
4. **Ease of Manufacturing:** Gears with involute teeth can be manufactured using a single cutting tool for a given module, resulting in more cost-effective and efficient construction.

These advantages contribute to the widespread adoption of involute geometry in gear systems (Wittel, Muhs, Jannasch, & Voßiek, 2015)[73].

In this thesis, involute geometry is used for the construction of the rack and pinion steering system. The geometry ensures smooth, efficient motion transfer and minimizes manufacturing complexity and widely employed by BMW in their steering gear systems.

70 See page 728, original language in German.

71 See page 43.

72 See page 39-40.

73 See page 730, original language in German.

4.3 Calculations for the Gear Geometries

The teeth and gear geometries of crossed helical gears are calculated using the same formulas for cylindrical helical gears as stated by Niemann and Winter (Niemann & Winter, 1986)[74] and taken from the ISO 21771 norm. The only difference compared to helical gears with parallel axis will be the calculation of the total contact ratio in order to describe the theoretical point contact rather than a line contact. The geometric parameters used for the rack and pinion calculations in this study are presented in **Table 2**.

Parameter	Value	Unit
$m_{n,1,2}$	2	mm
$\alpha_{n,1,2}$	20	$degree$
λ	26	$degree$
z_1	10	$-$
β_1	26	$degree\ (left\ helix)$
β_2	0	$degree$
b_1	30	mm
b_2	25	mm
d_2	25	mm
$C_{\beta,1}$	1	μm
r_k	1	μm
h_k	1	μm
δ_{hk}	45	$degree$

Table 2: *Geometric parameters used in this study*

4.3.1 Pinion Geometry

All the equations below are taken from ISO 21771 (International Standards Organisation, 2007) **unless stated otherwise.**

The first step of the geometry calculations is the calculations of the transverse module[75], the transverse pressure angle[76] and the normal[77] and transverse pitch[78] for the pinion:

$$m_{t,1} = \frac{m_{n,1}}{\cos(\beta_1)} = \frac{2\ mm}{\cos(26°)} = 2.2252\ mm \tag{1}$$

$$\alpha_{t,1} = \operatorname{atan}\left(\frac{tan(\alpha_{n,1})}{cos(\beta_1)}\right) = \operatorname{atan}\left(\frac{tan(20°)}{cos(26°)}\right) = 22.046° \tag{2}$$

$$p_{n,1} = m_{n,1} * \pi = 2\ mm * \pi = 6.2832\ mm \tag{3}$$

74 See page 2-5, original language in German.

75 See page 15 formula 2.

76 See page 20 formula 14.

77 See page 22 formula 24.

78 See page 22 formula 23.

$$p_{t,1} = m_{t,1} * \pi = 2.2252\ mm * \pi = 6.9907\ mm \tag{4}$$

The next step is to calculate the pitch circle[79] and base circle diameters[80] :

$$d_1 = z_1 * m_t = 10 * 2.2252\ mm = 22.252\ mm \tag{5}$$

$$r_1 = \frac{d_1}{2} = \frac{22.252\ mm}{2} = 11.126\ mm \tag{6}$$

$$d_{b,1} = d_1 * \cos(\alpha_{t,1}) = 22.252\ mm * \cos(22.046°) = 20.625\ mm \tag{7}$$

$$r_{b,1} = \frac{d_{b,1}}{2} = \frac{20.625\ mm}{2} = 10.313\ mm \tag{8}$$

In the following step we need to decide the profile shift and check if the value is larger than the minimum profile shift coefficient based on the used manufacturing tools. The minimum profile shift value is required to protect the teeth from undercut, which means the thinning and weakening of the root. The selection of profile shift (Weigand, Kral, & Dencsi, 2016)[81] has a huge impact on the contact ratio, because it changes the tooth profile as the contact point moves upwards or downwards based on positive or negative profile shift and altering the tooth thickness accordingly. A lower, even negative profile shift positively increases the contact ratio and therefore the lowest possible profile shift should be selected:

$$x_{min,1} = \kappa - \frac{z_1^2 * \sin(\alpha_{t,1})^2}{2} = 1 - \frac{10^2 * \sin(22.046°)^2}{2} = 0.2956 \tag{9}$$

$$x_{selected,1} = x_1 = 0.3 \tag{10}$$

After the profile shift has been selected, the tip clearance and the tip alteration factor[82]are selected. The higher the tip alteration we implement, the greater the contact ratio can be achieved, as it increases the contact surface area of the teeth. The problem with increased tip alteration is the danger of the tip of the pinion coming too close to the root of the opposite gear or rack and interfering with each other, which causes excessive friction, possible damages, and risk of overloading. An excessive tip alteration also causes the teeth to become "pointed" and thin, which causes poorer contact conditions, reduced loading capacity and risk of high

79 See page 14 formula 1.

80 See page 20 formula 13.

81 See page 264, original language in German.

82 See page 24.

mechanical deformation and breakage. Therefore, a review of the maximum tip circle diameter of the pinion is an absolute necessity for a correct design. Selected tip altering coefficient is 0.07 for the construction. Tip clearance on the other hand is given through pre-determined ISO 53 profiles of the gear geometries. For this thesis, both the rack and pinion are constructed using the ISO 53 Profile C (International Standards Organisation, 1998)[83], which uses a tip clearance factor c_p of 0.25:

$$k = k^* * m_{n,1} = 0.07 * 2\,mm = 0.14\,mm \tag{11}$$

$$c = c_p * m_{n,1} = 0.25 * 2\,mm = 0.5\,mm \tag{12}$$

Through the selection of tip alteration and the rack and pinion profiles, we can now calculate the tip circle[84] and root circle[85] diameters of the pinion. In the ISO 53 Profile C (International Standards Organisation, 1998)[86], the addendum coefficient[87] is equal to the normal module and the dedendum coefficient[88] is $1 + c_p$ times of the module:

$$\begin{gathered} h_{a,1} = m_{n,1} + x_1 * m_{n.1} + k = \\ 2\,mm + 0.3 * 2\,mm + 0.14\,mm = 2.74\,mm \end{gathered} \tag{13}$$

$$h_{f,1} = m_{n,1} * (1 + c_p) - x_1 * m_{n.1} = 2\,mm * 1.25 - 0.3 * 2\,mm = 1.9\,mm \tag{14}$$

Therefore, the total tooth depth[89] and the tip and root diameters are calculated as:

$$h_1 = h_{a,1} + h_{f,1} + c = 2.74\,mm + 1.9\,mm + 0.5\,mm = 5.14\,mm \tag{15}$$

$$\begin{gathered} d_{a,1} = d_1 + (h_{a,1} + x_1 * m_{n.1} + k) * 2 = \\ 22.252\,mm + (2\,mm + 0.3 * 2\,mm + 0.14\,mm) * 2 \end{gathered} \tag{16}$$

$$d_{f,1} = d_1 - (h_{f1} - x_1 * m_{n.1}) * 2 = 22.252\,mm - (2.5\,mm - 0.3 * 2\,mm) * 2 \tag{17}$$

$$d_{a,1} = 27.732\,mm, \qquad d_{f.1} = 18.452\,mm \tag{18}$$

$$r_{a,1} = \frac{d_{a,1}}{2} = \frac{27.732\,mm}{2} = 13.866\,mm \tag{19}$$

83 See page 5.

84 See page 24 formula 33.

85 See page 24 formula 34.

86 See page 5.

87 See page 25 formula 36.

88 See page 25 formula 37.

89 See page 24 formula 35.

$$r_{f,1} = \frac{d_{f,1}}{2} = \frac{18.452\ mm}{2} = 9.226\ mm \tag{20}$$

Now that the pinion geometries are calculated, it is necessary to control whether this geometry is prone to the pointing or undercut. As we previously selected the profile shift coherent with avoiding undercut, a further check is not needed. However, the verification of pointing requires the use of involute functions and the inverse involute function (24) that is derived from the series expansion $inv\ (x) = \tan(x) - x = \frac{1}{3}x^3 + \frac{2}{15}x^2 + \frac{17}{315}x^7$ ... Later in formula (22) the transverse angle in the tip is calculated:

$$inv_{\alpha_{t,1}} = \tan(\alpha_{t,1}) - \alpha_{t,1} = \tan(22.046°) - 22.046° = 0.0201 \tag{21}$$

$$inv_{\gamma_1} = \frac{\pi}{2 * z_1} + \frac{2 * x_1 * \tan(\alpha_{t,1})}{z_1} + inv_{\alpha_{t,1}} = \frac{\pi}{2 * 10} + \frac{2 * 0.3 * \tan(22.046°)}{10} + 0.0201 \tag{22}$$

$$inv_{\gamma_1} = 0.202 \tag{23}$$

$$\gamma_1 = \sqrt[3]{3 * inv_{\gamma_1}} - \frac{2}{5} * inv_{\gamma_1} = \sqrt[3]{3 * 0.202} - \frac{2}{5} * 0.202 = 43.831° \tag{24}$$

$$r_{a,1.max} = \frac{r_{b,1}}{\cos(\gamma_1)} = \frac{10.313\ mm}{\cos(43.831°)} = 14.295\ mm \tag{25}$$

$$r_{a,1} < r_{a,1.max} \tag{26}$$

4.3.2 Pinion Modifications

It is possible to make various geometrical modifications for pinions, namely tooth flank modifications. ISO 21771 describes them as desired alterations of the face compared to the main geometry (International Standards Organisation, 2007)[90]. Two types of pinion modifications are considered in this thesis: a tip rounding and crowning of the flank line (flank line helix crowning). The helix crowning shown in **Figure 19** decreases the misalignment errors during the meshing of the gear pair and again decreases the stress accumulation on the edges of the teeth. A tip rounding shown in **Figure 20** is effective to reduce stress as result of eliminating the sharp edges and further improve the meshing contact, but as the involute contact surface decreases, the contact ratio will be negatively influenced. The contact ratio on the other hand, similar with the tip rounding, decreases as the contact surfaces are lesser.

90 See page 44.

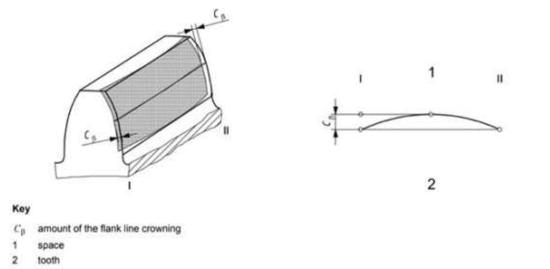

Figure 19: *Tooth flank modification of the pinion (KISSSOFT)*

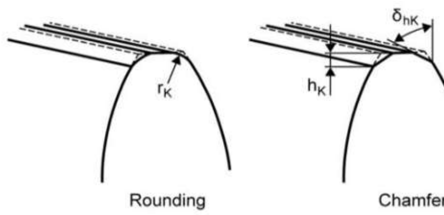

Figure 20: *Tooth tip modification of the pinion (KISSSOFT)*

4.3.3 Rack Geometry

The calculations for the rack geometry are simpler compared to the pinion, as we are not dealing with helical geometry and ISO 53 (International Standards Organisation, 1998)[91] profiles allow us to design a rack only using the addendum and dedendum:

$$m_{t,2} = \frac{m_{n,2}}{\cos(\beta_2)} = \frac{2\,mm}{\cos(0°)} = 2\,mm \tag{27}$$

$$\alpha_{t,2} = \text{atan}\left(\frac{tan(\alpha_{n,2})}{cos(\beta_2)}\right) = \text{atan}\left(\frac{tan(20°)}{cos(0°)}\right) = 20° \tag{28}$$

$$p_{n,2} = m_{n,2} * \pi = 2\,mm * \pi = 6.2832\,mm \tag{29}$$

$$p_{t,2} = m_{t,2} * \pi = 2\,mm * \pi = 6.2832\,mm \tag{30}$$

$$h_{a,2} = m_{n,2} = 2\,mm \tag{31}$$

$$h_{f,2} = m_{n,2} * (1 + c_p) = 2\,mm * 1.25 = 2.5\,mm \tag{32}$$

$$h_2 = h_{a,2} + h_{f,2} + c = 2\,mm + 2.5\,mm + 0.5\,mm = 5\,mm \tag{33}$$

Now that the geometries are calculated, we can find the centre distance and the calculations for the contact ratio can be made. For this design we are working with a round rack instead of a straight one as the suppliers of BMW is producing round racks for their steering gears. This means for the calculation of the centre distance; we will be using the radius of the rack as its height:

$$a = r_1 + x_1 * m_{n,1} + r_2 - h_{a,2} = \\ 11.126\,mm + 0.3 * 2\,mm + 12.5\,mm - 2\,mm = 22.226\,mm \tag{34}$$

91 See page 5.

4.3.4 Rack Modifications

The rack teeth are also modified to overcome high stress around the edge points. This is done by using chamfers instead of rounding as was on the pinion.

4.3.5 Contact Ratio

The contact ratio for crossed helical rack and pinion is in theory a point contact as mentioned above. In practice, the contact takes effect in an ellipsis due to the meshing and resulting elastic and plastic behaviour of the material (Niemann & Winter, 1986)[92] Consequently, the theoretical contact ratio that is calculated below will not exactly represent the physical model. The contact ratio has been calculated using three different methods and displays the same results:

- **Method 1: The Method of Niemann and Winter:**

Niemann and Winter uses the projection of the contact line AE (the contact from the tip circle of the pinion to the tooth begin of the rack) by dividing to the cosines of the base helix angles (International Standards Organisation, 2007)[93] to calculate the total contact ratio of the rack and pinion pair. In their calculations, the line from A to S represents the contact line from the dedendum begin of the rack teeth until the contact point or pitch point and the line S to E represents the contact line from the pitch point until the base circle of the pinion (Niemann & Winter, 1986)[94]:

$$\beta_{b,1} = \operatorname{asin}\left(\sin(\beta_1) * cos(\alpha_{n,1})\right) = \operatorname{asin}(\sin(26°) * \cos(20°)) = 24.326° \qquad (35)$$

$$\beta_{b,2} = \operatorname{asin}\left(\sin(\beta_2) * cos(\alpha_{n,2})\right) = \operatorname{asin}(\sin(0°) * \cos(20°)) = 0° \qquad (36)$$

$$AS = \frac{h_{a,2} - x_1 * m_{n,1}}{\cos(\beta_{b,2}) * \sin(\alpha_{t,2})} = \frac{2\,mm - 0.3 * 2\,mm}{\cos(0°) * \sin(20°)} = 4.093\,mm \qquad (37)$$

$$SE = \frac{0.5 * \left(\sqrt{d_{a,1}^2 - d_{b,1}^2} - \sqrt{d_1^2 - d_{b,1}^2}\right)}{\cos(\beta_{b,1})} \qquad (38)$$

$$SE = \frac{0.5 * \left(\sqrt{27.732\,mm^2 - 20.625\,mm^2} - \sqrt{22.252\,mm^2 - 20.625\,mm^2}\right)}{\cos(24.326°)} = 5.5894\,mm \qquad (39)$$

$$AE = AS + SE = 4.093\,mm + 5.5894\,mm = 9.6824\,mm \qquad (40)$$

---

92 See page 5, original language in German.

93 See page 18 formula 6.

94 See page 5, original language in German.

$$\varepsilon_{\gamma,1} = \frac{AE}{p_{n,1} * \cos(\alpha_{n,1})} = \frac{9.6824\ mm}{6.2832\ mm * \cos(20°)} = 1.6399 \tag{41}$$

- **Method 2: Method of Werner Krause and ISO 21771:**

This method divides the total contact ratio into its transverse and overlap ratios and calculates the total contact ratio by combining these two parts together. The formula of the transverse contact ratio in Formula (45) for rack and pinion is taken from the ISO 21771[95] norm, and the formula for the calculation of the overlap ratio comes from the journal article of Werner Krause "Überdeckung von Schraubenstirnradgetrieben"[96] (Krause, 2002)[97], who was specialised in the construction of crossed helical gears

$$g_{\alpha,2} = \sqrt{r_{a,1}^2 - r_{b,1}^2} - \sqrt{r_1^2 - r_{b,1}^2} + \frac{h_{a,1} - x_1 * m_{n,1}}{\sin(\alpha_{t,1})} \tag{42}$$

$$g_{\alpha,2} = \sqrt{13.866\ mm^2 - 10.313\ mm^2} - \sqrt{11.126\ mm^2 - 10.313\ mm^2} + \frac{2\ mm - 0.3 * 2\ mm}{\sin(22.046°)} \tag{43}$$

$$g_{\alpha,2} = 8.823\ mm \tag{44}$$

$$\varepsilon_{\alpha.2} = \frac{g_{\alpha,2}}{p_{t,1} * \cos(\alpha_{t,1})} = \frac{8.823\ mm}{6.9907\ mm * \cos(22.046°)} = 1.3617 \tag{45}$$

In the method of Krause, the transverse contact ratio is defined in (46) (Krause, 2002)[98] and the overlap contact ratio in (47) (Krause, 2002)[99]:

$$\varepsilon_{\alpha.K} = \frac{A_{n,1}E_{n,1} * \cos(\alpha_{n,1}) * \cos(\beta_1)}{p_{t,1} * \cos(\alpha_{t,1})^2} \tag{46}$$

95 See page 37 formula 90.

96 English: Contact Ratio of Cylindrical Screw Gears

97 See page 55, original language in German.

98 See page 55 formula 2a, 2b, original language German.

99 See page 55 formula 3a, 3b, original language German.

$$\varepsilon_{\beta,K} = \frac{A_{n,1}E_{n,1} * \cos(\alpha_{n,1}) * \sin(\beta_1) * \tan(\beta_1)}{p_{t,1}} \tag{47}$$

In order to find the correct overlap ratio, we have to convert the contact line $A_{n,1}E_{n,1}$ (Krause, 2002) [100]defined by Krause to a rack and pinion variant defined in ISO 21771. When we set the Formula (45) and Formula (47) together, we can find that the contact line defined by Krause and set it to find the overlap ratio:

$$\varepsilon_{\alpha,2} = \varepsilon_{\alpha,K} \rightarrow \frac{g_{\alpha,2}}{p_{t,1} * \cos(\alpha_{t,1})} = \frac{A_{n,1}E_{n,1} * \cos(\alpha_{n,1}) * \cos(\beta_1)}{p_{t,1} * \cos(\alpha_{t,1})^2} \tag{48}$$

$$A_{n,1}E_{n,1} = \frac{g_{\alpha,2} * \cos(\alpha_{t,1})}{\cos(\alpha_{n,1}) * \cos(\beta_1)} \tag{49}$$

After we define $A_{n,1}E_{n,1}$, we can now calculate the overlap ratio in (47) that is compatible with the ISO 21771 contact line:

$$\varepsilon_{\beta,2} = \frac{g_{\alpha,2} * \sin(\beta_1) * \tan(\beta_1) * \cos(\alpha_{t,1})}{p_{t,1} * \cos(\beta_1)} = \frac{8.823\ mm * \sin(26°) * \tan(26°) * \cos(22.049°)}{6.9907\ mm * \cos(26°)} \tag{50}$$

$$\varepsilon_{\beta,2} = 0.2783 \tag{51}$$

$$\varepsilon_{\gamma,2} = \varepsilon_{\alpha.2} + \varepsilon_{\beta,2} = 1.3617 + 0.2783 = 1.6399 \tag{52}$$

It is important to note the irregularity with the overlap contact ratio in this method. According to Krause, the total contact ratio of a crossed helical gear represents the contact ratio of a spur gear, more accurately the contact ratio of its substitute spur gear (Krause, 2002)[101]. This is due to the inconvenient point contact between the rack and pinion. It is also important to note that, contrary to parallel gear pairs, the overlap ratio of crossed helical gears is not dependent on the active face width of the gear pair and only need to satisfy the minimum face width (Niemann & Winter, 1986). Theoretically speaking, there are no contact outside of the points A to E (Wittel, Muhs, Jannasch, & Voßiek, 2015)[102].

100 See page 55 formula 8, original language in German.

101 See page 55, original language in German.

102 See page 816, original language in German.

- **Method 3:Use of KISSSOFT:**

A calculation for the contact ratio is also made using the gear calculation software KISSSOFT using the module ZE7 that was released with the KISSSOFT Release 2019 (KISSSOFT, 2019). The system uses user inputs regarding the normal module, helix angle, teeth number of the pinion, face widths of the rack and pinion, profile shift, and rack height to calculate the contact ratio. The results for the contact ratios are the same as two other methods without the teeth modifications (53) and the calculation report is attached in the Appendix A. When the teeth modifications are applied, the contact ratio slightly decreases (54) and illustrated in the Appendix A.

$$\varepsilon_{\gamma,3.1} = 1.6399 \tag{53}$$

$$\varepsilon_{\gamma,3.2} = 1.594 \tag{54}$$

4.4 Computer Aided Design Models of Rack and Pinion

4.4.1 Pinion

The design of the pinion was made using the KISSSOFT 3D export module, which allows the user to create a STP file of the geometry using parametric modelling and use it as a Part in SolidWorks. **Figure 21** illustrates the different viewpoints of the created pinion.

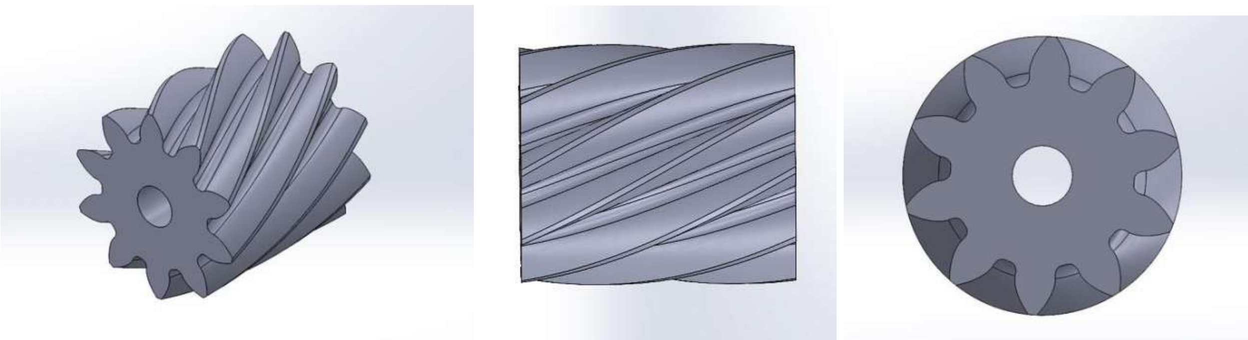

Figure 21: *CAD model of the pinion*

4.4.2 Involute Construction

KISSSOFT employs the involute construction method to create the pinion. The involute construction in CAD begins with first drawing the root circle, base circle, pitch circle and tip circle diameters. The second step is to find the pitch point “C”, which can be easily identified by drawing a horizontal line “Line 1” tangent to the pitch circle diameter. Later, another tangent line “Line 2” is drawn that is tangent to the base circle but also intersects the pitch point. We define the intersection point of the second tangent line on the base circle as point “A”. Now, the line between the point “A” and point “C” will be divided into **n** equal parts and the distance “L” between each part is to be noted. The “Line 2” also intersects the tip circle on the opposite side of point “A”, and the line will be divided into equal distances determined in the last step from point “A” until the tip circle. The next step is to project arcs on to the base circle using the point “A” as origin point and divided points as radius. After the points on the base circle are determined now tangent lines (projection lines) originating from these points must be drawn in the direction of the point “C”. The length of these tangent lines is determined through the distances between equally divided points on the “Line 2” and the number of points. The length of the first projection line that originated from the closest projection point to the pitch point has the length of “L”. The second projection line that originated from the second projection point next to the first one has the length of 2 times of “L”. This process continues until the n^{th} projection line is drawn, which is **n** times of “L” long. Now that all the projection lines are drawn, we can merge the end points using the spline function and create the involute tooth profile. The root of the tooth is then designed based on the ISO 53 teeth profiles.

4.4.3 Rack

KISSSOFT was not used to export the rack, as a round rack module does not exist in KISSSOFT modules therefore, the rack was constructed by using SolidWorks. The first step for the construction of the rack was to create a cylindric extrude with a diameter of 25 mm and length of 70 mm. 70 mm was selected as the length so that the pinion can rotate minimum of two times on the rack. The second step was to draw the tooth space profile of the rack on the edge of the cylinder and cut the tooth space from the cylinder. After we iterate the cut along the cylinder using the length of transverse pitch of the rack ($p_{t,2}$), we reach our desired rack profile. Finally, the rack is modified with chamfers on the tips of the teeth. **Figure 22** represent the rack model used for the assembly in SolidWorks.

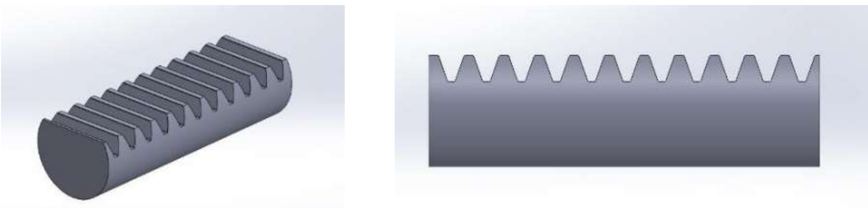

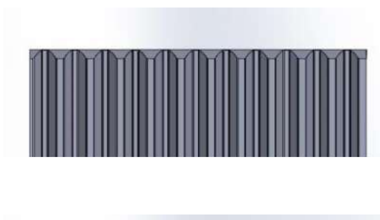

Figure 22: *CAD model of the rack*

4.4.4 Assembly

The assembly of the system was also done in SolidWorks. The mating functions in general are much more responsive and capable compared to ABAQUS, therefore SolidWorks shines as a favourable choice for the assembly. For the analysis in ABAQUS, the extra cylindric parts of the rack are not necessarily important and requires more computing power due to the created mesh (will be discussed in more detail in FEM modelling). Therefore, the rack is reduced to have a straight bottom and the volume underneath the centre point is deleted. Also, the number of teeth has been reduced to 7 full and a half tooth. The following four steps have been used for the assembly:

- The movement of the rack have been constrained everywhere except along its axis. This is done by creating two separate coincident mating, one between the top planes of rack and assembly default planes and one between the front planes of rack and assembly default planes. Coincident mating means that, the components occupy the same location and move together in the space.
- An extra plane was created off-set to the top plane with the centre distance and the pinion centre axis is mated with this plane using coincident mating so that the pinion can only move along this new plane.
- Next step is to align the pinion axis with the perpendicular axis of the rack. As we use a skew angle of 26°, the pinion axis is mated with the rack perpendicular axis with 26° angle mating.
- Last step is to define the initial contact. For this, the tooth flank of the pinion is mated tangentially with the rack tooth flank.

Figure 23 represents the assembly that is developed in SolidWorks and will be used for the further FEM analysis.

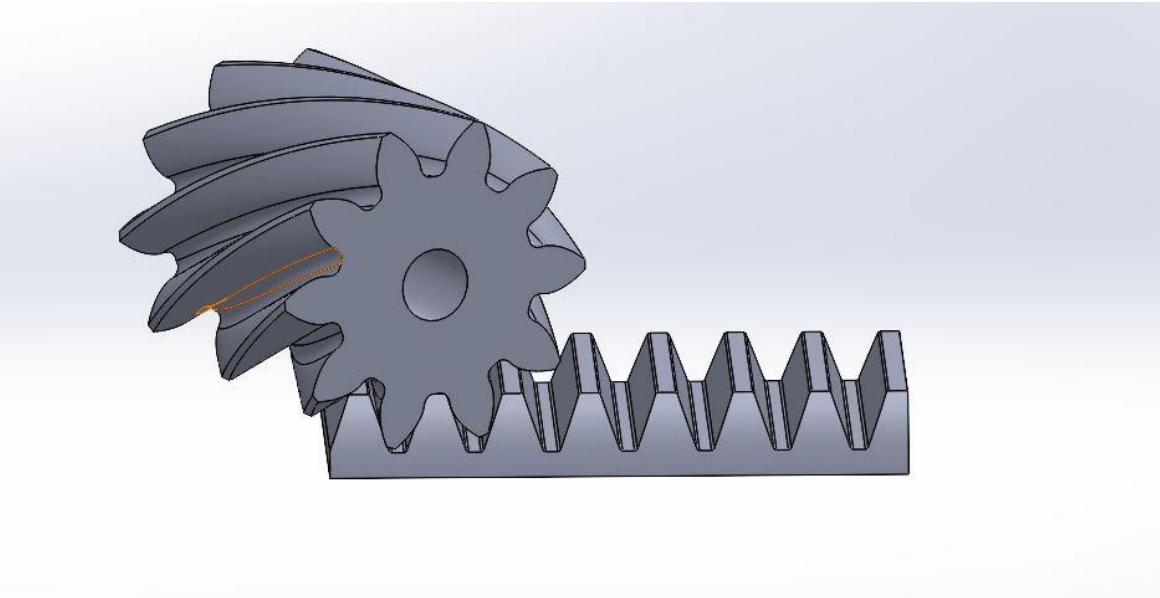

Figure 23: *Reduced CAD assembly of the rack and pinion system*

5 Finite Element Modelling

The FEM analysis was performed using ABAQUS Standard, a general-purpose finite element program (SIMULIA, Abaqus Analysis User's Guide, 2016)[103]. ABAQUS contains several components for creating a model that are used to define and solve a physical problem. At a minimum, the geometry and material definitions must be implemented in the ABAQUS model, while other optional modules can be used depending on the requirements of the problem (SIMULIA, Abaqus Analysis User's Guide, 2016)[104]. In this section, the necessary modules for the FEM analysis will be introduced and the different simulation cases will be presented for evaluation in Chapter 4.

5.1 Parts

The parts were imported directly using the SolidWorks STP files of the assembly. ABAQUS differentiates between the part and assembly data; therefore, the parts are imported separately with an already defined parametrisation for the assembly. In the parts module a section was created that is applied to both parts. This section property defines both the rack and pinion as homogeneous solid bodies.

5.2 Material

The material module defines the material properties for the parts. Steel is used as our material for both rack and pinion with following elastic properties and density:

- Density: 7850 $\frac{kg}{m^3}$
- Young's Modulus: 210 GPa
- Poisson's Ratio: 0.3

ABAQUS also allows users to define a material damping property to diminish the vibrations during the solving step. ABAQUS uses the Rayleigh Damping Coefficients to define damping properties of materials using a mass and stiffness dependent damping property (SIMULIA, Abaqus Analysis User's Guide, 2016)[105]. To calculate the Rayleigh Damping, the mass proportional coefficient α_R and stiffness proportional component β_R must be specified by identifying the natural frequencies ω_i and critical damping ζ_i of the system (SIMULIA, Abaqus Analysis User's Guide, 2016)[106]. This damping property is unnecessary when other types of damping are used in the dynamic analysis and therefore, it is excluded from this analysis section.

103 See 1.1.1 Introduction: General

104 See 1.3.1 Defining a model in Abaqus

105 See 26.1.1 Material Damping

106 See 26.1.1 Material Damping

5.3 Assembly

Assembly module is used to create and configure our system for the analysis. As the Assembly STP data is already imported, an interaction with the positioning of the rack and pinion is not necessary. A crucial step in this module is to create a proper coordinate system for the pinion. The Assembly comes with a global inertial coordinate system. In this system, the x-axis is perpendicular to the rack axis along the length and follows the transverse tooth section, the y-axis is perpendicular to the top plane (surface plane) of the rack and z-axis is along the length of the rack. Although this global coordinate system (x_1, y_1, z_1) is very suitable for the rack, it poses difficulties defining movement, loads, and BC's for the pinion and therefore, a second (local) coordinate system needs to be defined specifically for the pinion. The second inertial datum axis CSCY-2 (x_2, y_2, z_2) in the middle of the pinion with the x_2 axis parallel to the pinion axis and with the condition $y_1 \times y_2 = 0$. **Figure 24** illustrates both coordinate systems in the assembly module.

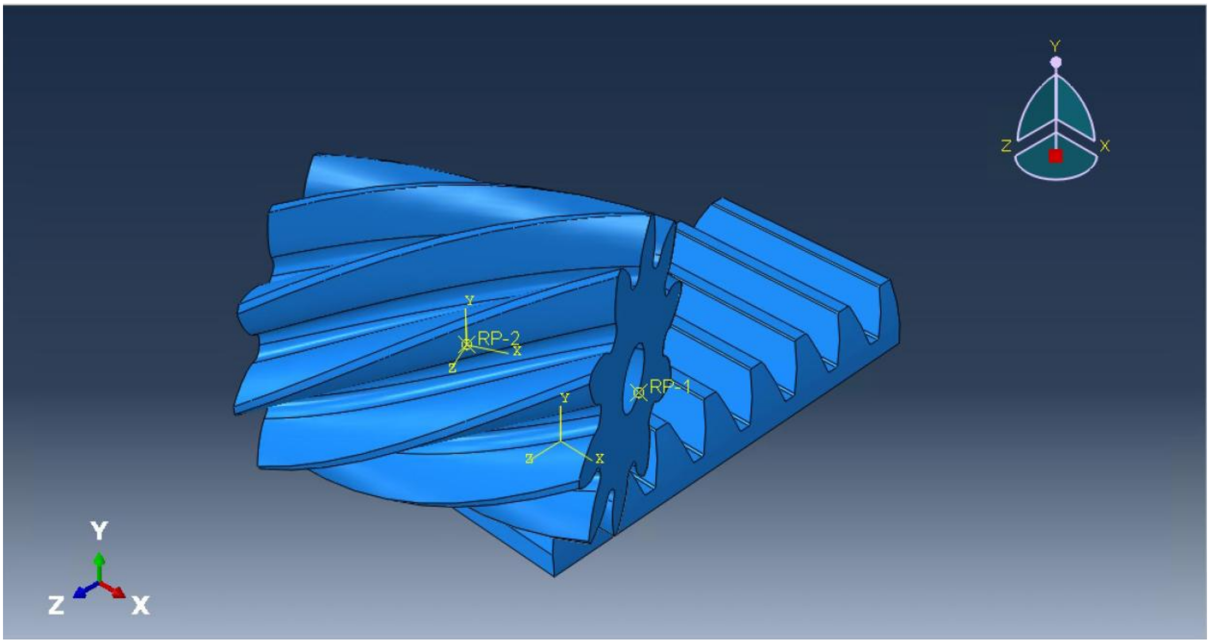

Figure 24: *Assembly of the part with the coordinate systems in ABAQUS*

5.4 Step

In this module, the type and properties of the analysis solver is defined. A dynamic implicit analysis is selected for all the simulation cases. An implicit analysis compared to an explicit analysis uses implicit operators and therefore, the operator matrix needs to be inverted (to solve the equations) and a set of nonlinear equations must be solved (SIMULIA, Abaqus Analysis User's Guide, 2016)[107]. An explicit analysis on the other hand, utilizes the central-difference method where the displacements and velocities are known quantities before each increment (SIMULIA, Abaqus Analysis User's Guide, 2016)[108]. Consequently, for our case, an implicit analysis is more suitable as a stiffness and contact analysis results in elastic and small deformations which require numerical stability and large time steps to solve, while explicit analysis limits the time steps. In the dynamic implicit analysis, a fixed incrementation with a

107 See 6.3.1 Dynamic analysis procedures: overview

108 See 6.3.1 Dynamic analysis procedures: overview

number of 2000 increments are used and it starts with the initial increment size of 0.0005 so that the results can be collected from the solver in uniform time intervals. To capture the deformations and the nonlinear kinematics more accurately, nonlinear geometric (NLGEOM) effects are included in the step, although at the cost of more computational requirements.

5.5 Interaction

The interaction module governs the connections between elements and parts, making it a crucial module for the analysis. In the interaction module relationships can be created between bodies with each other and with other impressed elements such as springs, dashpots and connector elements . In order to make the load module and interactions easier, the contact modelling is done using reference points. Reference points act as control points which are used to define the interactions and load modules that allows users to simplify their systems. For this purpose, two reference points have been created: RP_1 is on the bottom surface of the rack and RP_2 is in the middle of the pinion. A definition of the connection constraints is also needed for the reference points and target bodies so that their behaviours can be modelled. A coupling with all degrees of freedoms (DOF) locked is created between the reference points and their respective bodies that links reference points to the bodies and allows them to move and behave together. The equations (55) and (56) below illustrate the coupling vectors for the rack and the pinion. The first coupling constraint is applied to the bottom surface area of the rack and the second coupling constraint to the inner surface of the pinion. **Figures 25-26** show the coupling connections and the reference points.

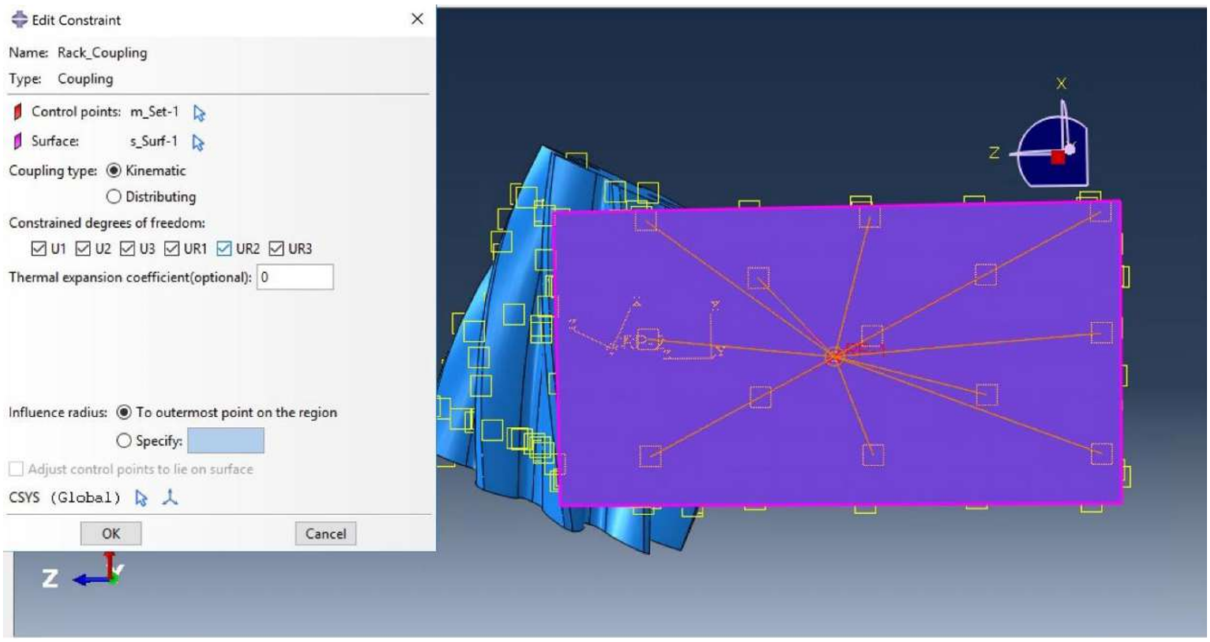

Figure 25: *Coupling constraint of the rack reference point and the rack bottom surface*

$$RP_{1,Coupling} = \begin{pmatrix} u_{1,1,c} \\ u_{2,1,c} \\ u_{3,1,c} \\ \varphi_{1,1,c} \\ \varphi_{2,1,c} \\ \varphi_{3,1,c} \end{pmatrix} \tag{55}$$

Figure 26: *Coupling constraint of the pinion reference point and the inner pinion surface*

$$RP_{2,Coupling} = \begin{pmatrix} u_{1,2,c} \\ u_{2,2,c} \\ u_{3,2,c} \\ \varphi_{1,2,c} \\ \varphi_{2,2,c} \\ \varphi_{3,2,c} \end{pmatrix} \tag{56}$$

The contact model was created using two different independent parts that find themselves in contact at the initial step. An initial clearing is introduced to overcome of overlapping nodes at the start of the simulation. The analysis starts with two of the pinion teeth in contact with the rack tooth flank. A surface-to-surface contact was chosen between the rack and pinion with finite sliding. In the finite sliding approach, the surfaces experience arbitrary separation, sliding and rotation (SIMULIA, Abaqus Analysis User's Guide, 2016)[109] and it accounts for the continuous change of nodes in the contact area. A surface-to-surface contact discretization allows the solver to consider the geometries of the surfaces of both contact bodies and therefore enables contact constraints to be spread over the geometry instead of being concentrated at single nodes as opposed to node to surface contact (SIMULIA, Abaqus Analysis User's Guide, 2016)[110]. Although a surface-to-surface contact cannot fully prevent large penetrations, these are greatly reduced making this type of contact the better alternative. ABAQUS requires a master and a slave surface to define the surface-to-surface contact. A slave surface should have these properties (SIMULIA, Abaqus Analysis User's Guide, 2016)[111]:

- Softer material compared to the master surface.
- Finer meshing.
- Less complex geometry.
- Less complex kinematics.

109 See 38.1.1 Contact formulations in Abaqus/Standard

110 See 38.1.1 Contact formulations in Abaqus/Standard

111 See 38.1.1 Contact formulations in Abaqus/Standard

Based on these requirements the rack was chosen as the slave surface and pinion was chosen as the master surface. This choice supports the motivation of this thesis, as the analysis of the contact phenomena on the rack is one of our primary objectives. **Figure 27** illustrates the selected master and slave surfaces. The surface smoothing setting is also activated for the contact to compensate for the irregularities that can exist due to curvature such as noncontinuous surface normals and contributes to the solver's ability to reach convergence (SIMULIA, Abaqus Analysis User's Guide, 2016)[112].

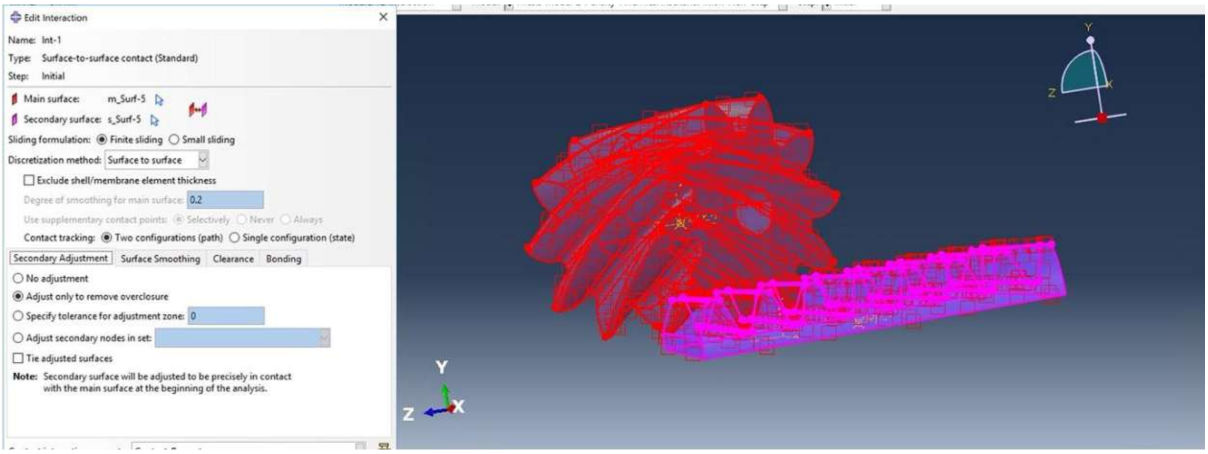

Figure 27: *Contact interaction of the master (red) and slave (purple) surfaces*

The definition of contact behaviours constitutes another critical step and plays a key role in influencing the results. An isotropic tangential behaviour without friction and a normal behaviour with hard contact that allows separation after contact is used for our analysis (For the second case, the "Penalty Method" for Normal Behaviour has been used for comparison). Ideally, a damping behaviour should also be added to the contact properties but contact damping is not available for implicit dynamic analysis and therefore not used in our analysis.

Interaction module also allows us to choose connector elements, which are useful to simulate various types of dependencies and movements. This connection is done by using an assembly-level wire feature and can be between two points in an assembly such as two parts or between a part and ground (SIMULIA, Abaqus/CAE User's Guide, 2016)[113]. Typical applications for the connector elements are for example, stopping mechanisms that restrict motion, internal friction like lateral forces or displacements, failure conditions where either the entire connection or a single relative motion can after break free after excessive BC's, and locking mechanism that locks the connection after necessary BC's are met (SIMULIA, Abaqus Analysis User's Guide, 2016). For the purpose of modelling a correct rack and pinion a connector element that could institute a bearing type restriction to the pinion is needed. Through this connector the forces, moments, and displacements of the pinion can be observed. A suitable option for this could be the Hinge Connector represented in **Figure 28** (SIMULIA, Abaqus Analysis User's Guide, 2016) (SIMULIA, Abaqus Analysis User's Guide, 2016)[114], that only allows one degree of freedom, which is rotation in the direction of the axis between two connector points and restricts all other degrees of freedoms.

112 See 38.1.1 Contact formulations in Abaqus/Standard

113 See 31.1.1 Understanding connectors

114 See 31.1.5 Connection-type library

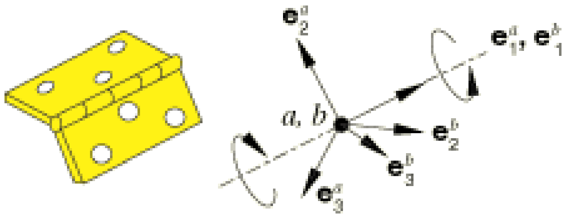

Figure 28: *Basic illustration of the hinge connector kinematics (SIMULIA, Abaqus Analysis User's Guide, 2016)*

The Hinge Connector has been connected to the reference point RP_2 and to the ground, while the coordinate system has been changed to the CSYS-2. Next step is to select the necessary Hinge Connector behaviours to model a bearing. The bearing BCs are:

- Translation:
  - Displacement, velocity, and acceleration in the pinion axis (x_2) need to be rigidly constrained.
  - Displacement, velocity, and acceleration in the first radial axis (y_2) need to be rigidly constrained.
  - Displacement, velocity, and acceleration in the second radial axis (z_2) need to rigidly constrained.

  The Hinge Connector satisfies all the above-mentioned BCs naturally.

- Rotation:
  - Displacement, velocity, and acceleration in the pinion axis (x_2) need to be free but constrained with damping to avoid oscillations after contact and to simulate a reaction moment against rotation.
  - Displacement, velocity, and acceleration in the first radial axis (y_2) need to be rigidly constrained
  - Displacement, velocity, and acceleration in the second radial axis (z_2) need to rigidly constrained.

  The Hinge Connector satisfies the second and third BC's naturally and a damping behaviour is added in the axis direction to create a reaction moment in the direction of axial rotation.

In order to match these requirements, ABAQUS defines elastic stiffness (elastic behaviour) and a damping behaviour is defined by the user to the Hinge Connector. C_R represents the damping matrix $\left(\frac{g}{s}\right)$ for rotation. A Hinge Connector behaves in such a way that it restricts the degrees of freedom using infinite stiffness values in the restricted directions. The damping matrix (57) is represented below. The through Hinge Connector exerted moment is calculated using the equation (58).

$$C_R = \begin{pmatrix} C_{R,11} & C_{R,12} & C_{R,13} \\ C_{R,21} & C_{R,22} & C_{R,23} \\ C_{R,31} & C_{R,32} & C_{R,33} \end{pmatrix} = \begin{pmatrix} 10000 & 0 & 0 \\ 0 & 0 & 0 \\ 0 & 0 & 0 \end{pmatrix} \tag{57}$$

$$M_x = C_{11} * \omega_{1,2} \tag{58}$$

5.6 Load

The load module contains the BC's and mechanical loadings that are defined in the present problem. First, the BC's for the rack and the pinion in the initial step needs to be defined. Both the rack and the pinion need to be in an inertial state before the dynamic analysis begins and therefore, a Displacement/Velocity/Rotation BC to both components is defined, where all DOF are locked. An important point not to miss here is to choose the proper coordinate system for rack and pinion, where the global coordinate system is selected for the rack and the CSYS-2 coordinate system is selected to define the BC's of the pinion. The vectors $BC_{1,i}$ (59) and $BC_{2,i}$ (60) illustrate the BC's in the initial step (BC_1 for the rack and BC_2 for the pinion). As our goal is to understand the contact occurrence on the rack teeth flanks and the reaction forces/moments on the pinion, a rack driven system that rotates the pinion is preferred. In this system, we can define a displacement and a velocity to the rack, which eventually rotates the pinion. During Step-1 of the analysis, the reduced rack model moves 40 mm per step time in Step-1 in the z_1 direction. It is also important to restrict all other DOF's to allow a pure translational movement in the z_1 axis. Accordingly, a positive velocity (distance per step time) in the z_1 direction is for the dynamic implicit analysis and the other DOF's are constrained. Although the pinion is only required to rotate along the x_2 axis, additional restrictions regarding other DOF's are not needed to analyse the forces and moments due to the use of the Hinge Connector. Accordingly, no BC's or loads are defined for the pinion during the dynamic analysis step. The vectors $BC_{1,step}$ (61) and $BC_{2,step}$ (62) define the displacement BC's in Step-1, while the vector $BC_{3,step}$ (63) illustrates the velocity BC of the rack in Step-1. The BC's introduced by the Hinge Connector are shown in vector $BC_{Hinge,step}$ (64).

$$BC_{1,i} = \begin{pmatrix} u_{1,1,i} \\ u_{2,1,i} \\ u_{3,1,i} \\ \varphi_{1,1,i} \\ \varphi_{2,1,i} \\ \varphi_{3,1,i} \end{pmatrix} = \begin{pmatrix} v_{1,1,i} \\ v_{2,1,i} \\ v_{3,1,i} \\ \omega_{1,1,i} \\ \omega_{2,1,i} \\ \omega_{3,1,i} \end{pmatrix} = \begin{pmatrix} a_{1,1,i} \\ a_{2,1,i} \\ a_{3,1,i} \\ \dot{\omega}_{1,1,i} \\ \dot{\omega}_{2,1,i} \\ \dot{\omega}_{3,1,i} \end{pmatrix} = \begin{pmatrix} 0 \\ 0 \\ 0 \\ 0 \\ 0 \\ 0 \end{pmatrix} \tag{59}$$

$$BC_{2,i} = \begin{pmatrix} x_{1,2,i} \\ y_{2,2,i} \\ z_{3,2,i} \\ \varphi_{1,2,i} \\ \varphi_{2,2,i} \\ \varphi_{3,2,i} \end{pmatrix} = \begin{pmatrix} v_{1,2,i} \\ v_{2,2,i} \\ v_{3,2,i} \\ \omega_{1,2,i} \\ \omega_{2,2,i} \\ \omega_{3,2,i} \end{pmatrix} = \begin{pmatrix} a_{1,2,i} \\ a_{2,2,i} \\ a_{3,2,i} \\ \dot{\omega}_{1,2,i} \\ \dot{\omega}_{2,2,i} \\ \dot{\omega}_{3,2,i} \end{pmatrix} = \begin{pmatrix} 0 \\ 0 \\ 0 \\ 0 \\ 0 \\ 0 \end{pmatrix} \tag{60}$$

$$BC_{1,step} = \begin{pmatrix} x_{1,2,step} \\ y_{2,2,step} \\ z_{3,2,step} \\ \varphi_{1,2,step} \\ \varphi_{2,2,step} \\ \varphi_{3,2,step} \end{pmatrix} = \begin{pmatrix} v_{1,2,step} \\ v_{2,2,step} \\ v_{3,2,step} \\ \omega_{1,2,step} \\ \omega_{2,2,step} \\ \omega_{3,2,step} \end{pmatrix} = \begin{pmatrix} a_{1,2,step} \\ a_{2,2,step} \\ a_{3,2,step} \\ \dot{\omega}_{1,2,step} \\ \dot{\omega}_{2,2,step} \\ \dot{\omega}_{3,2,step} \end{pmatrix} = \begin{pmatrix} Free \\ Free \\ Free \\ Free \\ Free \\ Free \end{pmatrix} \tag{61}$$

$$BC_{2,step} = \begin{pmatrix} u_{1,1,step} \\ u_{2,1,step} \\ u_{3,1,step} \\ \varphi_{1,1,step} \\ \varphi_{2,1,step} \\ \varphi_{3,1,step} \end{pmatrix} = \begin{pmatrix} 0 \\ 0 \\ Free \\ 0 \\ 0 \\ 0 \end{pmatrix} \tag{62}$$

$$BC_{3,step} = \begin{pmatrix} v_{1,1,step} \\ v_{1,2,step} \\ v_{1,3,step} \\ \omega_{1,4,step} \\ \omega_{1,5,step} \\ \omega_{1,6,step} \end{pmatrix} = \begin{pmatrix} 0 \\ 0 \\ 40 \\ 0 \\ 0 \\ 0 \end{pmatrix} \frac{mm}{Step\ time} \tag{63}$$

$$BC_{Hinge,step} = \begin{pmatrix} x_{1,2,step} \\ y_{2,2,step} \\ z_{3,2,step} \\ \varphi_{1,2,step} \\ \varphi_{2,2,step} \\ \varphi_{3,2,step} \end{pmatrix} = \begin{pmatrix} v_{1,2,step} \\ v_{2,2,step} \\ v_{3,2,step} \\ \omega_{1,2,step} \\ \omega_{2,2,step} \\ \omega_{3,2,step} \end{pmatrix} = \begin{pmatrix} a_{1,2,step} \\ a_{2,2,step} \\ a_{3,2,step} \\ \dot{\omega}_{1,2,step} \\ \dot{\omega}_{2,2,step} \\ \dot{\omega}_{3,2,step} \end{pmatrix} = \begin{pmatrix} Kinematically\ constrained \\ Kinematically\ constrained \\ Kinematically\ constrained \\ Damping\ applied \\ Kinematically\ constrained \\ Kinematically\ constrained \end{pmatrix} \tag{64}$$

Figures 29-31 show the applied BC's for the rack and for the pinion in the initial situation and in the Step-1.

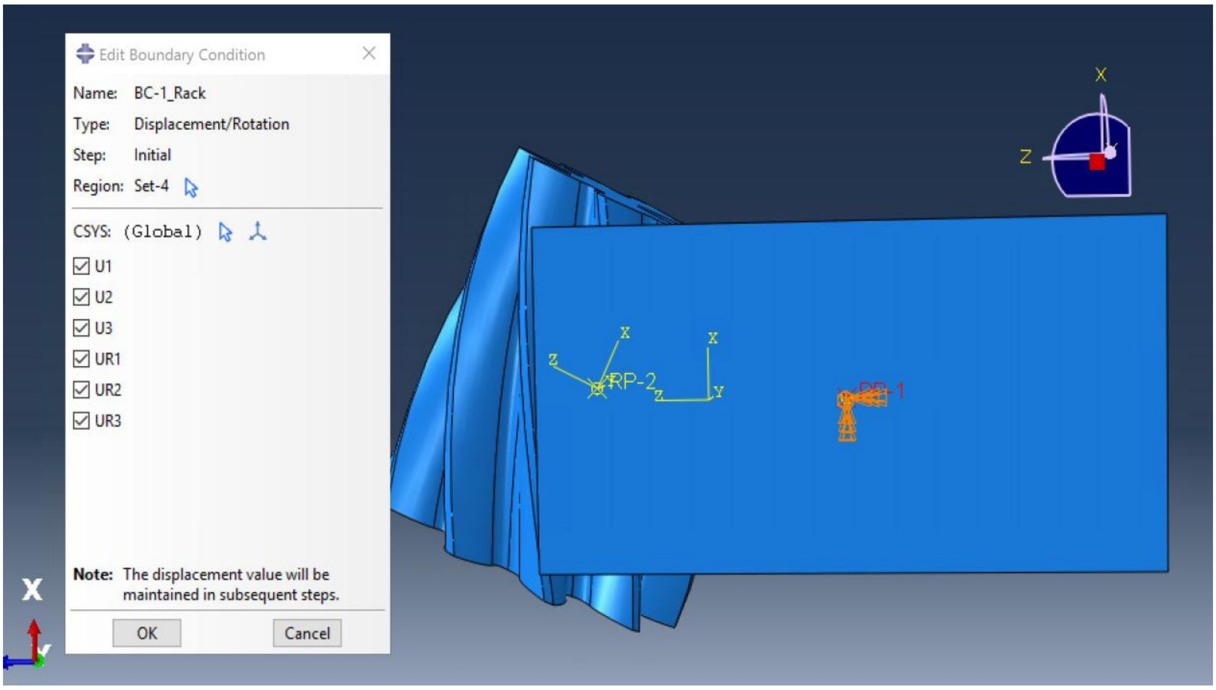

Figure 29: *Initial boundary conditions of the rack*

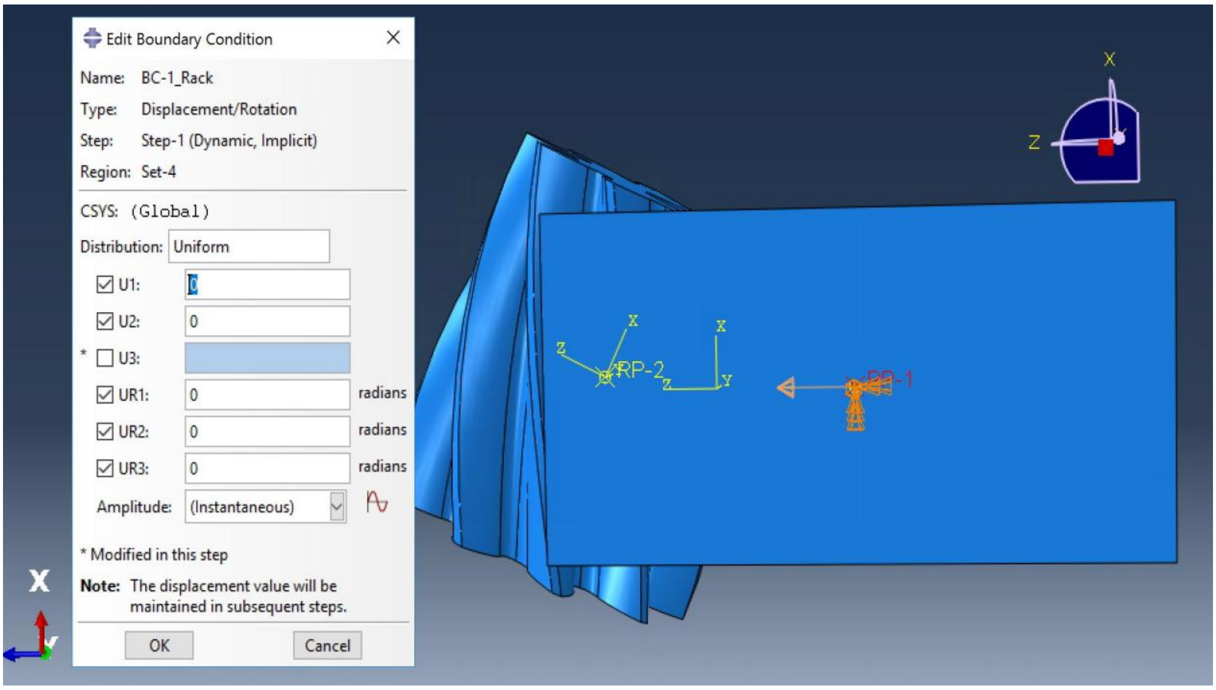

Figure 30: *Step-1 boundary conditions of the rack regarding displacement/rotation*

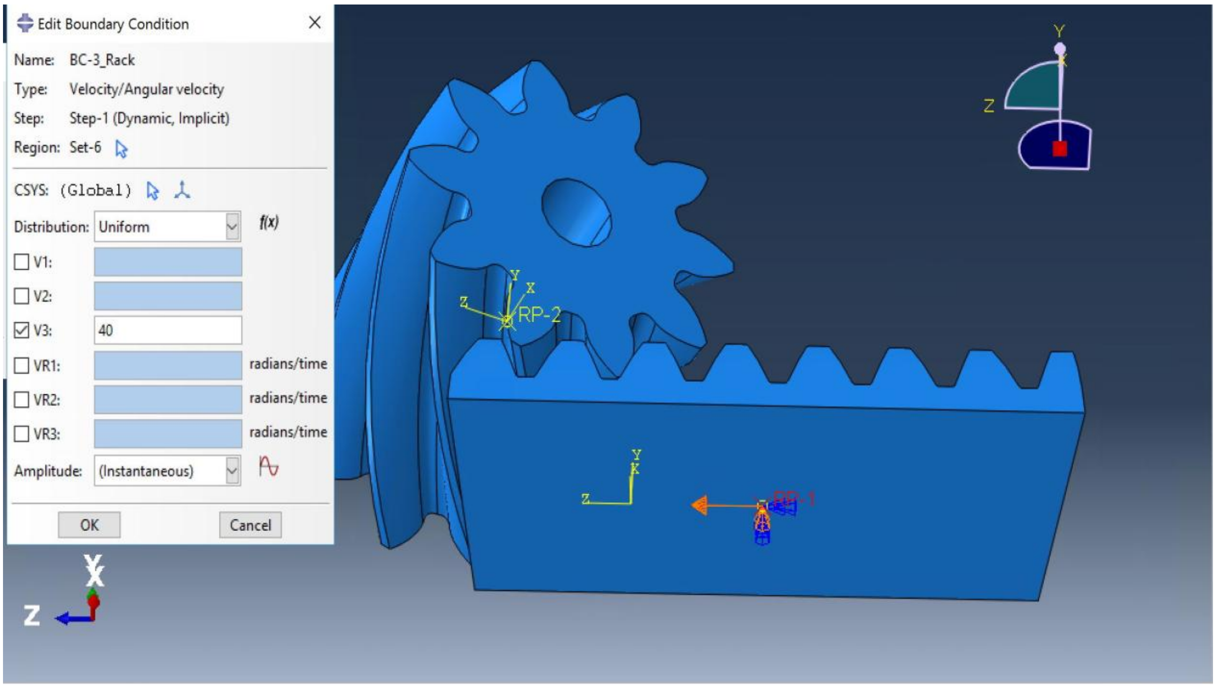

Figure 31: *Step-1 boundary conditions of the rack regarding velocity/angular velocity*

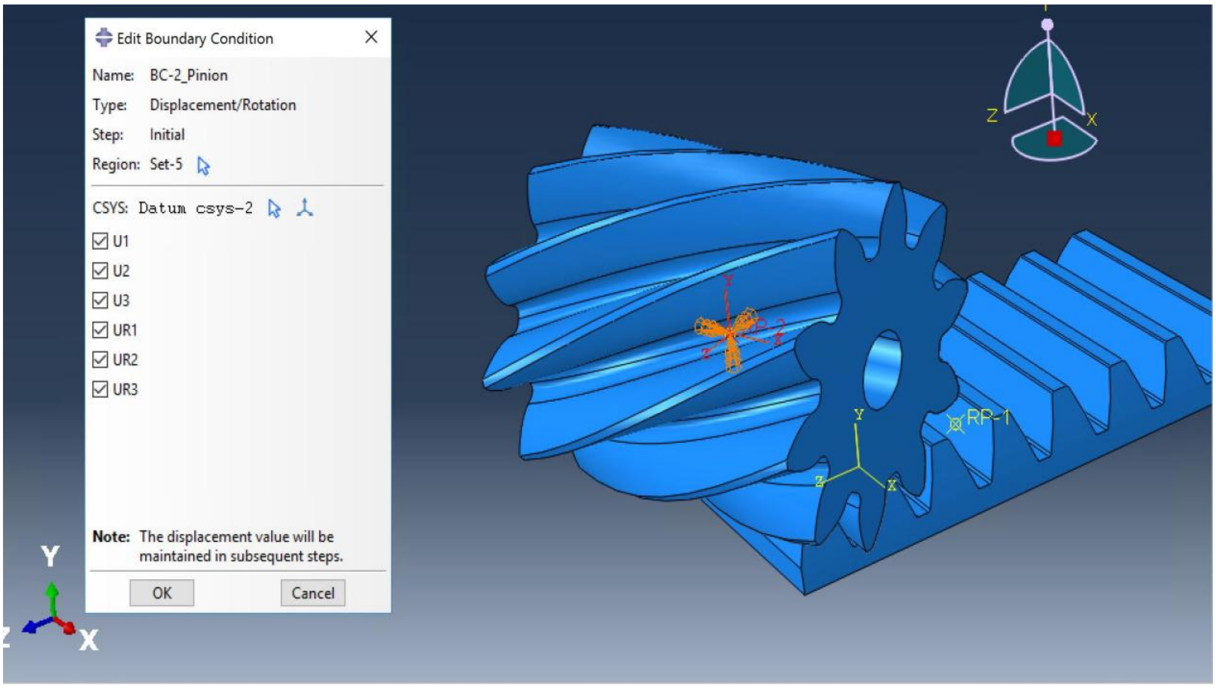

Figure 32: *Initial boundary condition of the pinion*

5.7 Field Output and History Output

The Field Output and History Output features deal with the results of the analysis and dictates what needs to be calculated during the simulation. It is of consequence to choose the right outputs in the right nodes or elements to receive the intended results and also optimize the computation time. The selected Field Outputs and domains are shown in **Table 3**:

Output Variables	Variable Code	Variable Description	Domain	Domain Description
Stress	S	Shows the existing stresses in regions where forces and moments act on	Whole Model	Both the rack and pinion stresses can be presented
Contact Pressure	CSTRESS	Shows the stresses and normal forces that exist due to contact	Whole Model	Both the rack and pinion stresses and normal forces can be presented
Translational Displacement	UT	Shows the translational displacement	Wire-2-Set-1 Set_Pinion_Coupling Set_Rack_Coupling	The displacements are shown in the connector, in the RP-1 and in the RP-2
Rotational Displacement	UR	Shows the rotational displacement	Wire-2-Set-1 Set_Pinion_Coupling Set_Rack_Coupling	The displacements are shown in the connector, in the RP-1 and in the RP-2
Translational Velocity	VT	Shows the translational velocities	Wire-2-Set-1 Set_Pinion_Coupling Set_Rack_Coupling	The velocities are shown in the connector, in the RP-1 and in the RP-2
Rotational Velocity	VR	Shows the rotational velocities	Wire-2-Set-1 Set_Pinion_Coupling Set_Rack_Coupling	The velocities are shown in the connector, in the RP-1 and in the RP-2
Reaction Forces	RF	Shows the reaction forces at supports	Wire-2-Set-1 Set_Pinion_Coupling Set_Rack_Coupling	The reaction forces are shown in the connector, in the RP-1 and in the RP-2

Reaction Moments	RM	Shows the reaction moments at supports	Wire-2-Set-1 Set_Pinion_Coupling Set_Rack_Coupling	The reaction moments are shown in the connector, in the RP-1 and in the RP-2
Total Forces	TF	Shows the total forces and moments	Wire-2-Set-1 Set_Pinion_Coupling Set_Rack_Coupling	The total forces and moments are shown in the connector, in the RP-1 and in the RP-2
Connector Total Forces	CTF	Shows the total forces occurred at the connector	Wire-2-Set-1 Set_Pinion_Coupling Set_Rack_Coupling	The total forces created by the connector are shown in the connector, in the RP-1 and in the RP-2
Connector Total Moments	CTM	Shows the total moments occurred at the connector	Wire-2-Set-1 Set_Pinion_Coupling Set_Rack_Coupling	The total moments created by the connector are shown in the connector, in the RP-1 and in the RP-2
Connector Relative Displacement	CU	Shows the relative translational displacement of the connector	Wire-2-Set-1 Set_Pinion_Coupling Set_Rack_Coupling	The total translational displacements created by the connector are shown in the connector, in the RP-1 and in the RP-2
Connector Relative Rotation	CUR	Shows the relative rotational dispalcement of the connector	Wire-2-Set-1 Set_Pinion_Coupling Set_Rack_Coupling	The total rotational displacements created by the connector are shown in the connector, in the RP-1 and in the RP-2

Table 3: *Field output history of the simulations*

5.8 Meshing

As mentioned in Chapter 1, the FEM uses geometry discretization into a finite number of elements that are connected to each other with nodes to analyse the system, thus making the mesh module one of the most important features that effects the accuracy of the results. Three important aspects need to be considered when strategizing for effective mesh generation (Okerke & Keates, 2018)[115]:

Simple Element Choice: Since the FEM solution is not an exact solution but an approximate one, the unnecessarily complex elements lead to higher inert solutions due to the higher assumptions connected to the complex elements (Okerke & Keates, 2018)[116]. Therefore, a wrong complex element will result in a worse outcome than a correct simple element.

Mesh Size Choice for Convergence: It is sometimes unclear to the user whether the mesh size used provides the most approximate solution or a convergent solution. A mesh sensitivity analysis is therefore necessary for the analysis in deciding the optimal mesh densities and helps

115 See page 176.

116 See page 176.

the user to start with coarser mesh that lightens the computing loads (Okerke & Keates, 2018)[117].

Appropriate Mesh Choice for Complex Geometries: Irregular and complex geometries must be taken into consideration in order to create continuous and structured meshes. This continuity of meshing ensures minimal variation of element parameters along the virtual domain axis loads (Okerke & Keates, 2018)[118].

The mesh process in ABAQUS consists of five main steps:

1) Seeding
2) Element Choice
3) Mesh Method
4) Mesh Generation
5) Mesh Verification

5.8.1 Seeding

The seeding module creates mesh nodes on the meshing geometry. The smaller seeding is, the more mesh nodes will be generated and consequently the final mesh will be finer. ABAQUS allows users to create uniform and biased seedings where the bias seeding allows concentrated seed density near a region or node. **Figure 33** shows the difference between uniform and biased seeding where the white elements represent a uniform seed distribution and pink ones show biased distribution near the top left corner (SIMULIA, Abaqus/CAE User's Guide, 2016)[119].

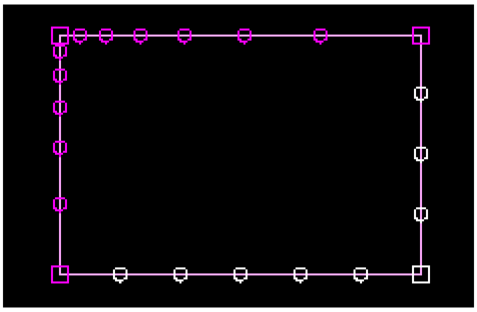

Figure 33: *Seeding variants in ABAQUS (SIMULIA, Abaqus Analysis User's Guide, 2016)*

ABAQUS also allows the user to choose different seeding densities for different surfaces of the same element and therefore allows a heterogenous seeding that is especially useful for contact problems. In order to analyse the contact regions more precisely without increasing the computing load, the contact regions of the rack and pinion are seeded denser than non-contact regions.

117 See page 176.

118 See page 176.

119 See 17.4.1 Understanding seeding

5.8.2 Element Choice

An understanding of the mesh elements is therefore a necessity for rigorous results. ABAQUS offers us various mesh elements (SIMULIA, Abaqus/CAE User's Guide, 2016)[120] that are described in **Table 4**:

Dimension	Element Shape	Element Description
One-Dimensional	Lines	
Two-Dimensional	Triangles	
	Quadrilaterals	
Three-Dimensional	Tetrahedra	
	Triangular prisms (Wedges)	
	Hexahedra	

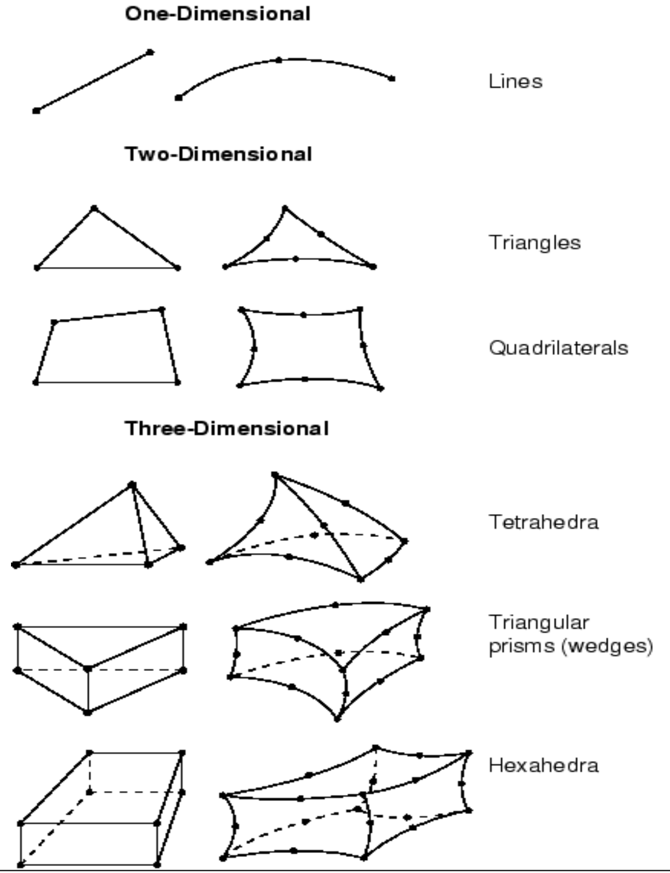

Table 4: *Mesh element types in ABAQUS (SIMULIA, Abaqus Analysis User's Guide, 2016)*

The selection of the element type is highly dependent on the geometry and the intended outcome of the FEM. For example, a thin structure (shell structure) can be discretised using two-dimensional elements as the stresses are dominated in the in-plane region and compression along the normal can be neglected, but objects that experience a three-dimensional stress need to be meshed using three-dimensional mesh elements (Okerke & Keates, 2018)[121]. Hence, it is clear to use three-dimensional mesh elements for our analysis to consider three-dimensional stresses and stiffnesses. "*It is widely known that FEM solutions are more accurate if quadrilateral or hexahedral elements shapes are used to solve 2D or 3D problems respectively. However, meshing of complex geometries are easiest with triangular (for 2D problems) or tetrahedral elements (for 3D problems)*" (Okerke & Keates, 2018)[122]. In general, the more connection points a mesh element has, the more DOF's can be utilized and it provides more realistic results. A mixture of hexahedral and tetrahedral elements are therefore the befitting element types.

120 See 17.5.1 Understanding seeding

121 See page 171.

122 See page 18.

The rack geometry is relatively simple and has lots of straight surfaces such as the bottom surface, the teeth surfaces, and the tips. The only comparatively complex regions are the teeth roots which have tangential connections and are in circular shape. The hexahedral element choice can be used with this geometry properly and allows us to model the whole part with hexahedral elements.

The pinion geometry on the other hand, is more challenging to mesh, because of the involute geometry and the inclusion of the helix angle with the flank crowning and tip rounding modifications. The use of hexahedral elements is not reasonable, and thus the element type must be switched to the tetrahedral elements.

5.8.3 Meshing Method

ABAQUS offers four types of meshing methods, which are described in **Table 5**.

Meshing Method	Illustration	Description
Structured Meshing	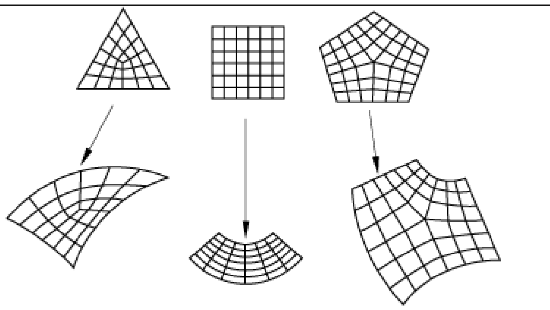	"*The structured meshing technique generates structured meshes using simple predefined mesh topologies. Abaqus/CAE transforms the mesh of a regularly shaped region, such as a square or a cube, onto the geometry of the region you want to mesh.*" (SIMULIA, Abaqus/CAE User's Guide, 2016)[123].
Swept Meshing	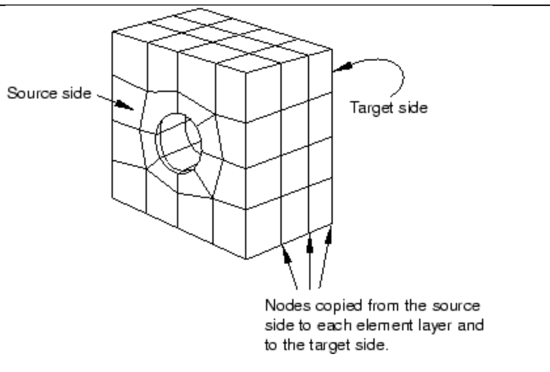	The swept meshing technique occurs in two steps, first being the mesh generation on one region – the source side and later the created meshes and nodes are copied until the other surface – target surface is reached and then the meshing follows the edge as a path between the target and source paths (SIMULIA, Abaqus/CAE User's Guide, 2016)[124].
Free Meshing	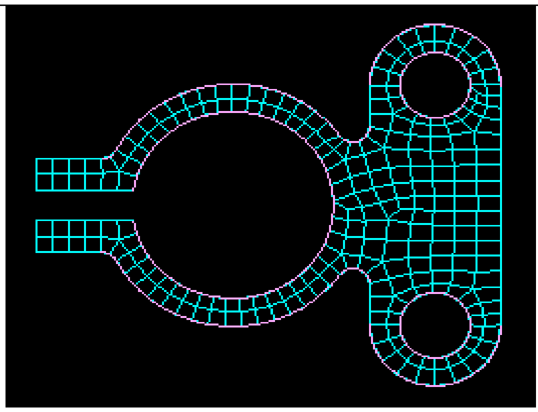	Free meshing allows more flexibility to the meshing method as there is no structure in the process of meshing and thus very suitable for complex geometries (SIMULIA, Abaqus/CAE User's Guide, 2016)[125].
Bottom-up Meshing	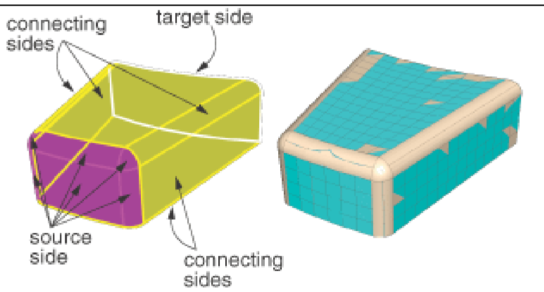	Bottom-up meshing is a manual method that is used to mesh hexahedral elements without relying on the geometry and is a good alternative when other methods fail (SIMULIA, Abaqus/CAE User's Guide, 2016)[126].

Table 5: *Meshing methods in ABAQUS (SIMULIA, Abaqus Analysis User's Guide, 2016)*

123 See 17.8.1 What is structured meshing?

124 See 17.9.1 What is swept meshing?

125 See 17.10.1 What is free meshing?

126 See 17.11.1 What is bottom-up meshing?

5.8.4 Mesh Generation

The Mesh Generation in ABAQUS is created by a "top-down" fashion where the mesh is created in harmony with the meshed regions and geometries and works down to the element and node positions (SIMULIA, Abaqus/CAE User's Guide, 2016)[127]. ABAQUS follows 2 steps for mesh generation (SIMULIA, Abaqus/CAE User's Guide, 2016)[128]:

1. *"Generate a mesh on each top-down region using the meshing technique currently assigned to that region. By default, Abaqus/CAE generates meshes with first-order line, quadrilateral, or hexahedral elements throughout."*
2. *"Merge the meshes of all regions into a single mesh. Typically, Abaqus/CAE merges the nodes along the common boundaries of neighbouring regions into a single set of nodes. However, in certain cases Abaqus/CAE creates tied surface interactions instead of merging these nodes; for example, along the common interface between hexahedral and tetrahedral meshes."*

Figure 34 (SIMULIA, Abaqus/CAE User's Guide, 2016)[129] represents the summarization of ABAQUS mesh generation for a part instance (SIMULIA, Abaqus/CAE User's Guide, 2016)[130]:

- *"A node is generated at each geometric vertex."*
- *"A connected set of element edges is generated along each geometric edge. "*
- *"A connected set of element faces is generated along each geometric face."*
- *"Nodes that are on the boundary of the mesh (including the midside nodes of second-order elements) are also on the boundary of the geometry."*
- *Midside nodes of internal second-order elements are centered between the end nodes of the element edges."*

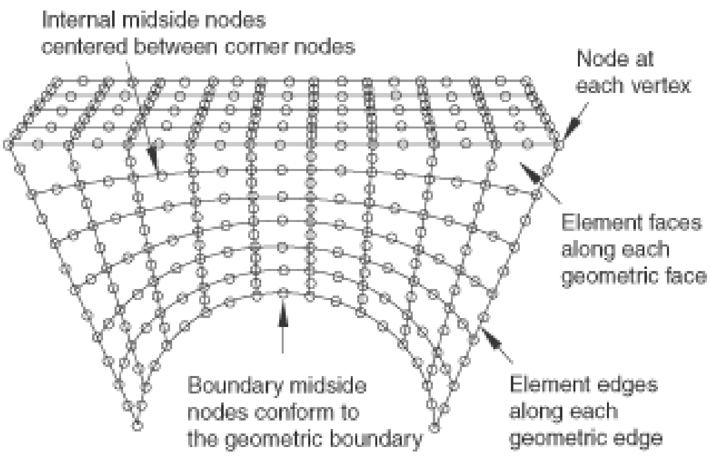

Figure 34: *ABAQUS mesh generation principle (SIMULIA, Abaqus Analysis User's Guide, 2016)*

127 See 17.7.1 Overview

128 See 17.7.1 Overview

129 See 17.7.1 Overview

130 See 17.7.1 Overview

5.8.5 Mesh Verification

Mesh Verification step is required to analyse how good, appropriate, and effective is the used meshing for a part instance. ABAQUS offers an indication of bad or distorted elements after the mesh generation that helps the user to make decisions at early stages. Additionally, ABAQUS also offers various mesh verification tools and fields that provides insights about the mesh quality and about the nodes (SIMULIA, Abaqus/CAE User's Guide, 2016)[131]. An important and widely relevant tool is the Shape Metrics tool of ABAQUS that creates a shape analysis based on the shape factor, small- and large face corner angles, and the aspect ratio (SIMULIA, Abaqus/CAE User's Guide, 2016)[132]. Initially, the program is arranged to highlight elements and shapes based on the criteria that is shown in **Table 6** (SIMULIA, Abaqus/CAE User's Guide, 2016)[133].

Selection Criteria	Quadrilateral	Triangle	Hexahedra	Tetrahedra	Wedge
Shape factor	N/A	0.01	N/A	0.0001	N/A
Smaller face corner angle	10	5	10	5	10
Larger face corner angle	160	170	160	170	160
Aspect ratio	10	10	10	10	10

Table 6: *Mesh verification standards in ABAQUS (SIMULIA, Abaqus Analysis User's Guide, 2016)*

Shape Factor: Shape Factor describes the ratio of the element area/volume to the optimal element area/volume and ranges from 0 to 1 with 1 being the optimal element shape (SIMULIA, Abaqus/CAE User's Guide, 2016)[134].

Small Face Corner Angle: *"Abaqus/CAE highlights elements containing faces where two edges meet at an angle smaller than a specified angle."* (SIMULIA, Abaqus/CAE User's Guide, 2016)

Large Face Corner Angle: *"Abaqus/CAE highlights elements containing faces where two edges meet at an angle larger than a specified angle."* (SIMULIA, Abaqus/CAE User's Guide, 2016)[135]
Aspect Ratio: *"Abaqus/CAE highlights elements with an aspect ratio larger than a specified value. The aspect ratio is the ratio between the longest and shortest edge of an element."* (SIMULIA, Abaqus/CAE User's Guide, 2016)[136]

Figures 35-40 illustrate the meshing obtained in the present study for different cases.

131 See 17.6.1 Verifying your mesh
132 See 17.6.1 Verifying your mesh
133 See 17.6.1 Verifying your mesh
134 See 17.6.1 Verifying your mesh
135 See 17.6.1 Verifying your mesh
136 See 17.6.1 Verifying your mesh

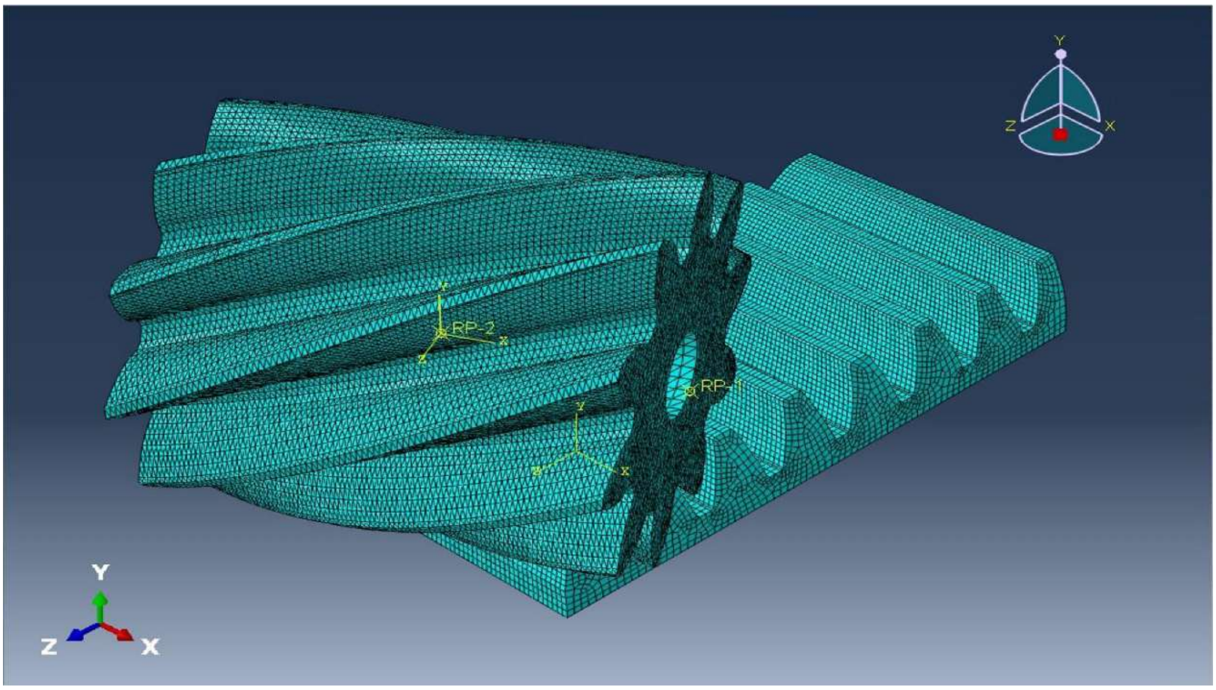

Figure 35: *Mesh of the rack and pinion system in Job-1 and Job-2 (coarse meshing)*

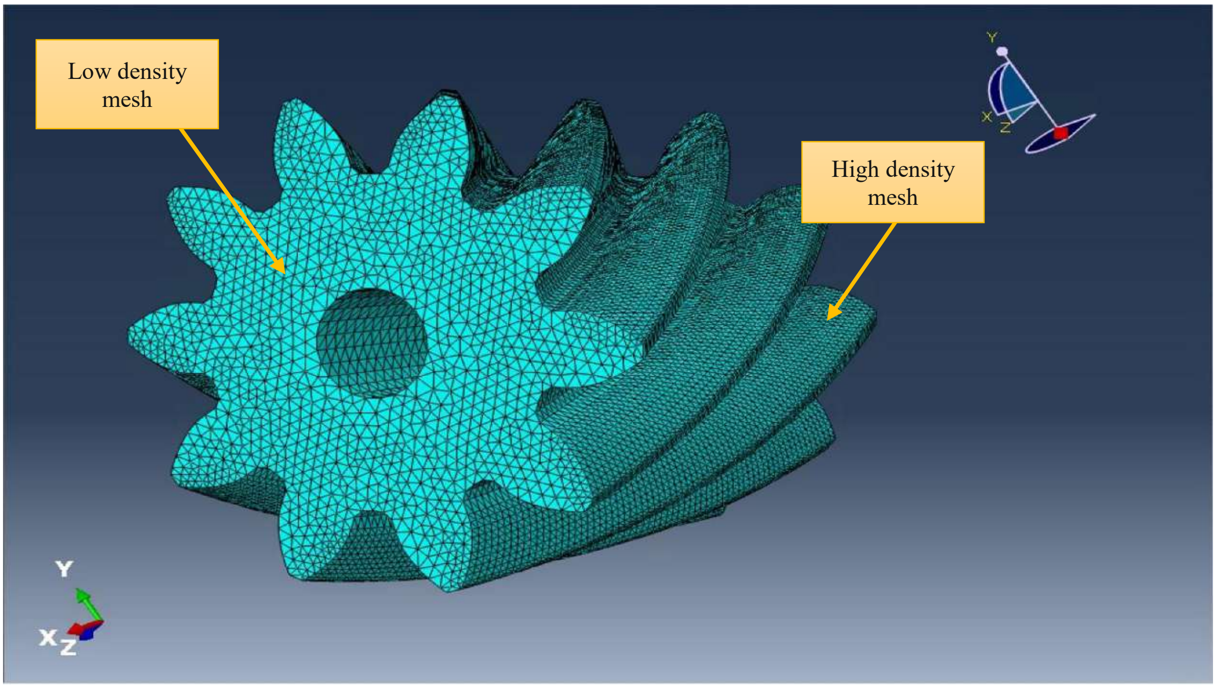

Figure 36: *Mesh of the pinion in Job-1 and Job-2 (coarse meshing)*

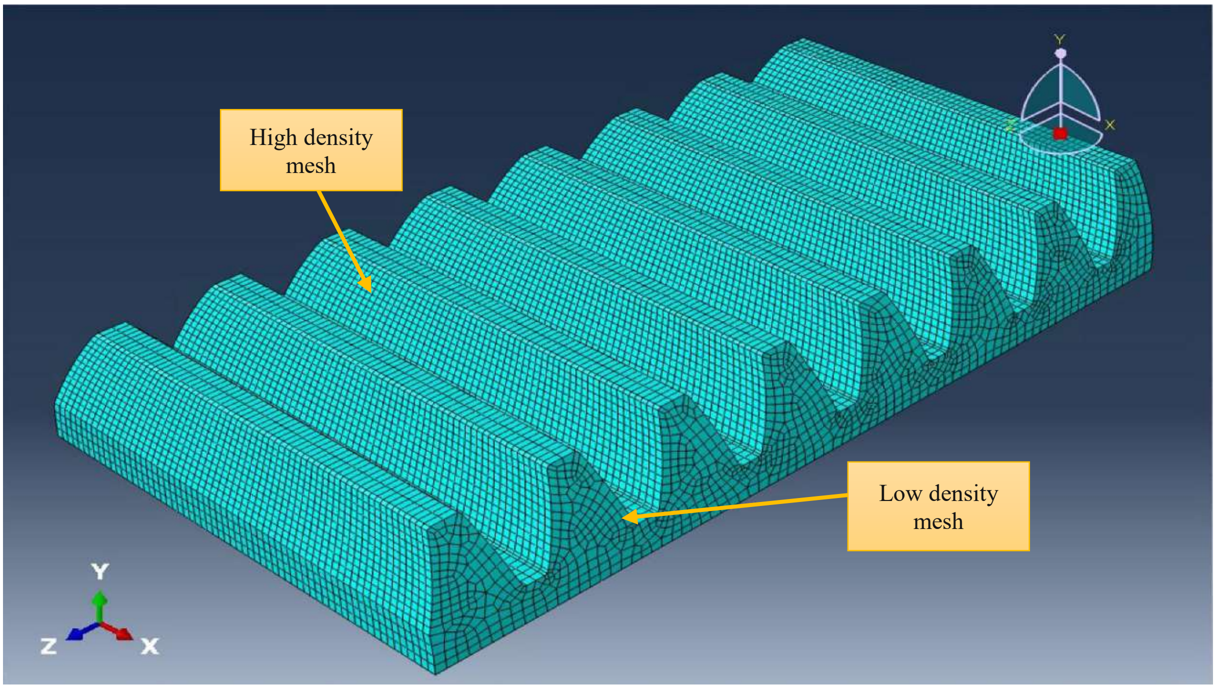

Figure 37: *Mesh of the rack in Job-1 and Job-2 (coarse meshing)*

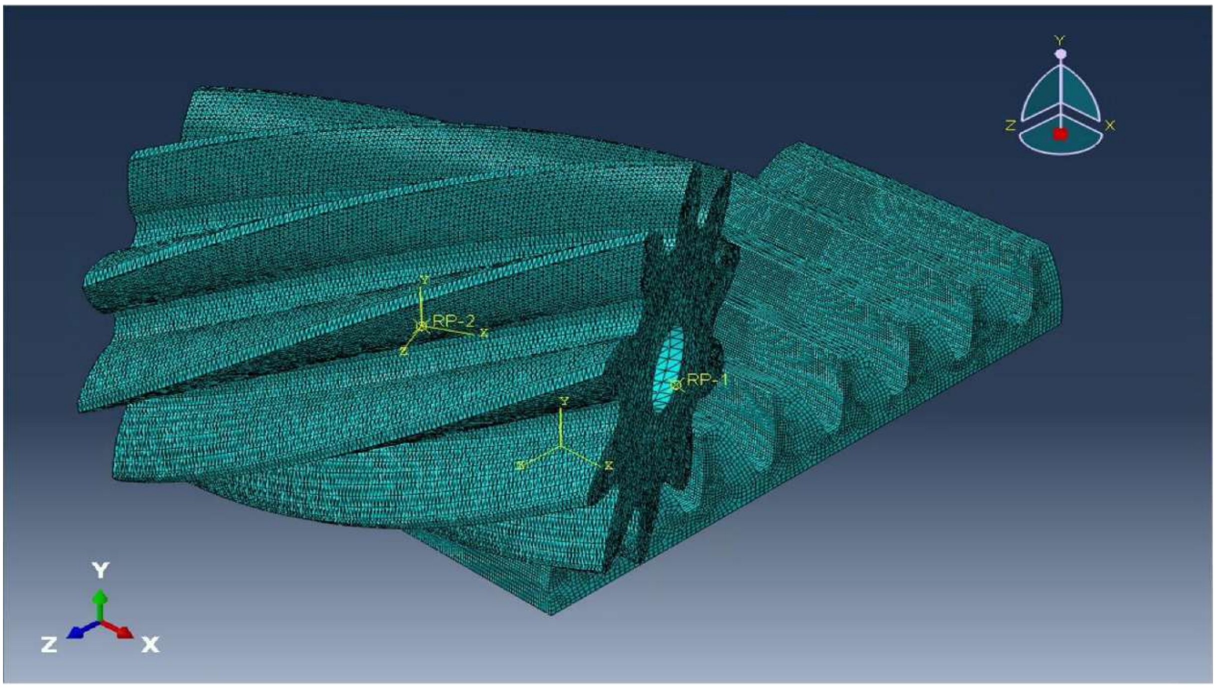

Figure 38: *Mesh of the rack and pinion system in Job-3 (fine meshing)*

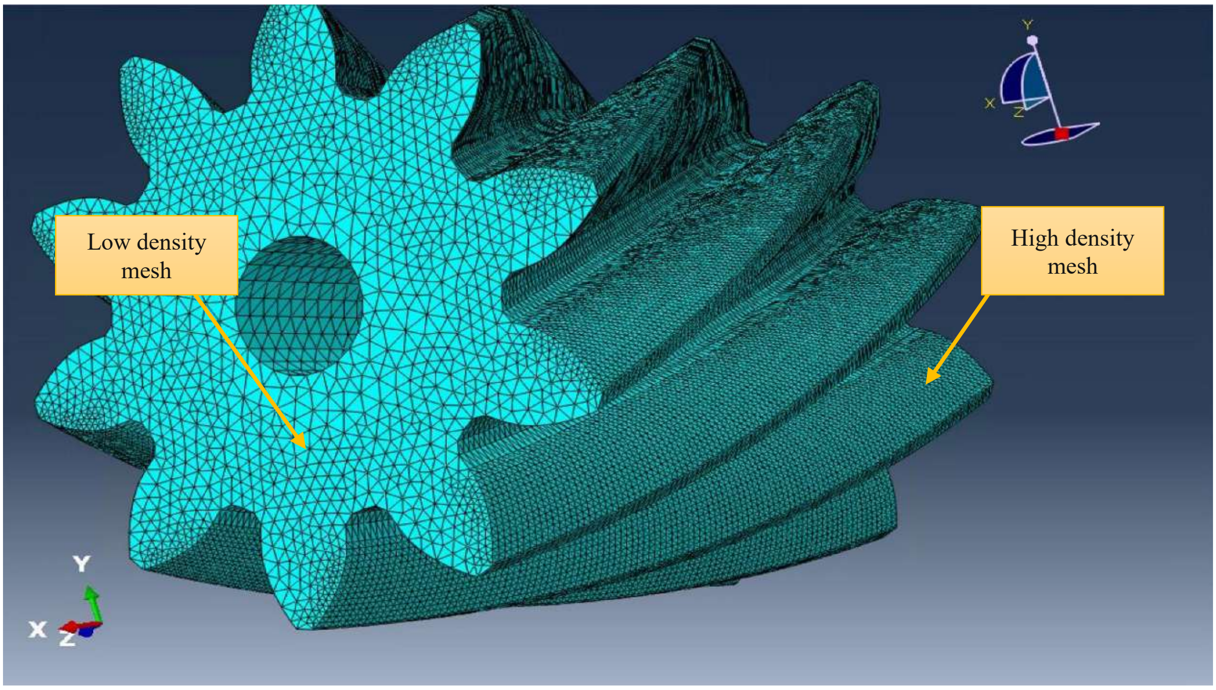

***Figure 39:** Mesh of the pinion in Job-3 (fine meshing)*

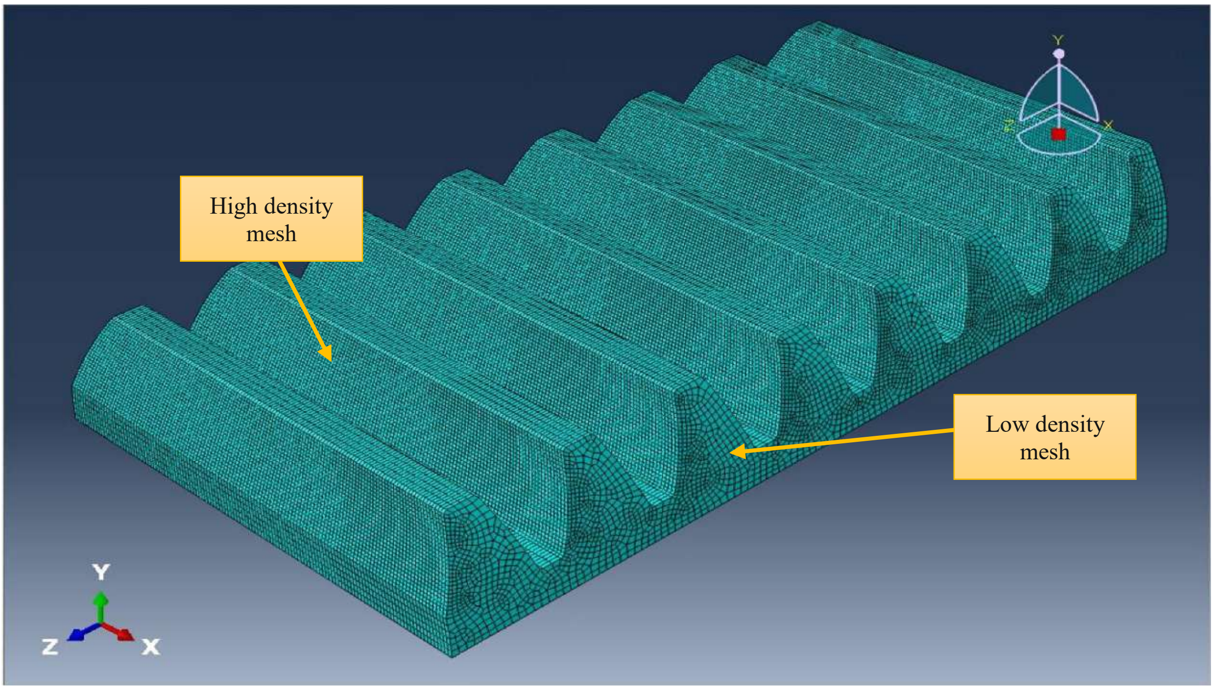

***Figure 40:** Mesh of the rack in Job-3 (fine meshing)*

5.9 Job

Different simulation cases (referred to as "Job" in this study) are then created based on the FEM model developed in ABAQUS.

Job	Contact	Rack Meshing	Pinion Meshing
Job-1	• Normal Contact: Hard Contact & Default Enforcement • Tangential Contact: Frictionless	• Seed size in Part: 0.6 • Number of Seeds in Contact Zones: 0.4 • Element Type in Part: Hex • Element Type in Contact Zones: Hex • Mesh Method in Part: Sweep • Mesh Method in Contact Zones: Sweep • Geometric Order: Linear • Shape Factor: N/A • Small Face Corner Angle: 30 • Large Face Corner Angle: 145 • Aspect Ratio: < 4	• Number of Seeds in Part: 0.8 • Number of Seeds in Contact Zones: 0.4 • Element Type in Part: Tet • Element Type in Contact Zones: Tet • Mesh Method in Part: Free • Mesh Method in Contact Zones: Free • Geometric Order: Linear • Shape Factor: < 0.1 • Small Face Corner Angle: 10 • Large Face Corner Angle: 135 • Aspect Ratio: < 5
Job-2	• Normal Contact: Hard Contact & Penalty Method • Tangential Contact: Frictionless	• Seed size in Part: 0.6 • Number of Seeds in Contact Zones: 0.4 • Element Type in Part: Hex • Element Type in Contact Zones: Hex • Mesh Method in Part: Sweep • Mesh Method in Contact Zones: Sweep • Geometric Order: Linear • Shape Factor: N/A • Small Face Corner Angle: 30 • Large Face Corner Angle: 145 • Aspect Ratio: < 4	• Number of Seeds in Part: 0.8 • Number of Seeds in Contact Zones: 0.4 • Element Type in Part: Tet • Element Type in Contact Zones: Tet • Mesh Method in Part: Free • Mesh Method in Contact Zones: Free • Geometric Order: Linear • Shape Factor: < 0.1 • Small Face Corner Angle: 10 • Large Face Corner Angle: 135 • Aspect Ratio: < 5
Job-3	• Normal Contact: Hard Contact & Default Enforcement • Tangential Contact: Frictionless	• Seed size in Part: 0.4 • Number of Seeds in Contact Zones: 0.2 • Element Type in Part: Hex • Element Type in Contact Zones: Hex • Mesh Method in Part: Sweep • Mesh Method in Contact Zones: Sweep • Geometric Order: Linear • Shape Factor: N/A • Small Face Corner Angle: 40 • Large Face Corner Angle: 140 • Aspect Ratio: < 2.8	• Number of Seeds in Part: 0.8 • Number of Seeds in Contact Zones: 0.3 • Element Type in Part: Tet • Element Type in Contact Zones: Tet • Mesh Method in Part: Free • Mesh Method in Contact Zones: Free • Geometric Order: Linear • Shape Factor: < 0.1 • Small Face Corner Angle: 15 • Large Face Corner Angle: 130 • Aspect Ratio: < 3.5

Table 7: *Mesh properties for each job*

Chapter 4

6. Numerical Results

All of the numerical results regarding the moments, forces and relative pinion motion are obtained in the Pinion Coupling location RP_2. The part where the force distribution on the contact lines are drawn and analysed on the rack is excluded from Job-1 and Job-2, as the mesh size is not fine enough to make a valuable analysis, only the contact situation for three different frames will be shown. The contact lines and the force distribution on these lines for Job-3 are drawn for selected start and end points on the tooth flank. ABAQUS plotter then divides this path into 100 equal paces. In total there will be three different contact lines in each contact zone for three different frames. Zone 1 is described as the right side of the tooth flank, beginning from the bottom until the edge of the flank. Zone 2 is the contact zone in the middle of the tooth flank. Zone 3 is defined as the left side of the tooth that starts from the edge and ends in the tip of the tooth flank.

6.1 Job-1

For the first case, a hard contact (between the rack and pinion) with default enforcement in the normal direction and a frictionless tangential contact was selected. The rack has a mesh size of 0.6 and a mesh size of 0.4 in the contact zones (tooth flanks). The pinion was meshed with a size of 0.8 and 0.4 in the contact zones (tooth flanks) similar to the rack.

6.1.1 Moments, Forces and Relative Rotation

The reaction moments and forces emerge from the rack driven contact and through the Hinge Connector originating damping. The reaction moments in the x_2 axis can be calculated using the equation (58) and the reaction moments around the y_2 axis are reacting against the movement of the rack in the z_1 axis. The reaction moments on the z_2 axis on the other hand exists due to the rotation of the pinion due to the tangential contact. The reaction forces are more straightforward and orderly with the rack movement. These conditions apply to all cases.

For the first case, the change of the moments in each increment are illustrated in **Figure 41** (The values after increment 1800 0.9 step time will not be considered for the analysis as the rack length is not enough to ensure a proper contact after this increment and therefore the values are not reliable. Therefore, the steady falling moments around y_2 and steady rising moments around z_2 are evaluated.). The definition of the axes (x_2, y_2, z_2) were already provided in **Figure 24**. Here we can see that the reaction moments in the x_2 axis are relatively stable in the region of 40.000 Nmm which is compatible with the values that are being used in the FEM analysis. We can calculate the exerted moment through a damper as:

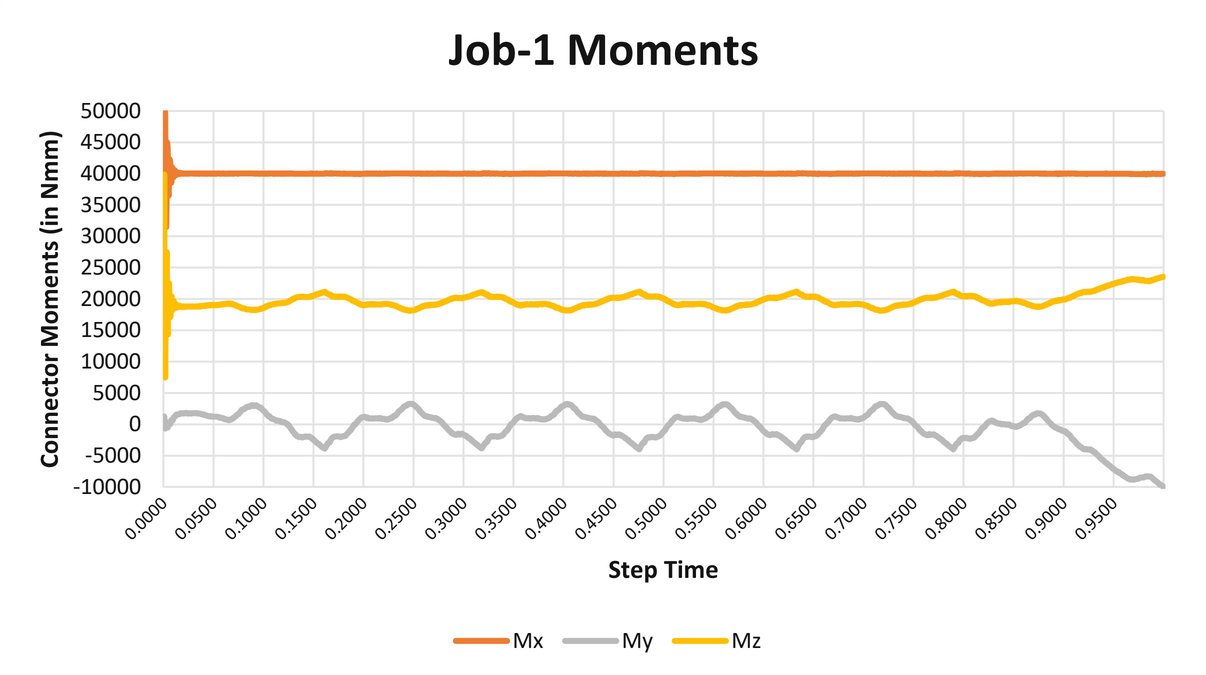

Figure 41: *Reaction moments at the pinion support for Job-1*

As the contact point of the pinion is moving 40 $mm/step$ an approximate moment calculation for the x_2 axis results in the region of 40.000 Nmm. A relatively stable moment through the damping was an expected result for us, although there are slight variations depending on the mesh contact. The reaction moments around the y_2 axis on the pinion on the other hand exhibit a periodic change depending on the contact positions of the pinion and the rack teeth, in approximately every 0.15 step time approximately starting from 0.110 step time. A positive high moment of 3272 Nmm at step time 0.2460 and a negative high moment of -3996 Nmm at step time at 0.4760 was calculated. The reaction moments around the z_2 axis on the pinion also exhibit a periodic behaviour, however with less amplitude than the moments around y_2. A positive high moment of 21171 Nmm at step time 0.6335 and a negative high moment of 18132 Nmm at step time at 0.2470 was calculated.

The maximum and minimum values for the moments are excluding the oscillations in the beginning of the simulation. The values are taken starting from 0.1005 time (Increment 201) and ends at 0.9 step time (Increment 1800).

The reaction forces occurring at the pinion support in Job-1 are represented in **Figure 42**. In comparison to the moment values, the forces are strictly linear with only minor changes during the simulation. This result is also an expected result, as the movement of the rack and the rotation of the pinion should not create strongly changing values for the forces in the CSYS-2 axis. As expected, the highest forces are observed in the z_2 axis, as this axis together with the portion of the x_2 axis are mainly responsible for the reaction against the rack displacement. The y_2 axis on the other hand is the least stressed axis as the forces in the normal orientation are not as prominent as the axial forces.

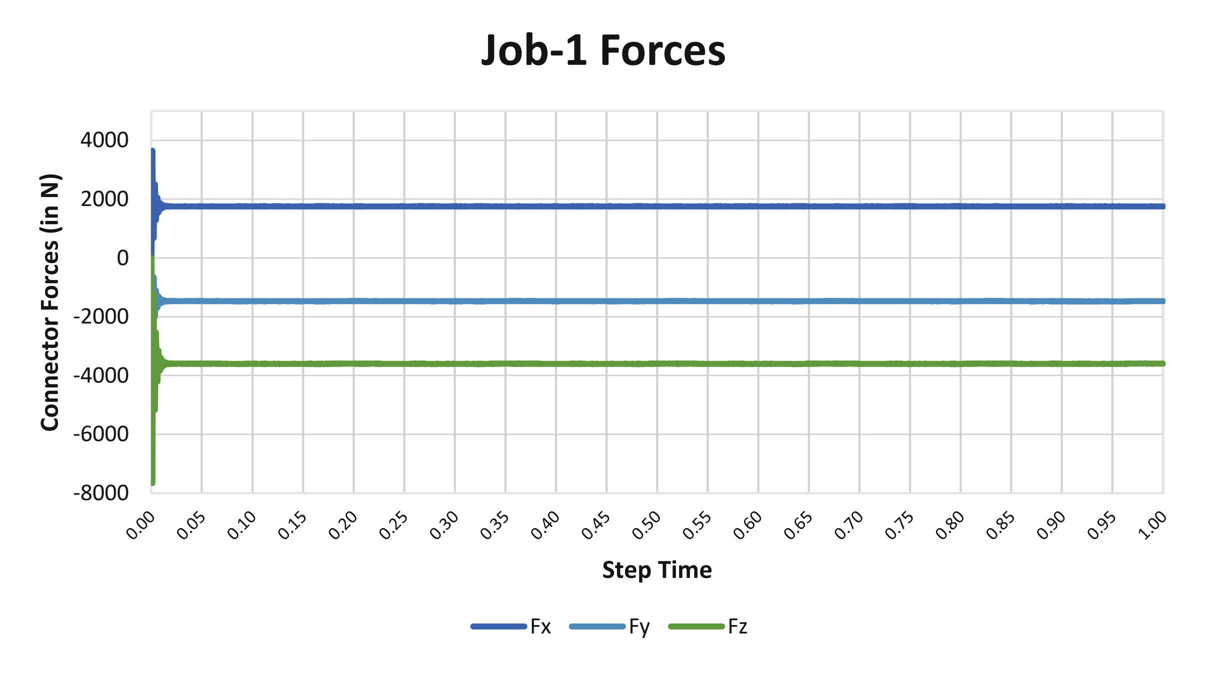

Figure 42: *Reaction forces at the pinion support for Job-1*

The pinion rotational velocity around the $-x_2$ axis seems constant with 4 $rotations/step$ and therefore, a linear change of the rotation angle through the step is observed and illustrated in **Figure 43**. This implicates that, the pinion is always stays in contact with the rack and the movement of the rack is the driver for the pinion movement.

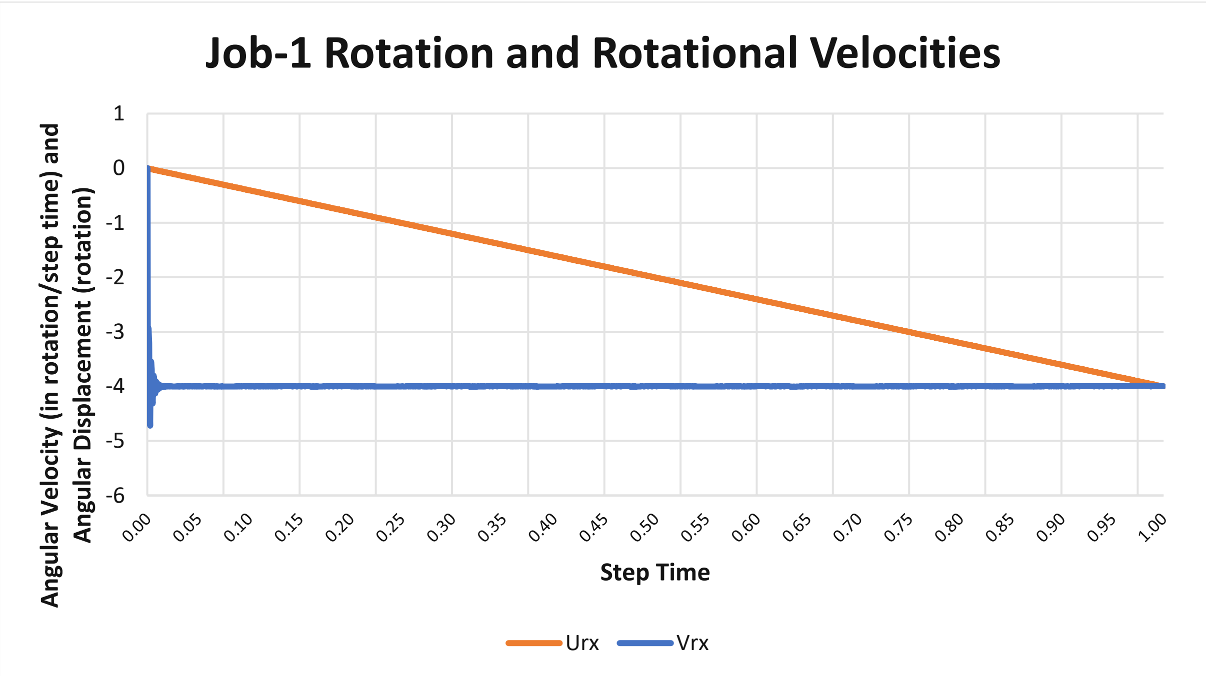

Figure 43: *Rotation angle and angular velocity of the pinion for Job-1*

6.1.2 Contact Forces

The contact status and contact forces for Job-1 for three different simulation frames are presented in **Figures 44-46**. A slipping contact is exclusively observed for this case, while contact forces are clustered in the regions of slipping contact.

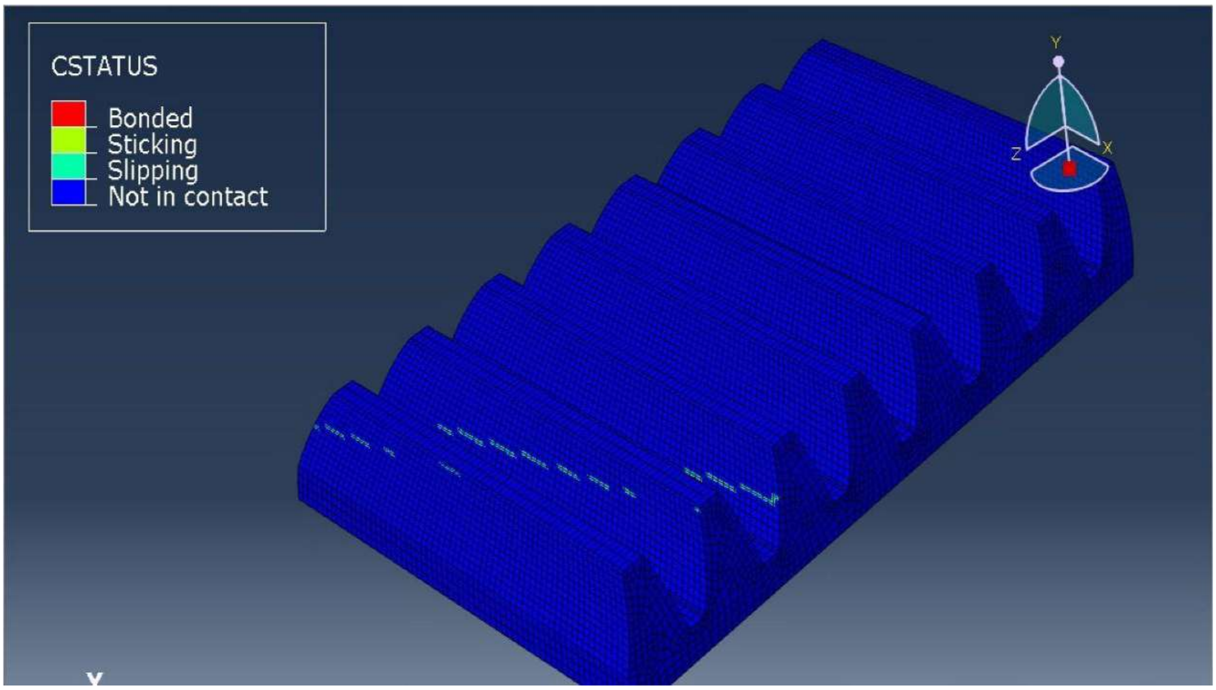

Figure 44: *Contact status on the rack for Job-1 in Frame 150*

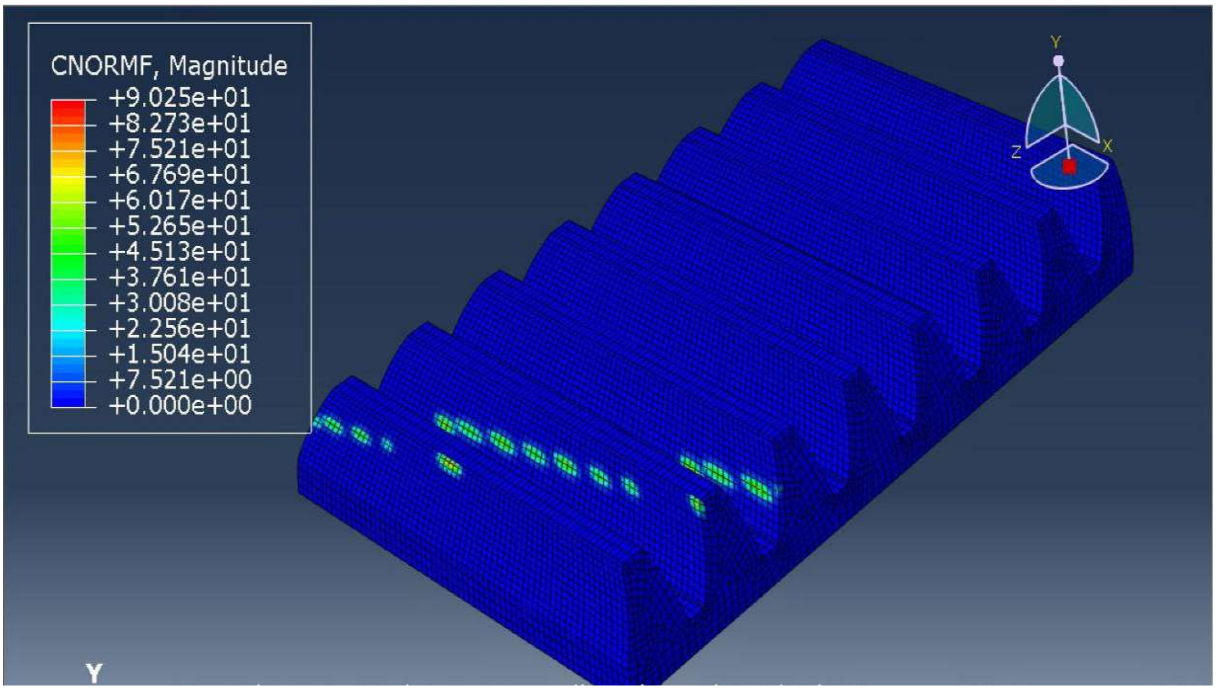

Figure 45: *Normal contact forces on the rack for Job-1 in Frame 150*

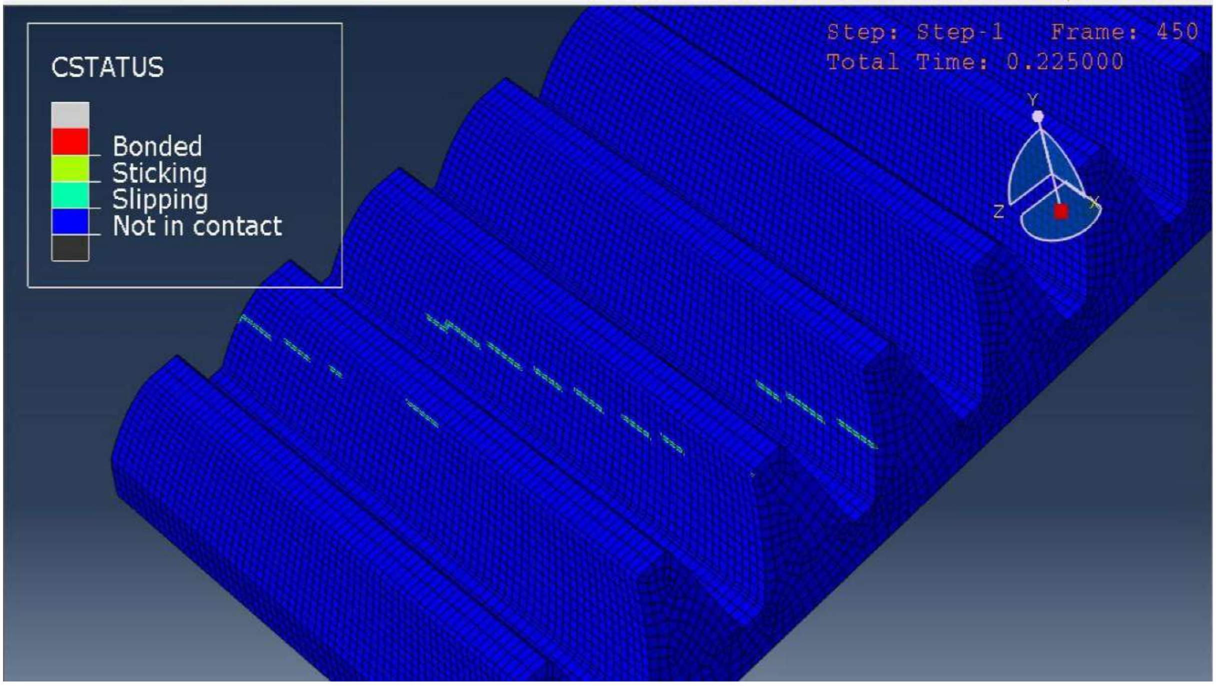

Figure 46: *Contact status on the rack for Job-1 in Frame 450*

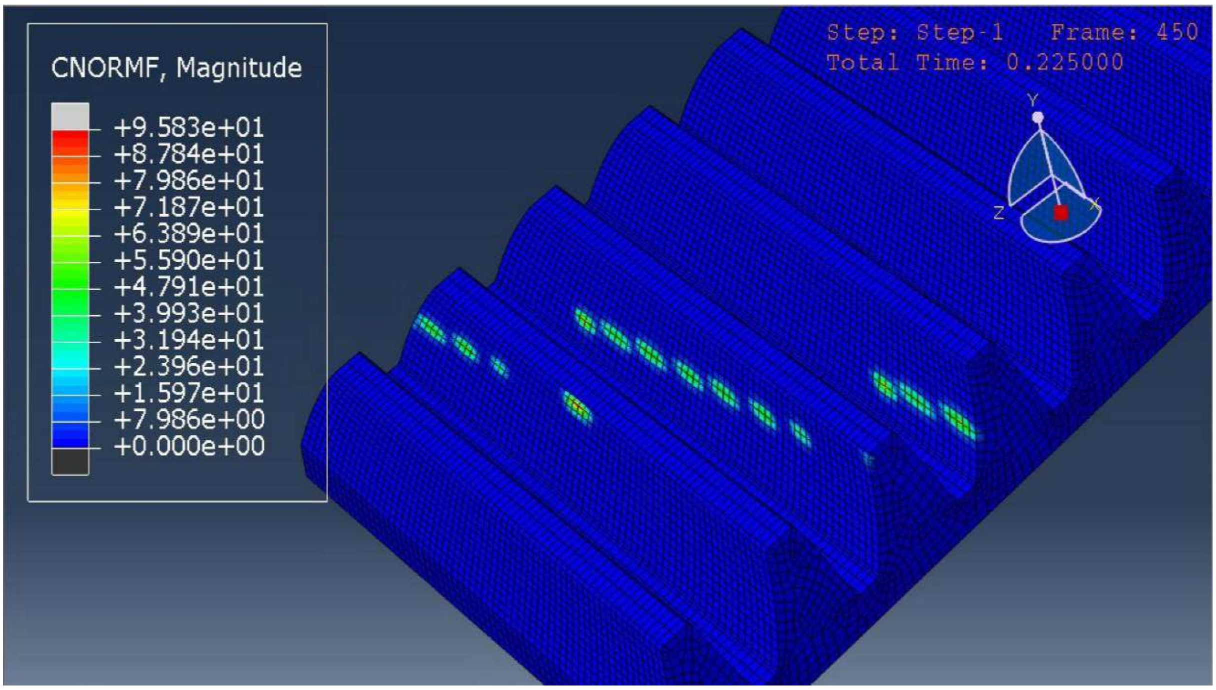

Figure 47: *Normal contact forces on the rack for Job-1 in Frame 450*

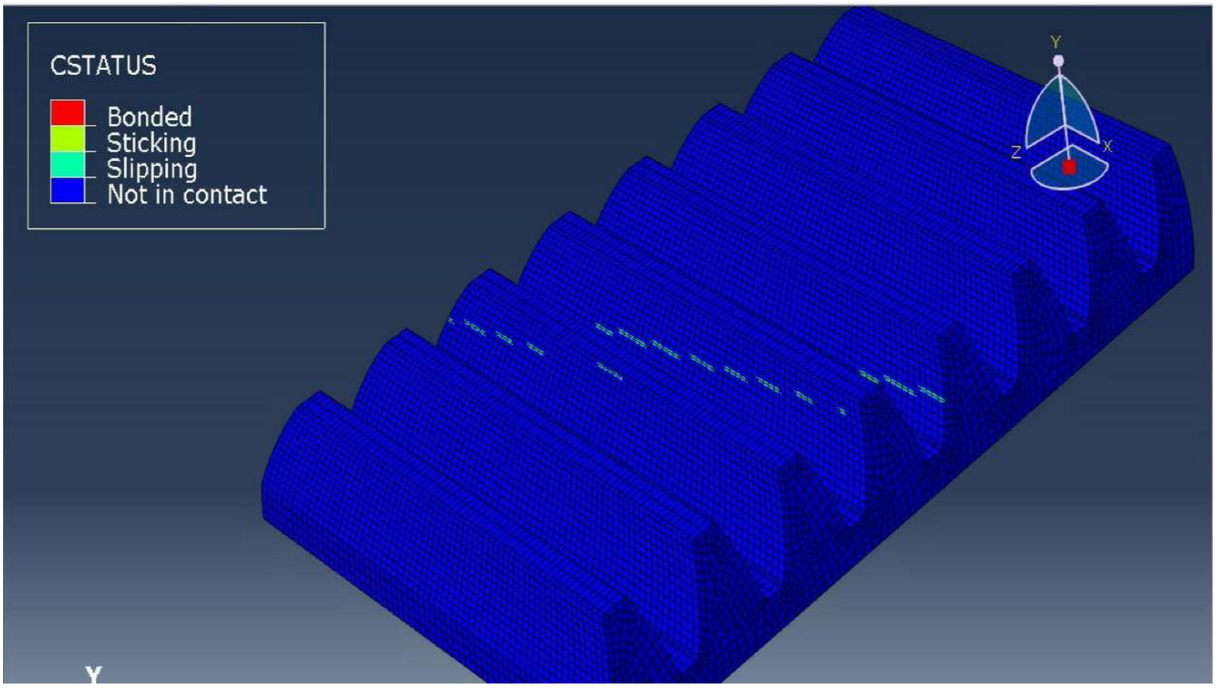

Figure 48: *Contact status on the rack for Job-1 in Frame 750*

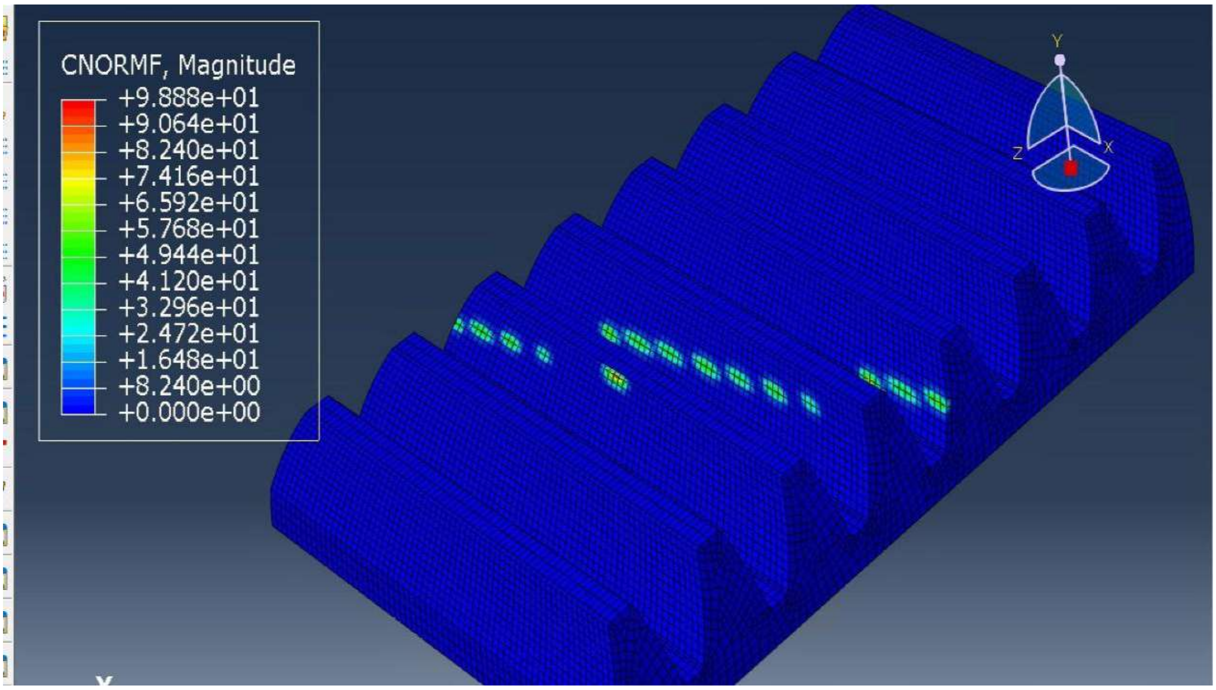

Figure 49: *Normal contact forces on the rack for Job-1 in Frame 750*

6.2 Job-2

For the second case, a hard contact with penalty method in the normal direction and a frictionless tangential contact is selected. The rack has a mesh size of 0.6 and a mesh size of 0.4 in the contact zones (tooth flanks). The pinion was meshed with a size of 0.8 and 0.4 in the contact zones (tooth flanks) similar to the rack.

6.2.1 Moments, Forces and Relative Rotation

The only difference between Job-1 and Job-2 is the used method of the normal contact behaviour. Job-1 uses a default method , while in Job-2 the influence of a “Penalty Method” was investigated. The reaction moments on the pinion in all x_2, y_2, z_2 axes are exactly the same as Job-1 and illustrated in **Figure 50**.

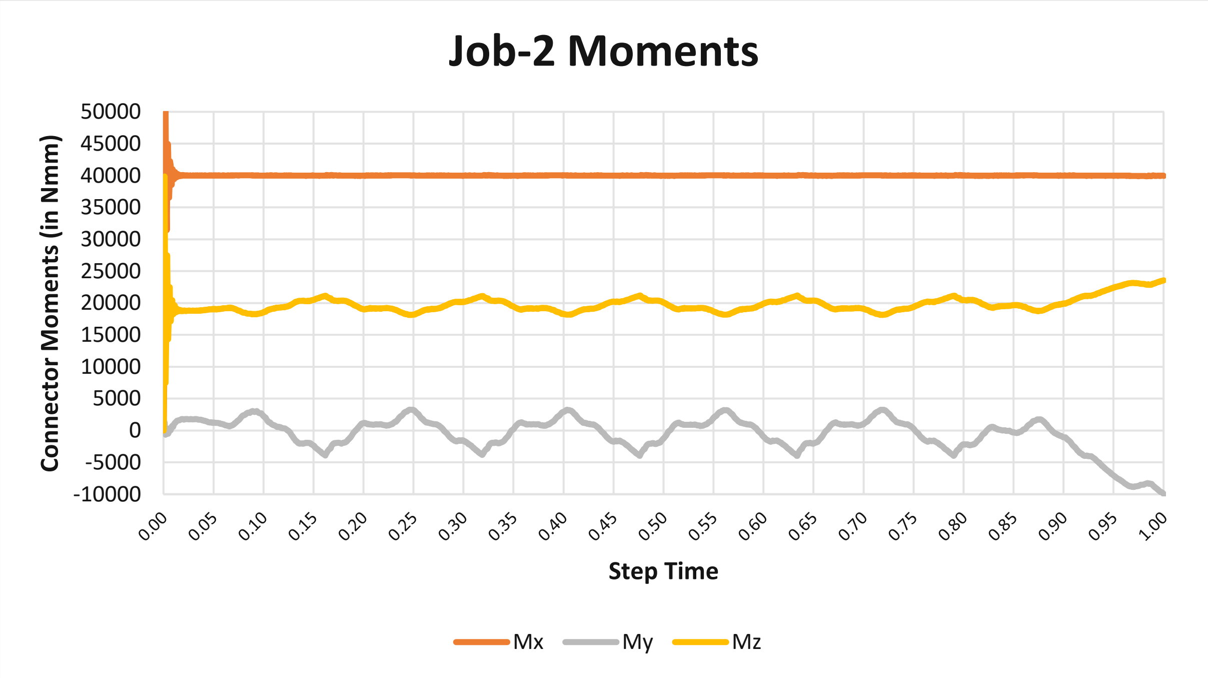

Figure 50: *Reaction moments at the pinion support for Job-2*

The same applies to the forces and relative motion of Job-2 as well and they exhibit the same behaviour as Job-1 and are represented in **Figures 51-52**.

Figure 51: *Reaction forces at the pinion support for Job-2*

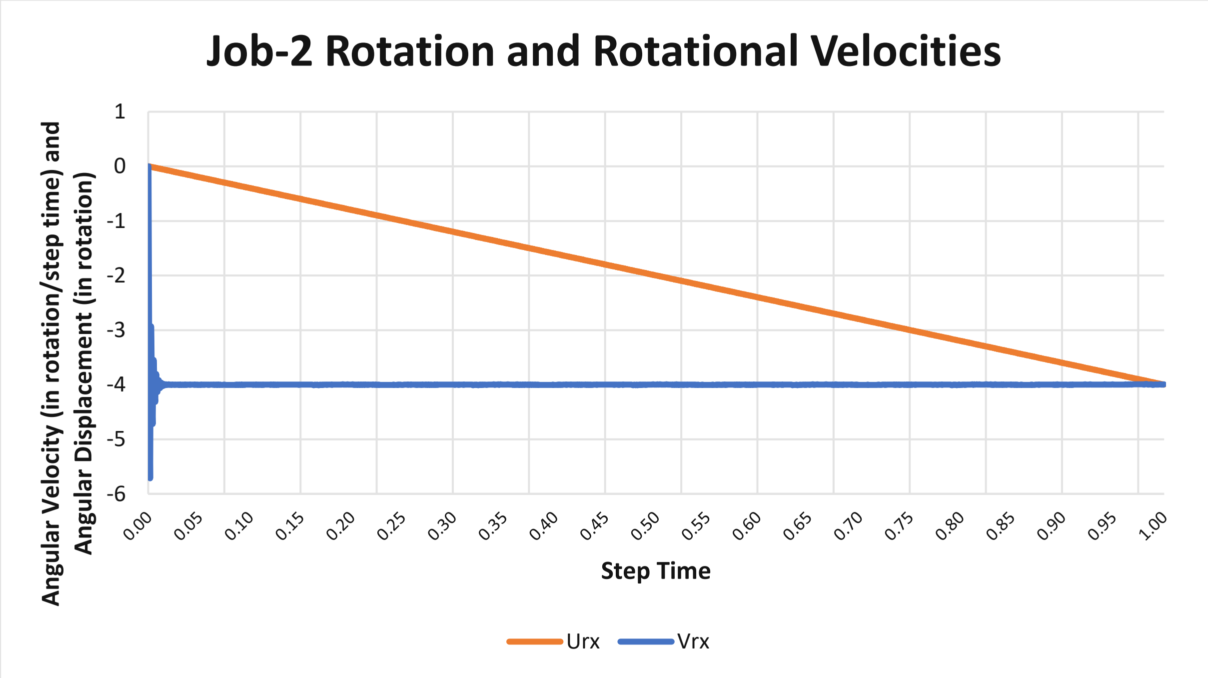

Figure 52: *Rotation angle and angular velocity of the pinion for Job-2*

6.2.2 Contact Forces

Comparable arguments can be presented for the contact status and contact forces for Job-2 as to Job-1. Consequently, a noticeable difference between default hard contact and penalty method is not present.

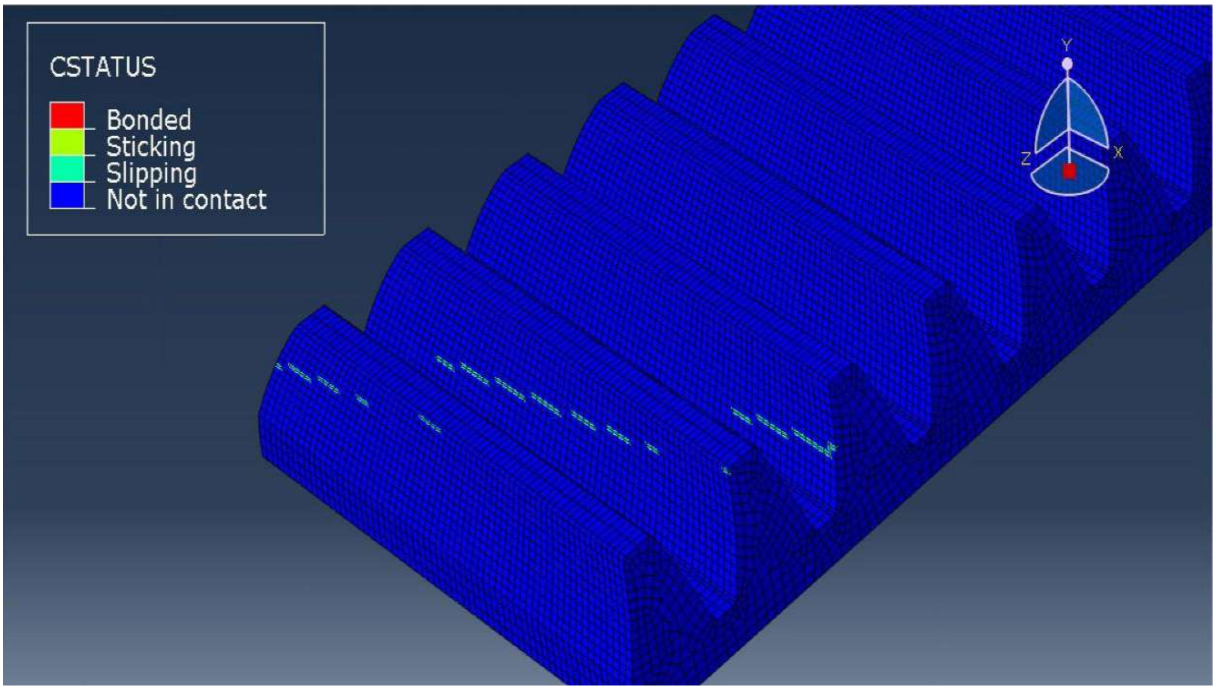

Figure 53: *Contact status on the rack for Job-2 in Frame 150*

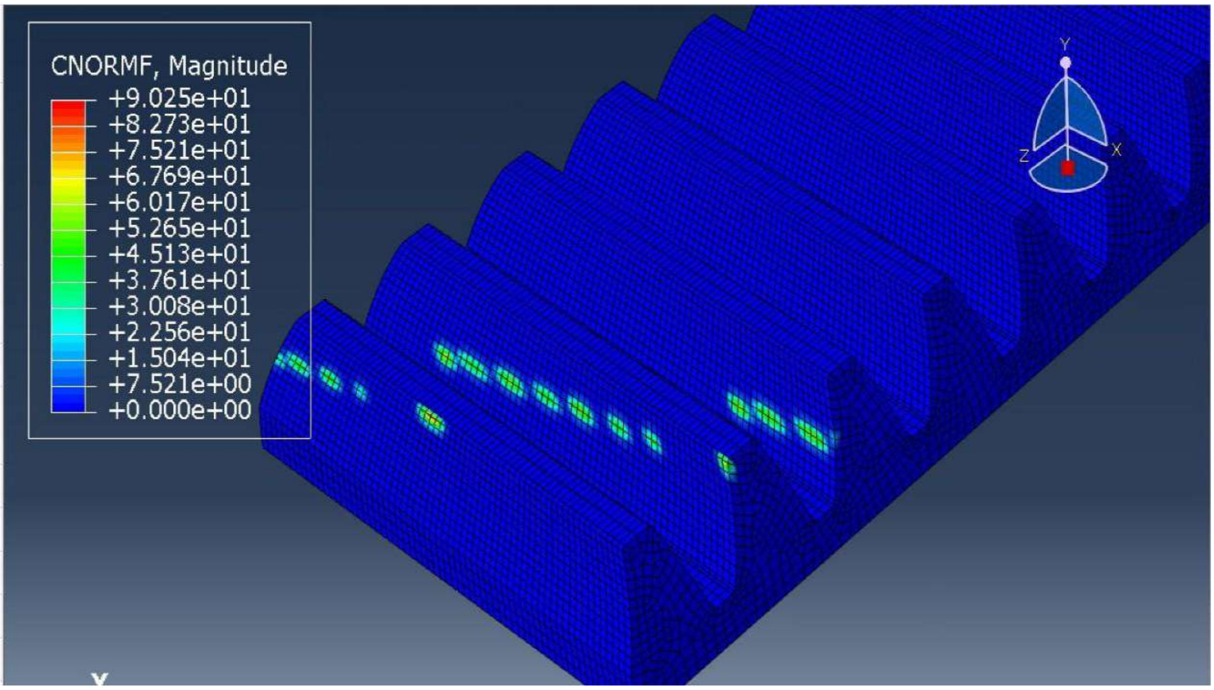

Figure 54: *Normal contact forces on the rack for Job-2 in Frame 150*

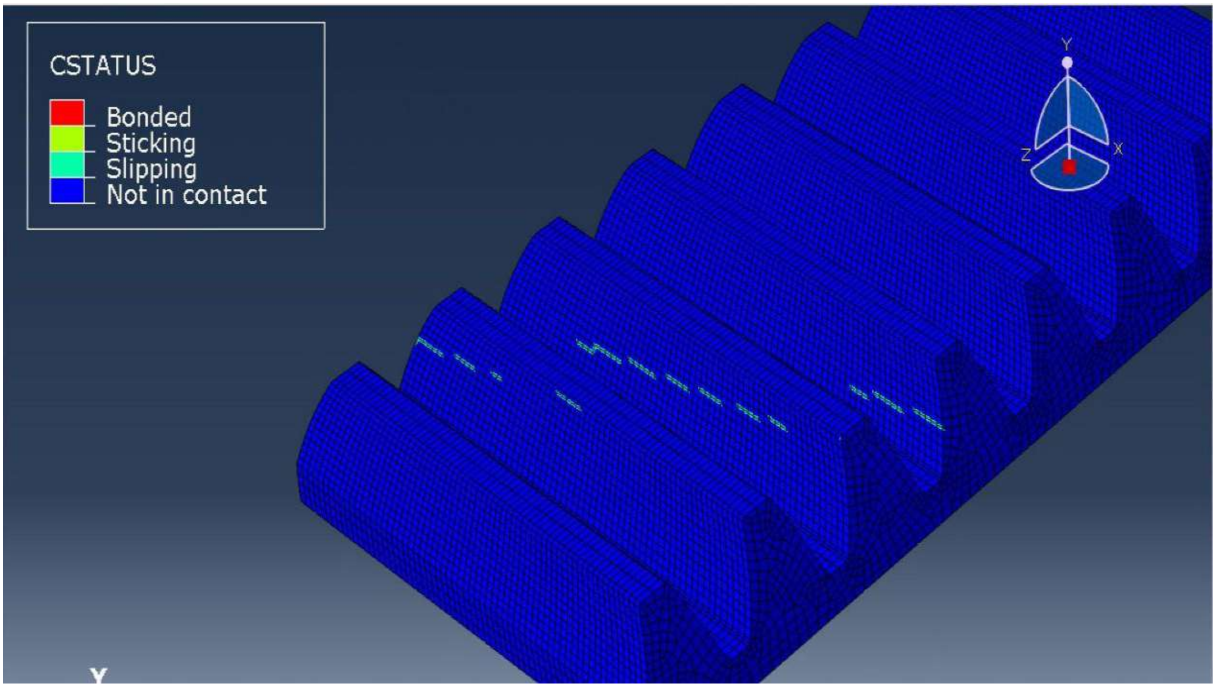

Figure 55: *Contact status on the rack for Job-2 in Frame 450*

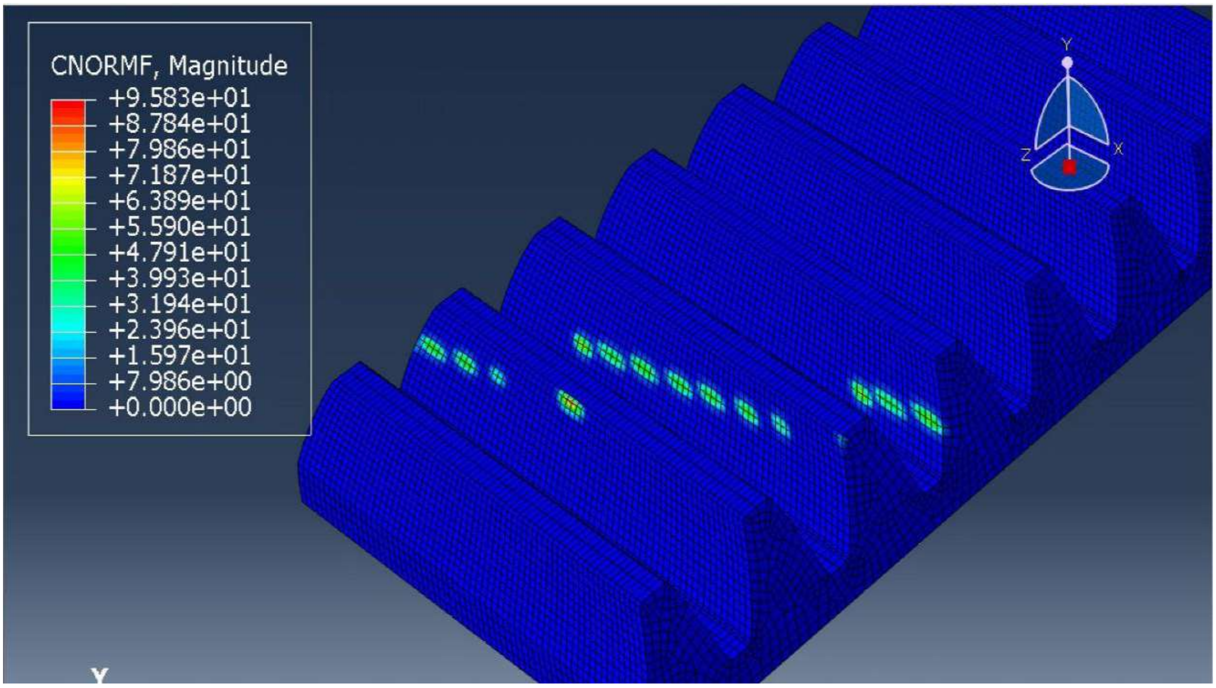

Figure 56: *Normal contact forces on the rack for Job-2 in Frame 450*

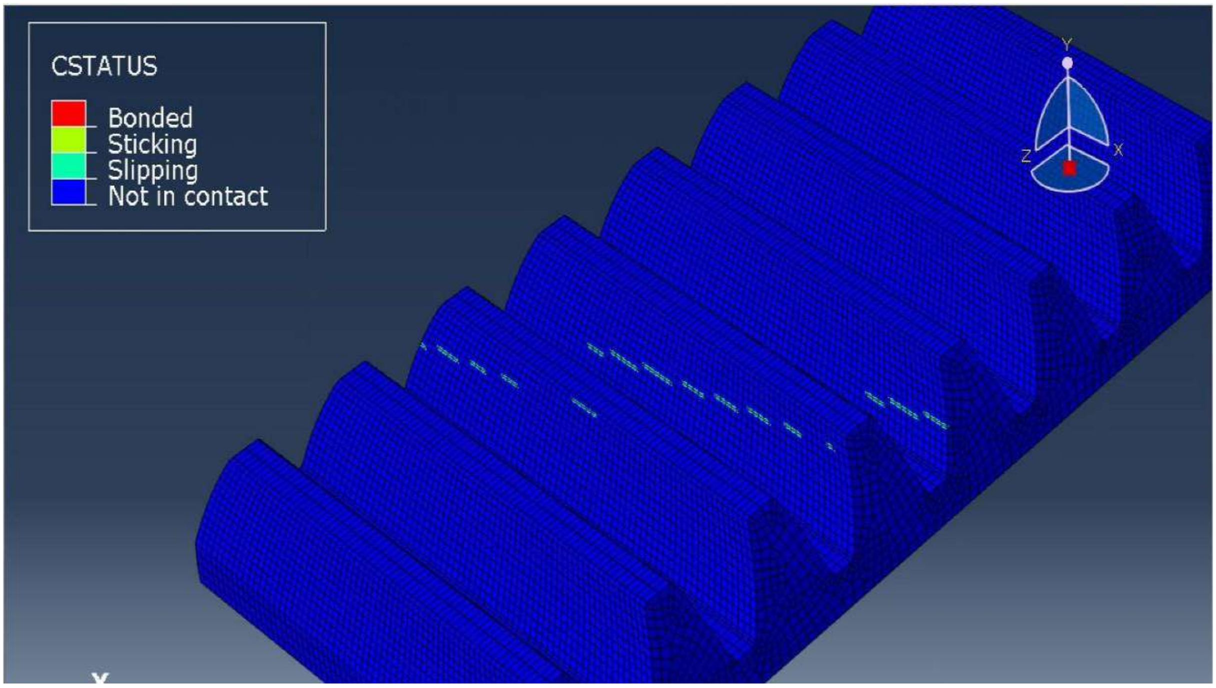

Figure 57: *Contact status on the rack for Job-2 in Frame 750*

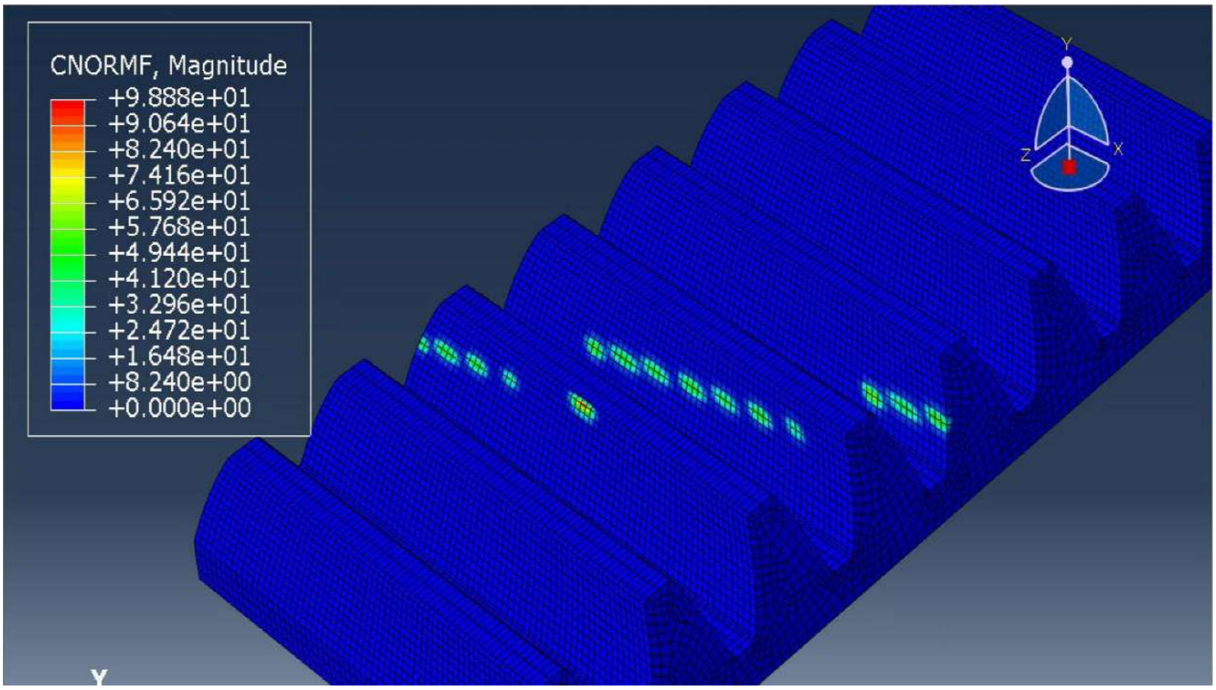

Figure 58: *Normal contact forces on the rack for Job-2 in Frame 750*

6.3 Job-3

Job-3 compared to Job-1 and Job-2 has a finer mesh and therefore needs significantly more computation time to complete the simulation. For this case, a hard contact with default enforcement in the normal direction and a frictionless tangential contact was selected. The rack has a mesh size of 0.4 and a mesh size of 0.2 in the contact zones (tooth flanks). The pinion was meshed with a size of 0.8 and 0.3 in the contact zones (tooth flanks). In terms of this thesis, it was decided that, a step time a little over 0.5 (0.531) step time (equals to 1063 increments) was sufficient to analyse the moments, forces, relative pinion motion and the contact situation on the rack for this job. In this time frame, two full periodic cycles for the moments can be seen.

6.3.1 Moments, Forces and Relative Rotation

The diagram for the moments in Job-3 starts again similar to Job-1 and Job-2 with strong fluctuations in the beginning where the rack and pinion contact is not in the ideal situation, but then continues in a steady state. On one hand, the values and direction of the reaction moments are again resembling the first two cases but on the other hand a more uniform distribution is observed. The moments in the x_2 axis results with again in the region of 40.000 Nmm. The moments around the y_2 axis exhibits a periodic distribution depending on the contact positions of the pinion and the rack teeth in approximately every 0.15 step time. This periodicity starts approximately from 0.1110 step. A positive high moment of $2660.07\ Nmm$ at step time 0.2490 and a negative high moment of $-2589.81\ Nmm$ at step time at 0.4695 was calculated in y_2 axis. The moments around the z_2 axis also exhibit a periodic behaviour, although with less amplitude than the moments around y_2. A positive high moment of $20586.6\ Nmm$ at step time 0.4700 and a negative high moment of $18351\ Nmm$ at step time at 0.4035 was calculated.

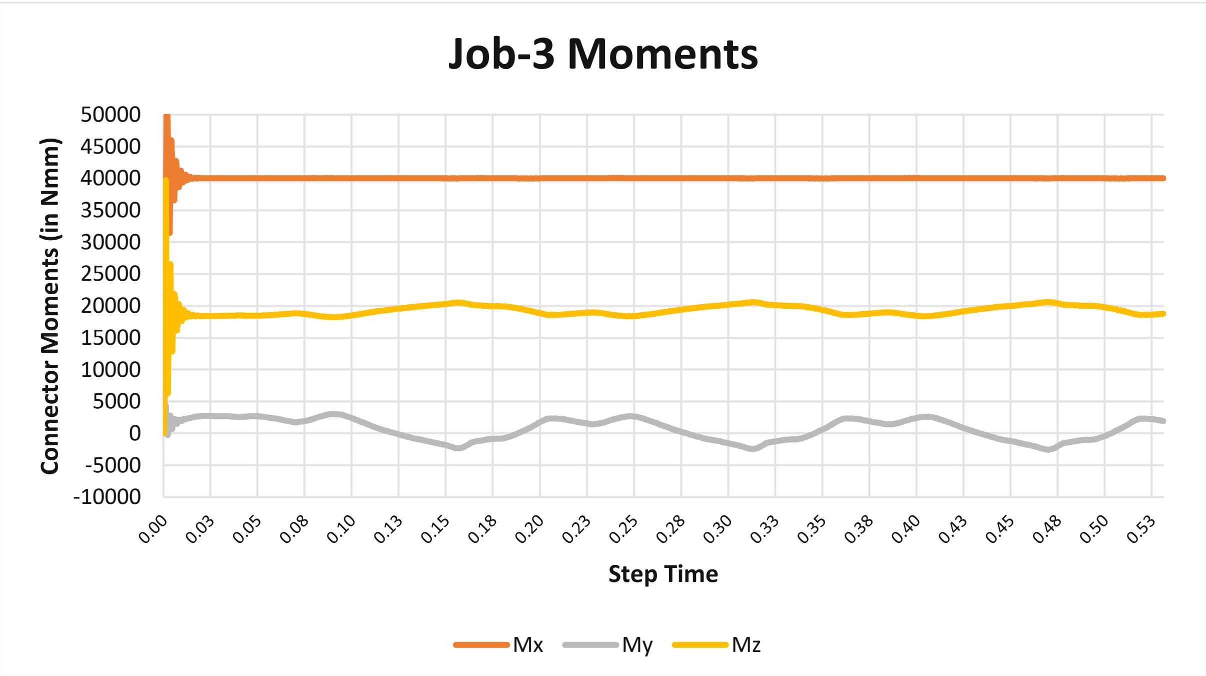

Figure 59: *Reaction moments at the pinion support for Job-3*

In terms of the reaction forces at the pinion support for Job-3, once more an analogous diagram compared to Job-1 and Job-2 can be seen. As expected, the highest forces are observed in the z_2 axis. The y_2 axis on the other hand is again the least loaded axis as the forces in the normal orientation are not as prominent as the axial forces. The maximum value for the forces around the x_2 axis is $1760.26\ N$ at step time 0.4770 and the minimum is $1752.7\ N$ at step time 0.5095. The maximum value for the forces around the y_2 axis is $-1482.51\ N$ at step time 0.1320 and the minimum is $-1466.17\ N$ at step time 0.3810. The maximum value for the forces around the z_2 axis is $-3608.51\ N$ at step time 0.4 and the minimum is $-3589.78\ N$ at step time 0.5070.

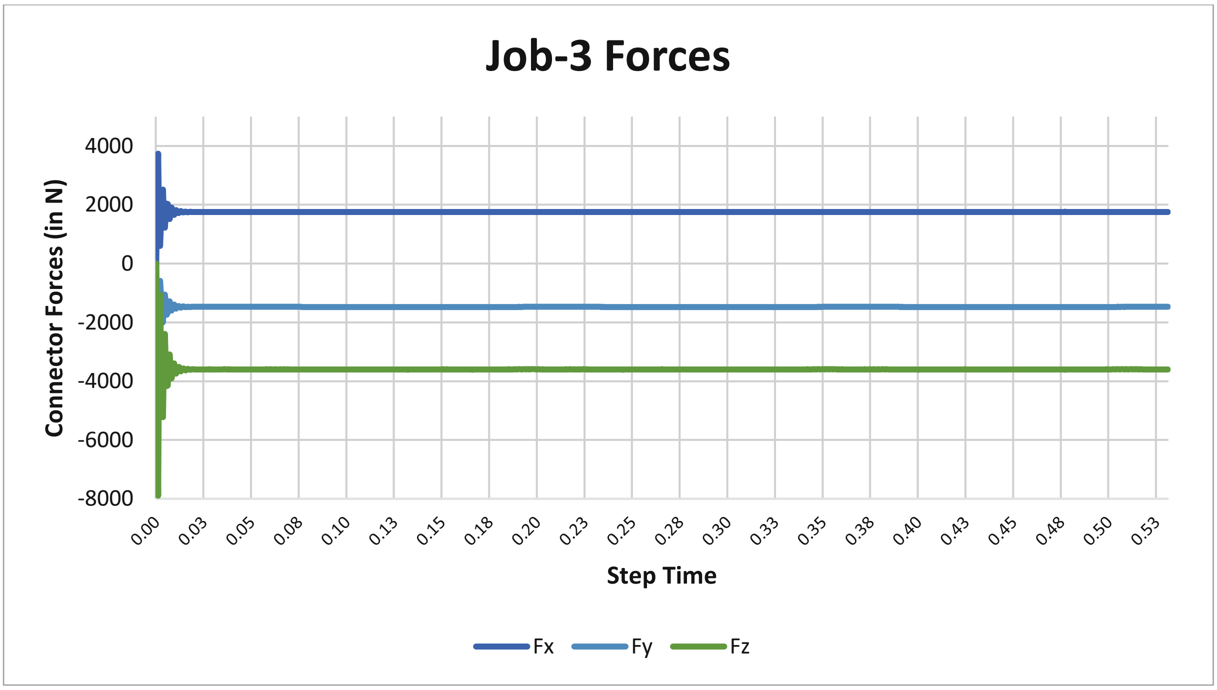

Figure 60: *Reaction forces at the pinion support for Job-3*

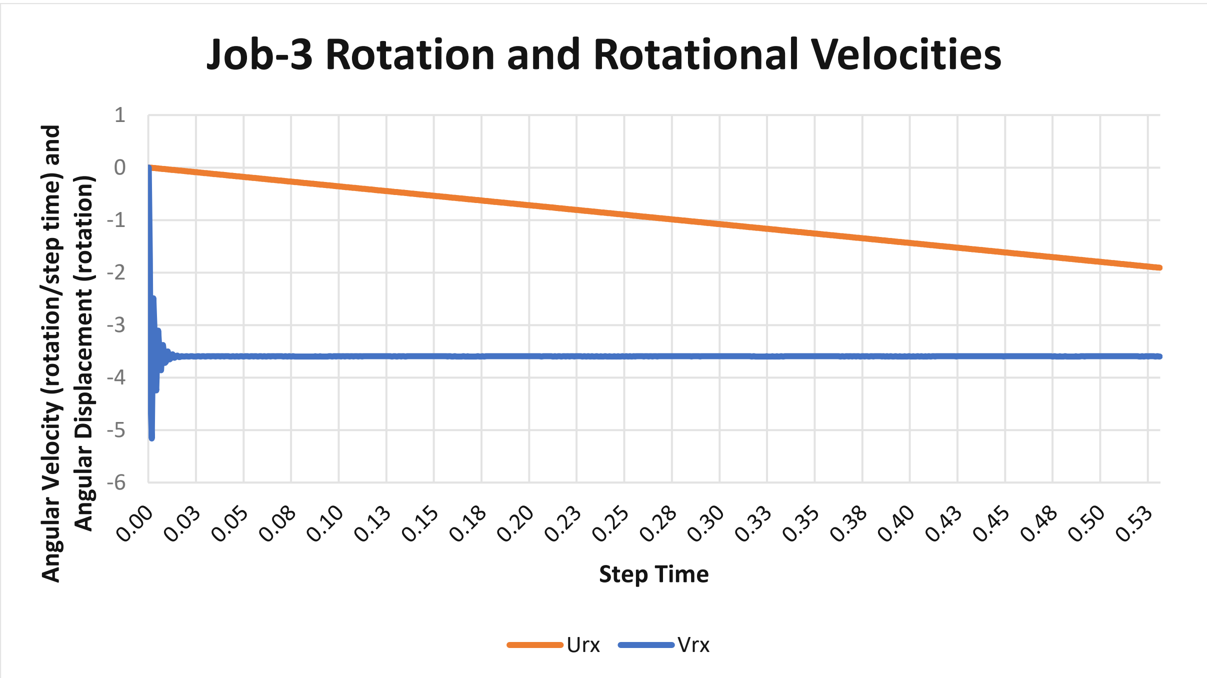

Figure 61: *Rotation angle and angular velocity of the pinion for Job-3*

The relative rotation of the pinion exhibits less fluctuations in the beginning compared to the Job-1 and Job-2 but as the simulation runs, they all exhibit a steady state behaviour.

6.3.2 Contact Forces Distribution

The contact status and contact forces are much more uniform and homogeneous compared to the previous cases with coarser mesh. This indicates that, ABAQUS solver can calculate a constantly occurring line contact between the rack and pinion instead of a clustered point contact. The numerical results are presented for different simulation frames, such as 150, 450 and 750, which corresponds to the same step times respectively.

- **Increment/Frame 150**

Contact Zone 1

The contact line in Zone 1 in the simulation Frame 150 is located on third tooth flank and is approximately 13 mm long, and consists 100 equally spaced path points. The first 50 path points (from length 0 mm to 6.24962 mm) do not measure any normal force (0 N) caused by the pinion contact, and therefore not included in the analysis and illustrated in **Figure 63**. Additionally, the last 3 path points are also excluded as they are on the edge of the tooth flank and shows concentrated high forces. The values point out that, the tooth is experiencing an average of 13.49 N normal force, which are stronger as the force distribution is further away from the tooth edge. The maximum force in this section is calculated 20.82 N at 11.85 mm length. The force distribution is not exactly uniform as the mesh is not fine enough to allow a high quality continuous uniform behaviour. The local maximum and minimum points exist due to the force concentration on the meshes and due to the positioning of nodes. The green dotted line represents the polynomial regression line of the contact forces for this path and is describes through $y = -0.0028x^2 + 0.1729x + 11.518$.

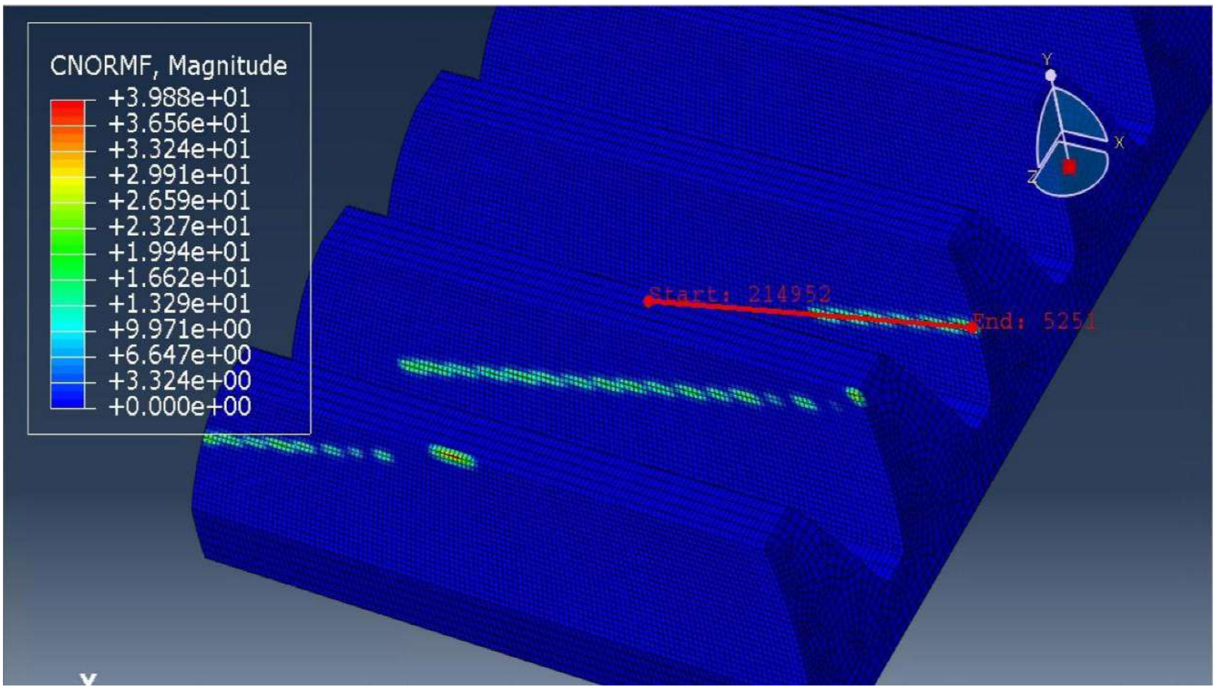

Figure 62: *Contact line in Zone 1 for Job-3 in Frame 150*

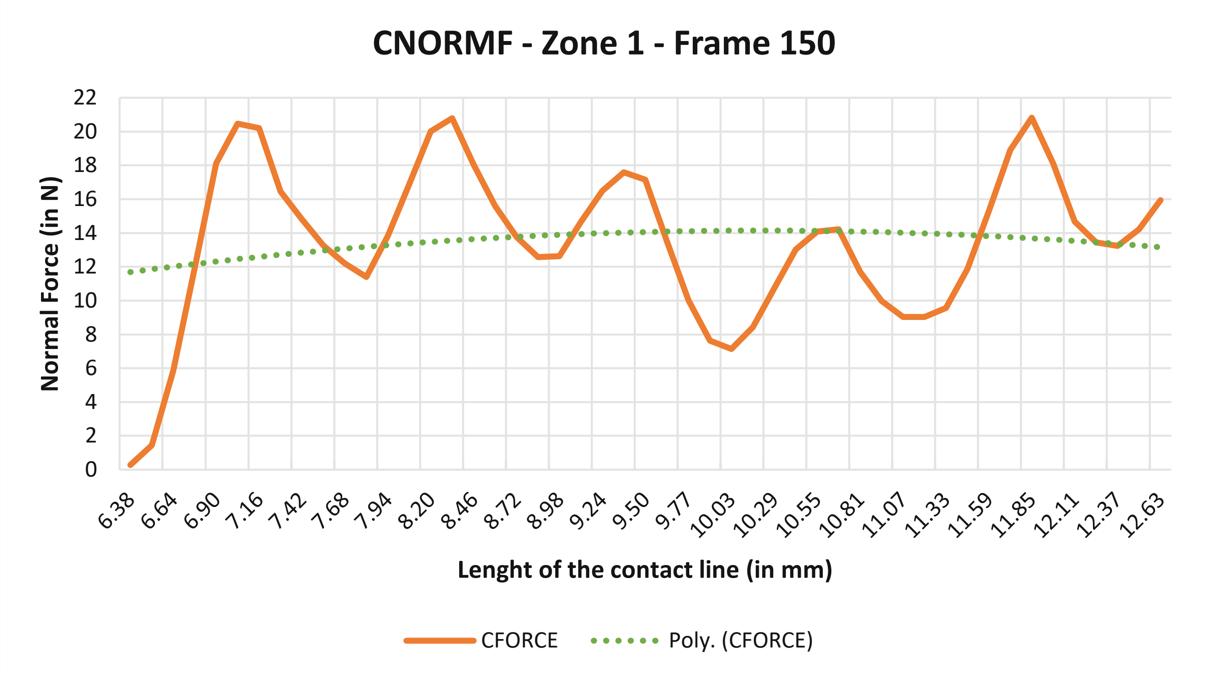

Figure 63: Normal forces distribution on the contact line in Zone 1 for Job-3 in Frame 150

Contact Zone 2

The contact line in Zone 2 is located on second tooth flank. Similar to the first contact zone, the first 18 path points and the last 5 path points are excluded from the analysis. The force distribution in the Zone 2 (approximately 23.41 mm long) can be interpreted as an inverted parabolic function where the average force is 11.97 N and the maximum force is 21.52 N at the length of 4.681 mm. This can be interpreted that, compared to Zone 1, the tooth flank is less stressed and able to scatter forces more efficiently and the highest forces are where the teeth engagement begins and ends. Similar with the problem in Zone 1, the normal forces are clustered in meshes and thus administer lower forces in between these clusters. The green dotted polynomial function is defined through $y = -0.0043x^2 + 0.2556x + 10.778$.

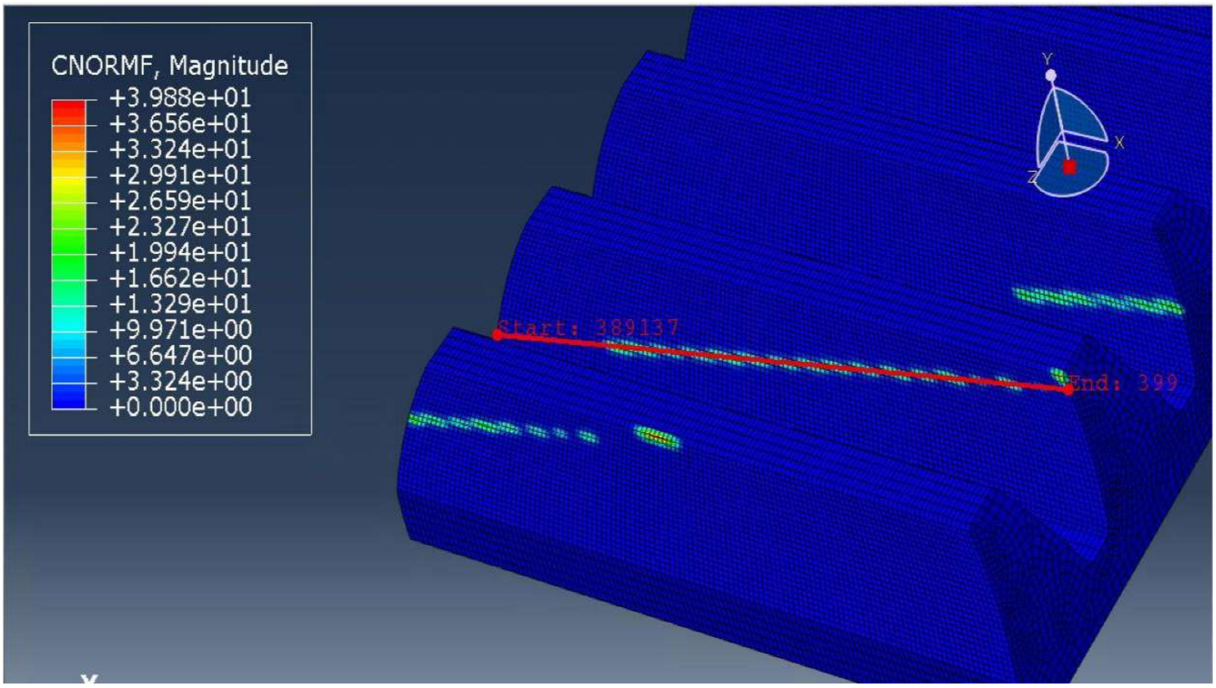

Figure 64: *Contact line in Zone 2 for Job-3 in Frame 150*

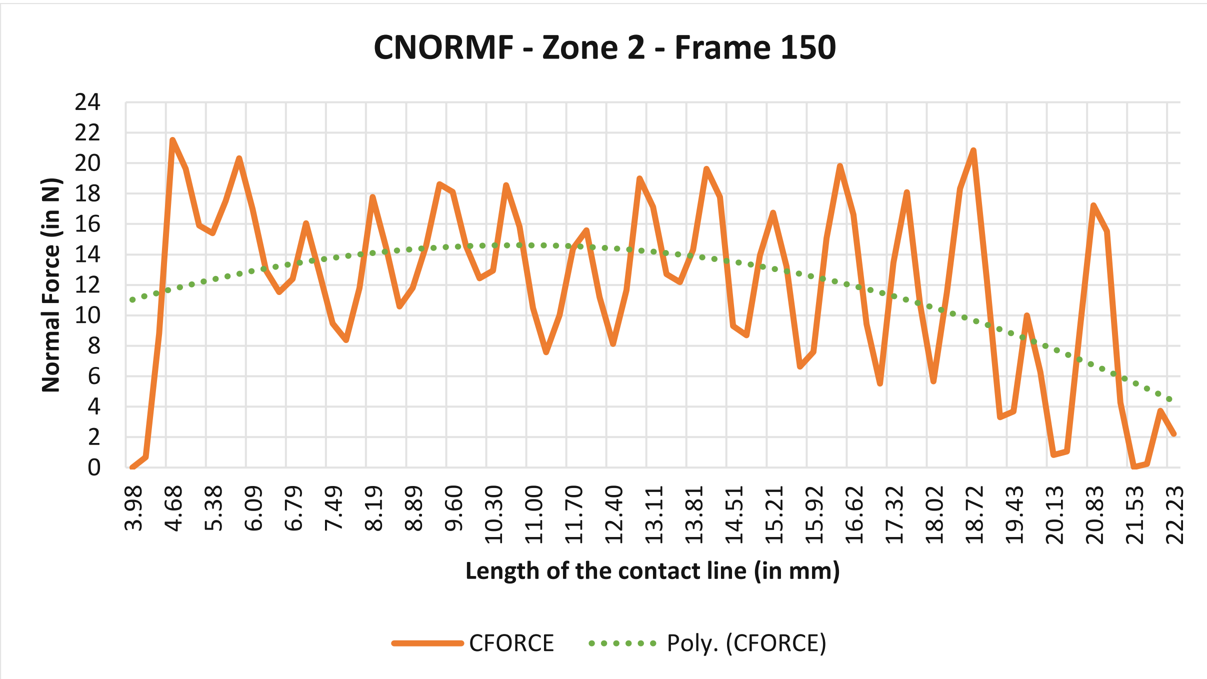

Figure 65: *Normal forces distribution on the contact line in Zone 2 for Job-3 in Frame 150*

Contact Zone 3

The contact line in Zone 3 is located on the first tooth flank and is approximately 11.15 mm, closer to the Zone 1 contact line length and calculates an average of 10.16 N in the length of the contact line. An important consideration here in this Zone is that, there is a gap between the lengths 8.365 mm and 9.146 mm. The cause for this gap is the contact on the top edge of the tooth flank where the highest force concentration can be observed. It is therefore decided to exclude the last 21 path points in order to understand the contact behaviour accurately. The first

3 path points are also excluded because of the high stresses on the edge. The maximum force on this line is 21.55 N at 3.12 mm. The polynomial force function is defined through $y = -0.0011x^2 - 0.0949x + 15.54$.

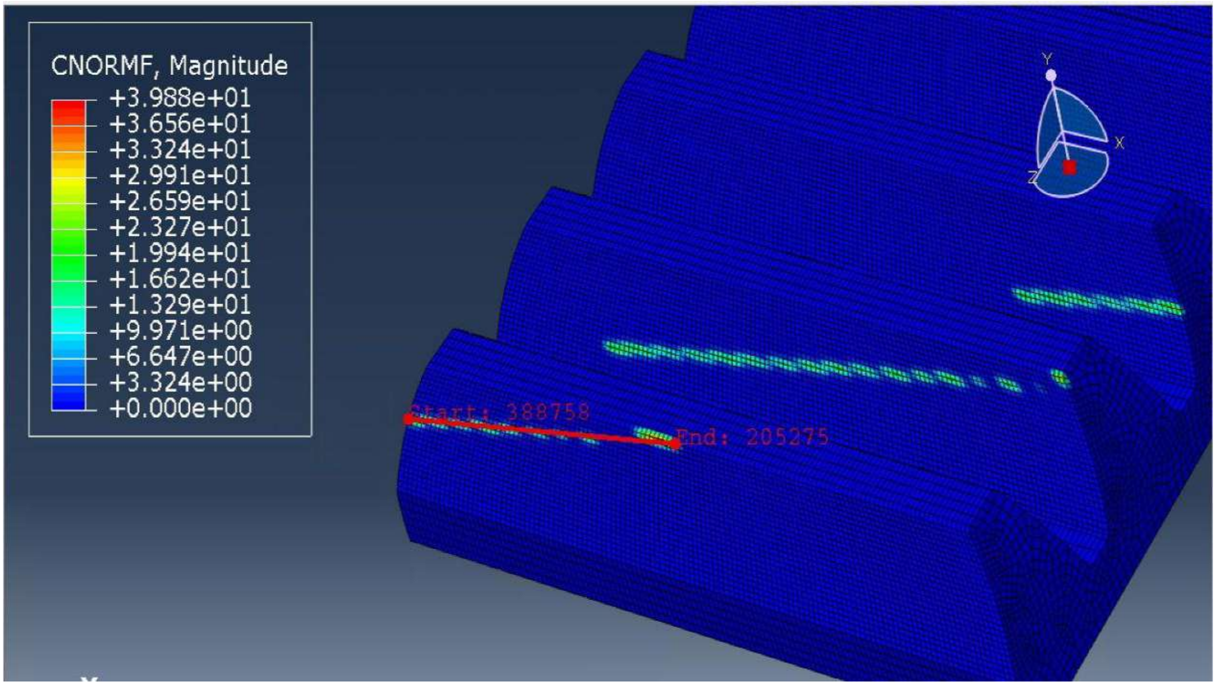

Figure 66: *Contact line in Zone 3 for Job-3 in Frame 150*

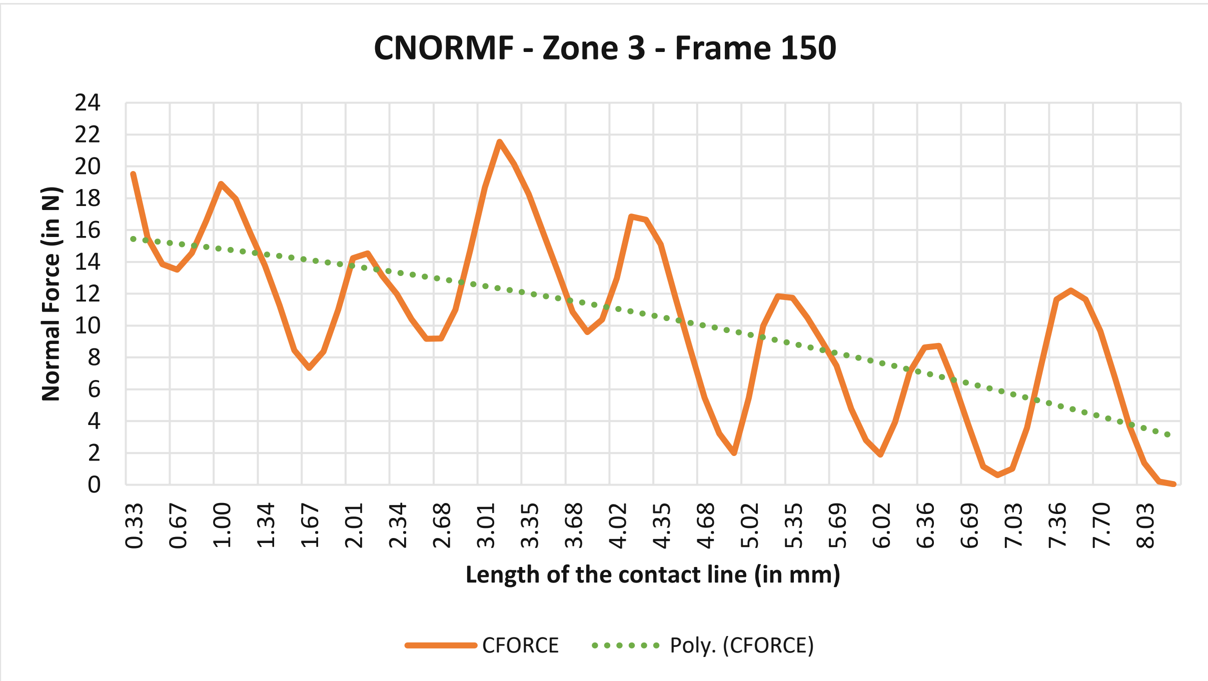

Figure 67: *Normal forces distribution on the contact line in Zone 3 for Job-3 in Frame 150*

- **Increment/Frame 450**

Contact Zone 1

The contact line in Zone 1 is located on the fourth tooth flank and is approximately 12.05 mm long and calculates on average 13.77 N. The first 48 path points and the last 3 path points are excluded once more for the same reason as the Increment/Frame 150. This contact line does exhibit its maximum calculated force of 21.96 N at 10.96 mm. Once again similar to Frame 150 we observe force clusters that creates this non-uniform force distribution. The polynomial function is graphed through the function $y\ ==-0.0017x^2\ +\ 0.1387x\ +\ 11.666$.

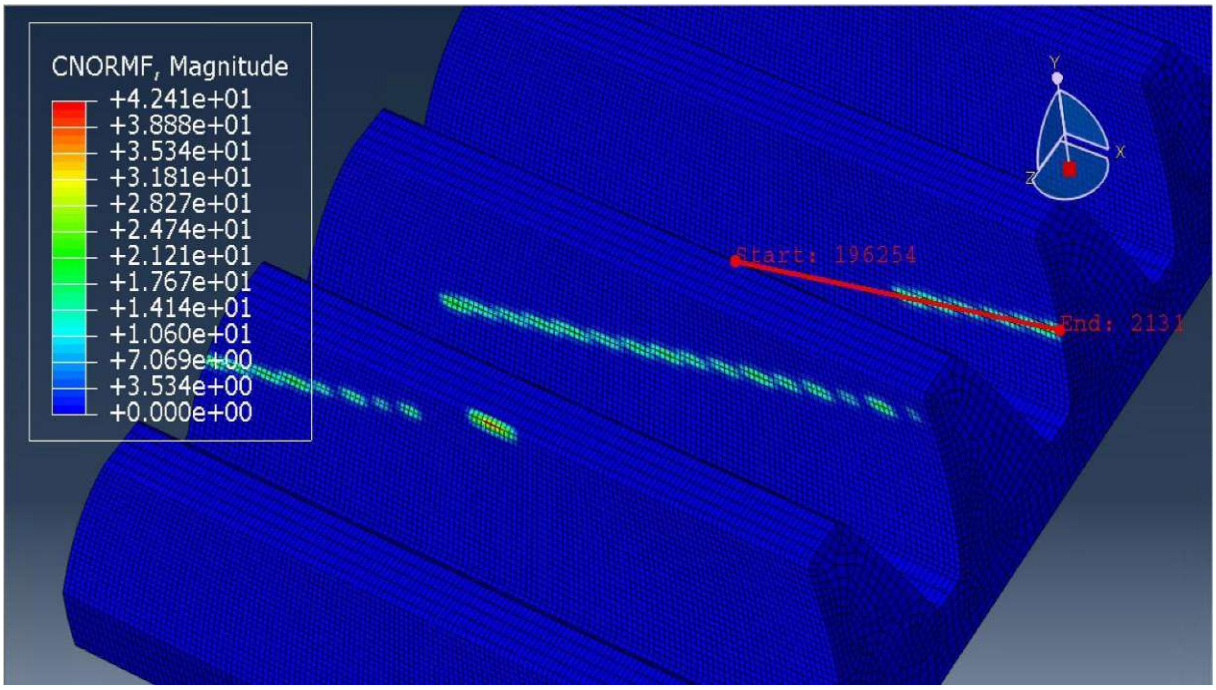

Figure 68: *Contact line in Zone 1 for Job-3 in Frame 450*

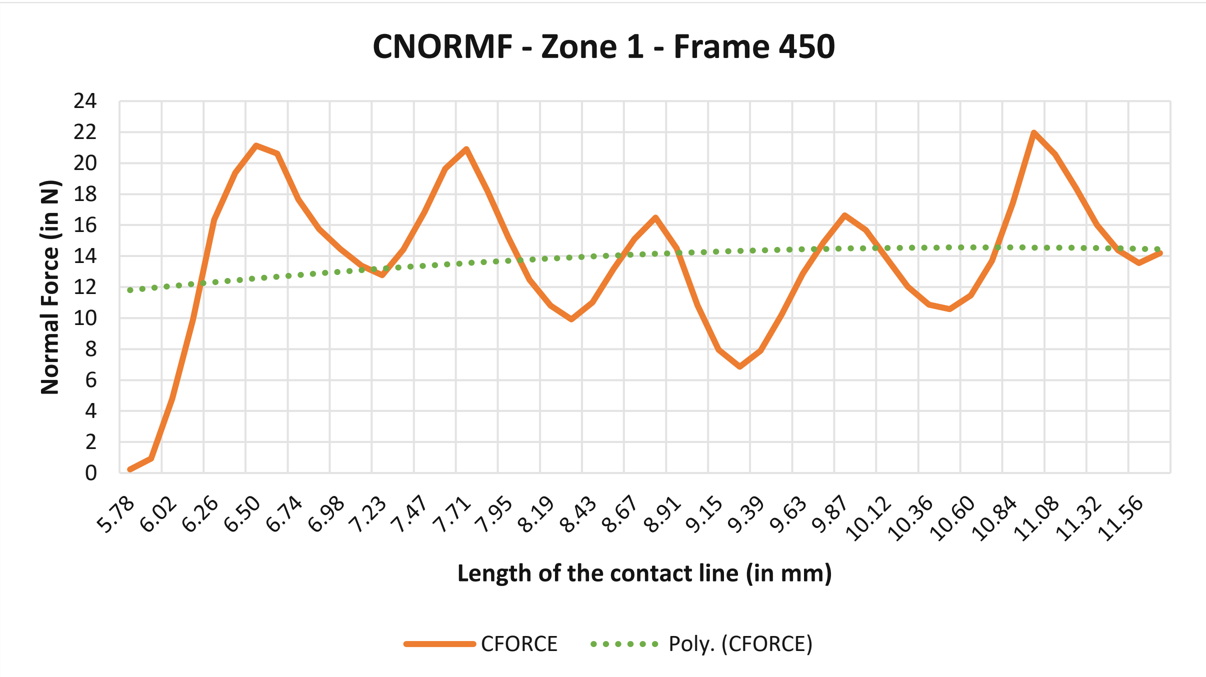

Figure 69: *Normal forces distribution on the contact line in Zone 1 for Job-3 in Frame 450*

Contact Zone 2

The contact line in Zone 2 is located on the third tooth flank and has a length of 22.93 mm. The first 21 and the last 3 path points are excluded. The average force calculated on this contact line is 12.18 N and the maximum force on the line is 20.879 N at length 17.20 mm. The parabolic function is defined by $y = -0.0032x^2 + 0.2112x + 10.382$.

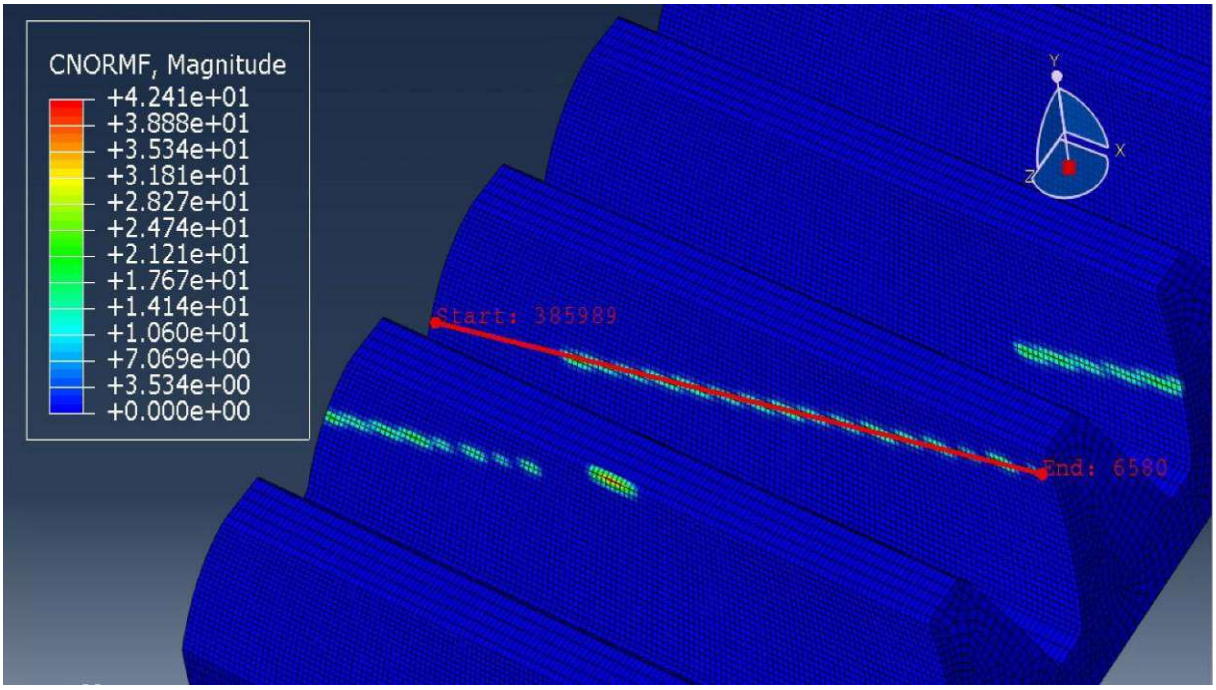

Figure 70: *Contact line in Zone 2 for Job-3 in Frame 450*

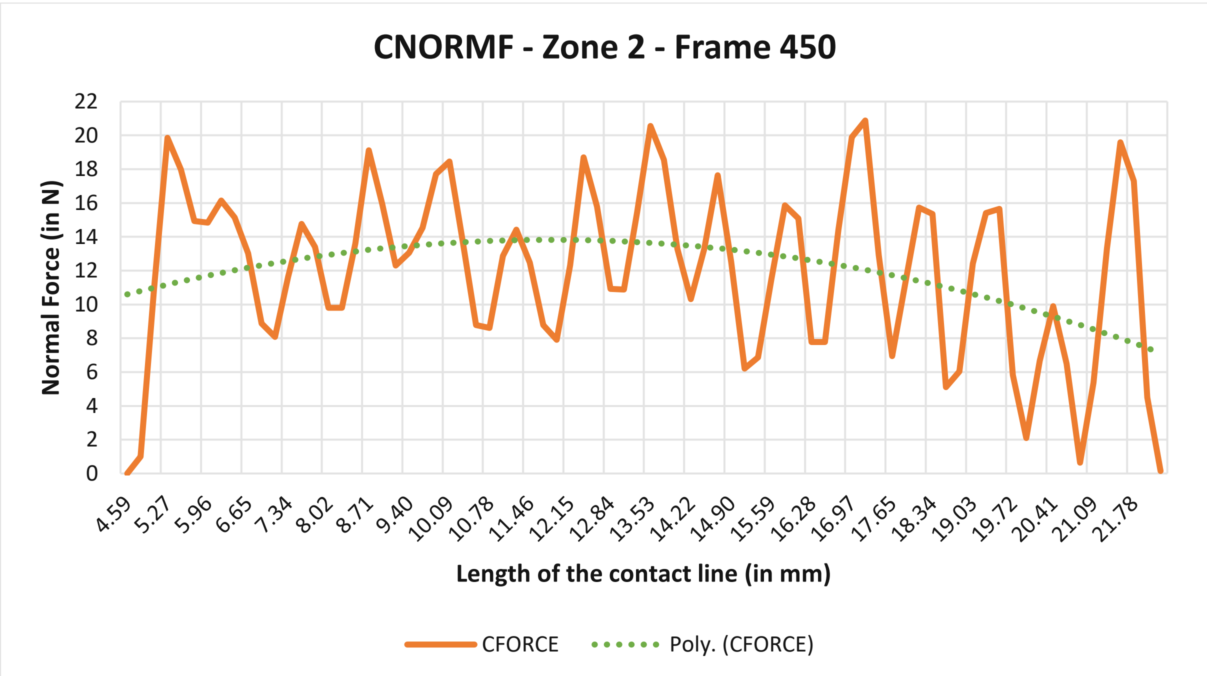

Figure 71: *Normal forces distribution on the contact line in Zone 2 for Job-3 in Frame 450*

Contact Zone 3

The contact line in Zone 3 is located on the second tooth flank is approximately $11.873\ mm$ long. The first 3 and the last 27 path points are excluded. The average force on the contact line is $11.10\ N$ and the maximum force is calculated $22.35\ N$ at $3.32\ mm$. The parabolical definition is made through the function $y = -0.0015x^2 - 0.0498x + 15.448$.

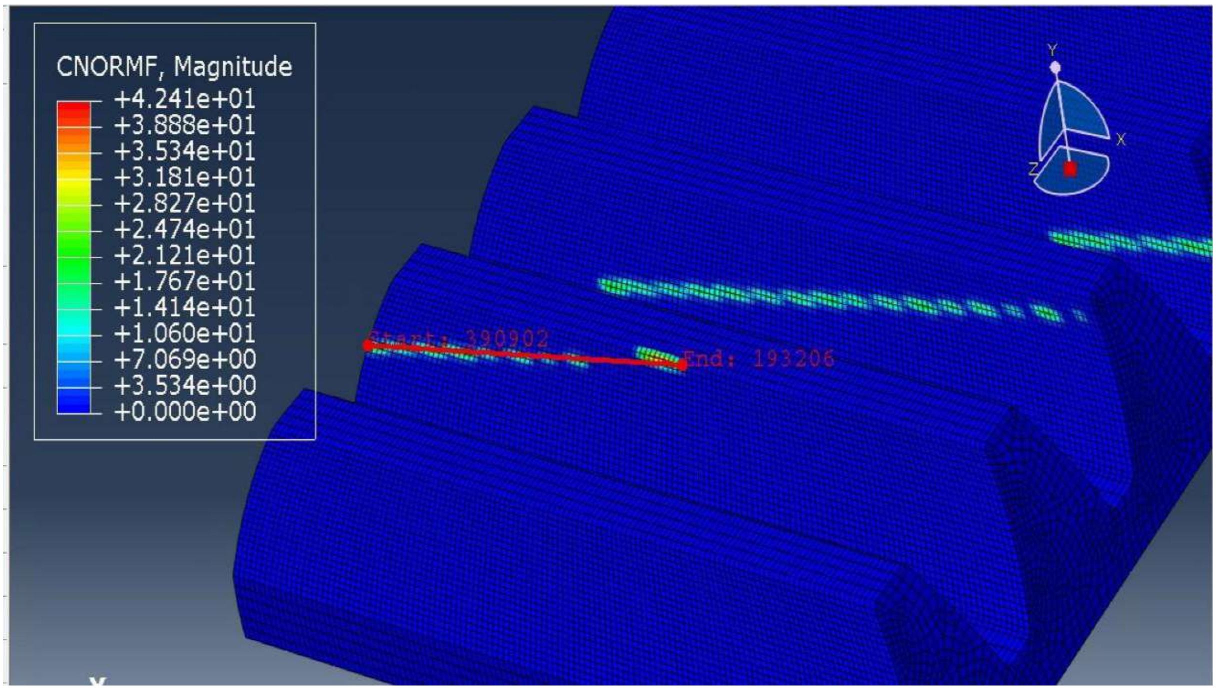

Figure 72: *Contact line in Zone 3 for Job-3 in Frame 450*

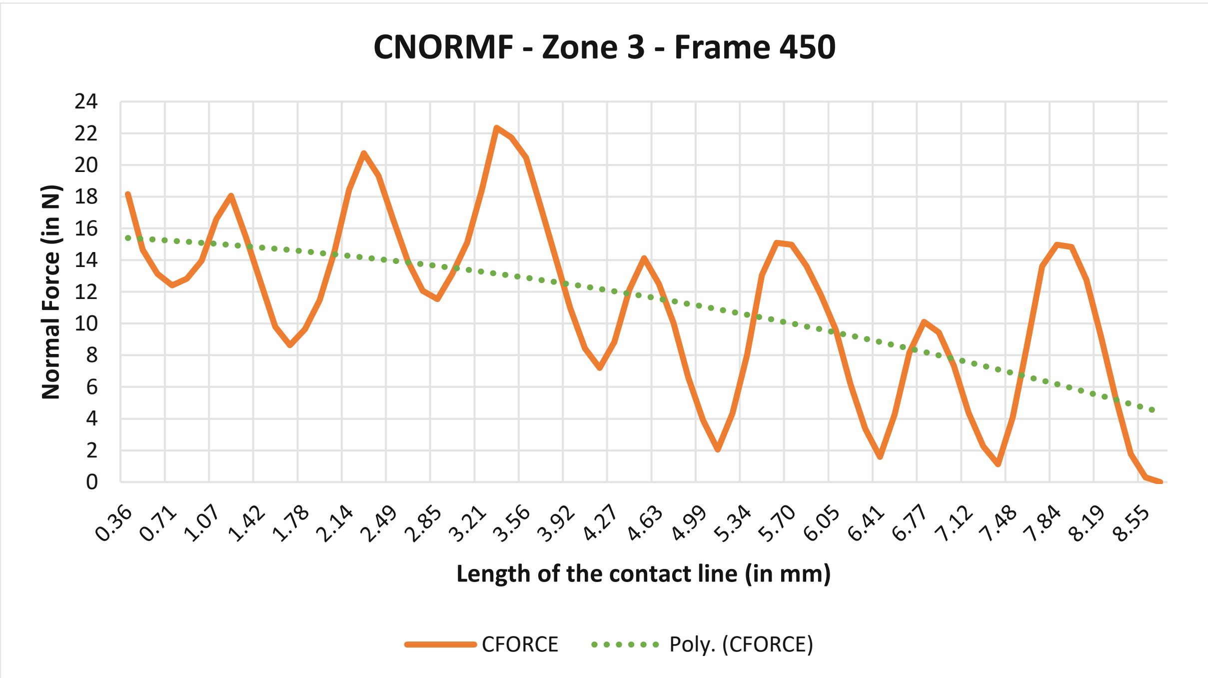

Figure 73: *Normal forces distribution on the contact line in Zone 3 for Job-3 in Frame 450*

- **Increment/Frame 750**

Contact Zone 1

The contact line in Zone 1 of the Frame 750 is located on the fifth tooth flank and has a length of 12.266 mm. The first 52 and last 3 path points are excluded. The average force on the line is 12.46 N and the maximum force calculated on this line is 22.54 N at length 7.237 mm. The parabolic function is defined through $y = -0.0038x2 + 0.2476x + 9.4396$.

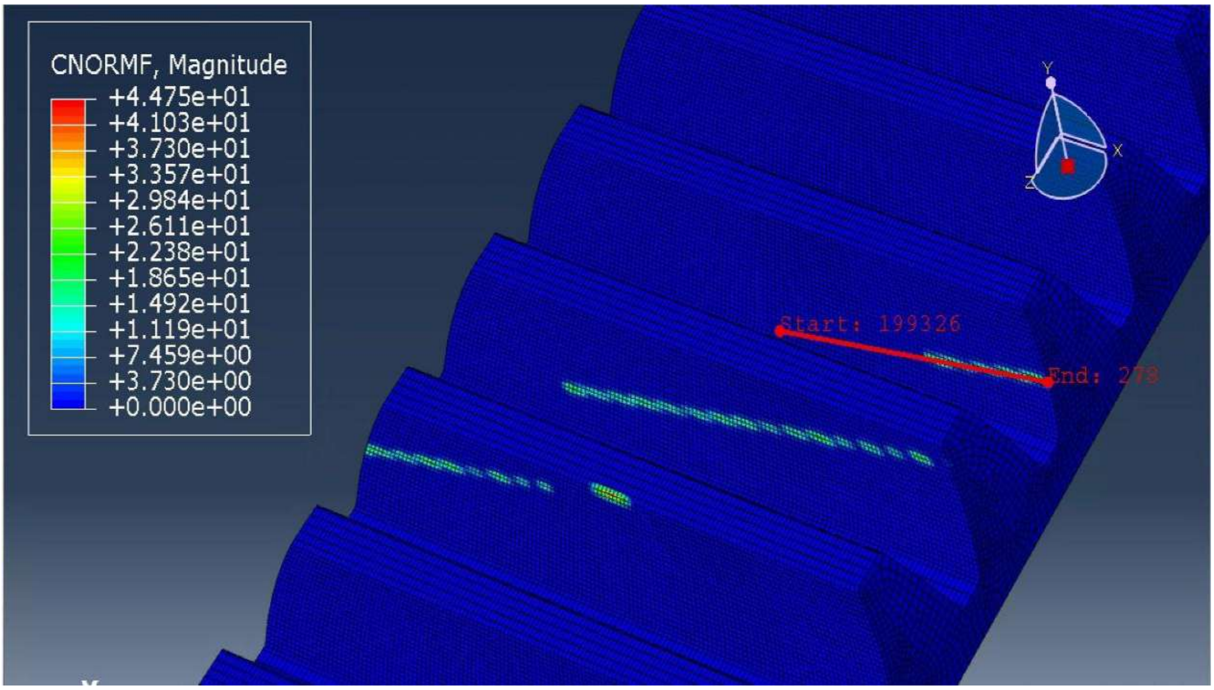

Figure 74: *Contact line in Zone 1 for Job-3 in Frame 750*

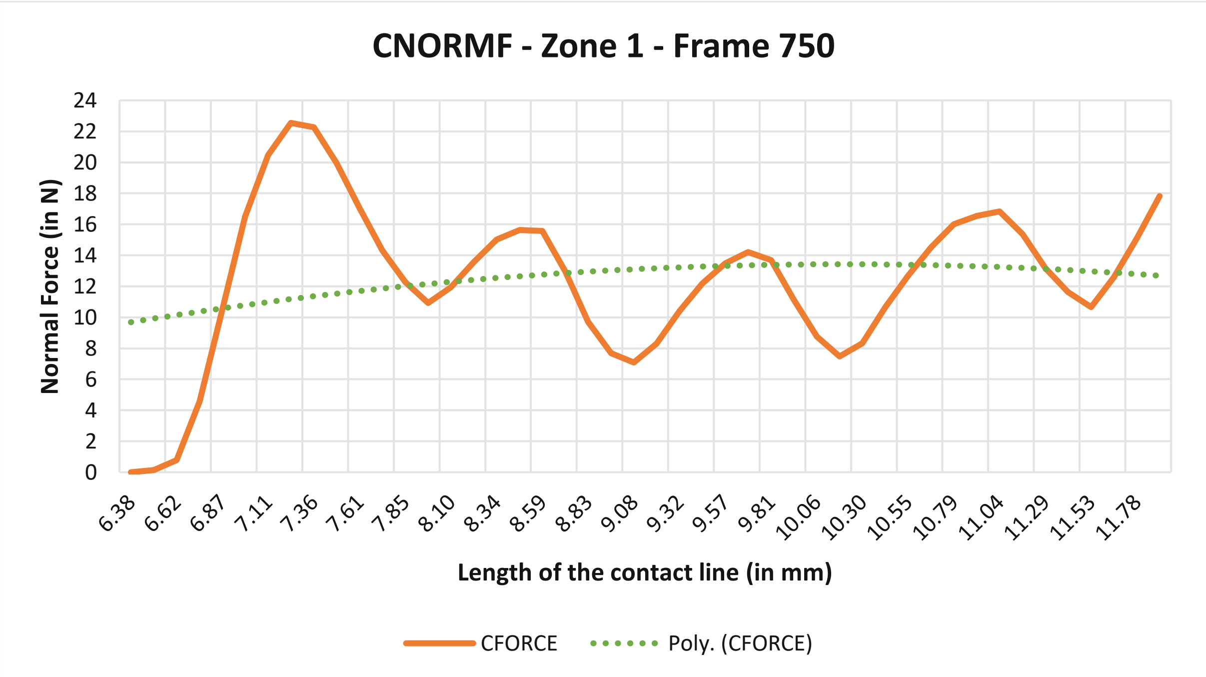

Figure 75: *Normal forces distribution on the contact line in Zone 1 for Job-3 in Frame 750*

Contact Zone 2

The contact line in Zone 2 is located on the fourth tooth flank and is approximately 23.54 mm. The first 23 and the last 3 path points are excluded. The average force on the line is calculated 12.68 N and the maximum force is 24.5 N at 6.12 mm. The parabolic function is defined through $y = -0.0016x^2 + 0.0916x + 12.188$.

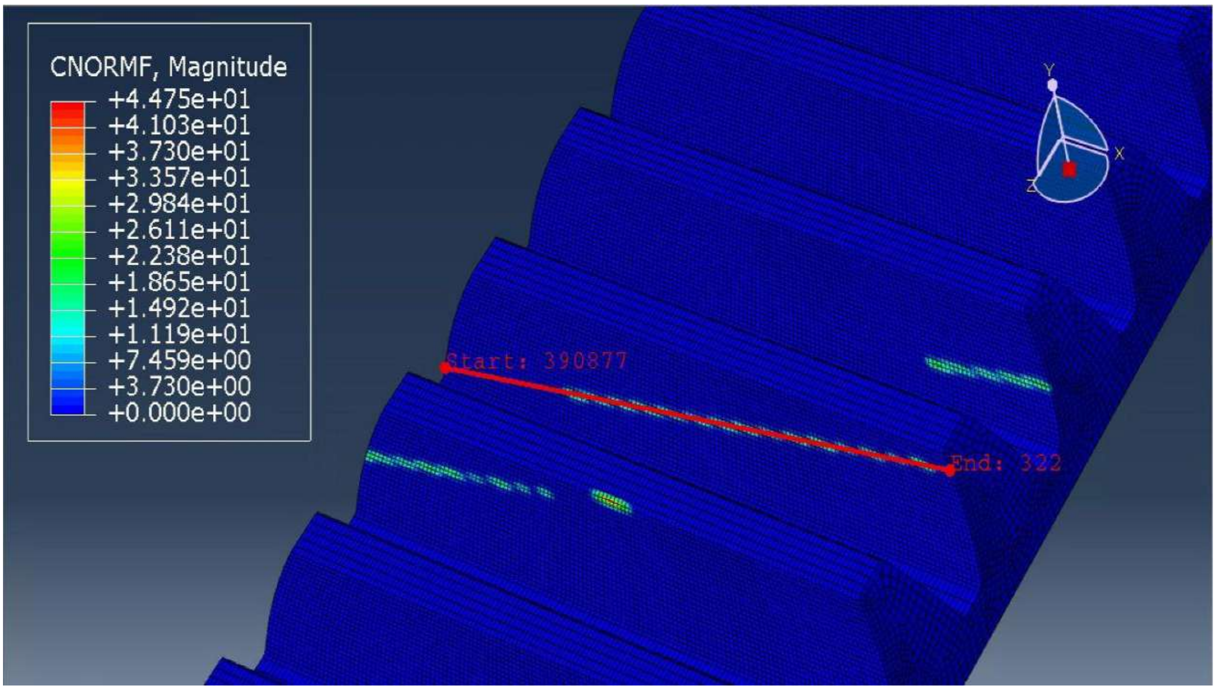

Figure 76: *Contact line in Zone 2 for Job-3 in Frame 750*

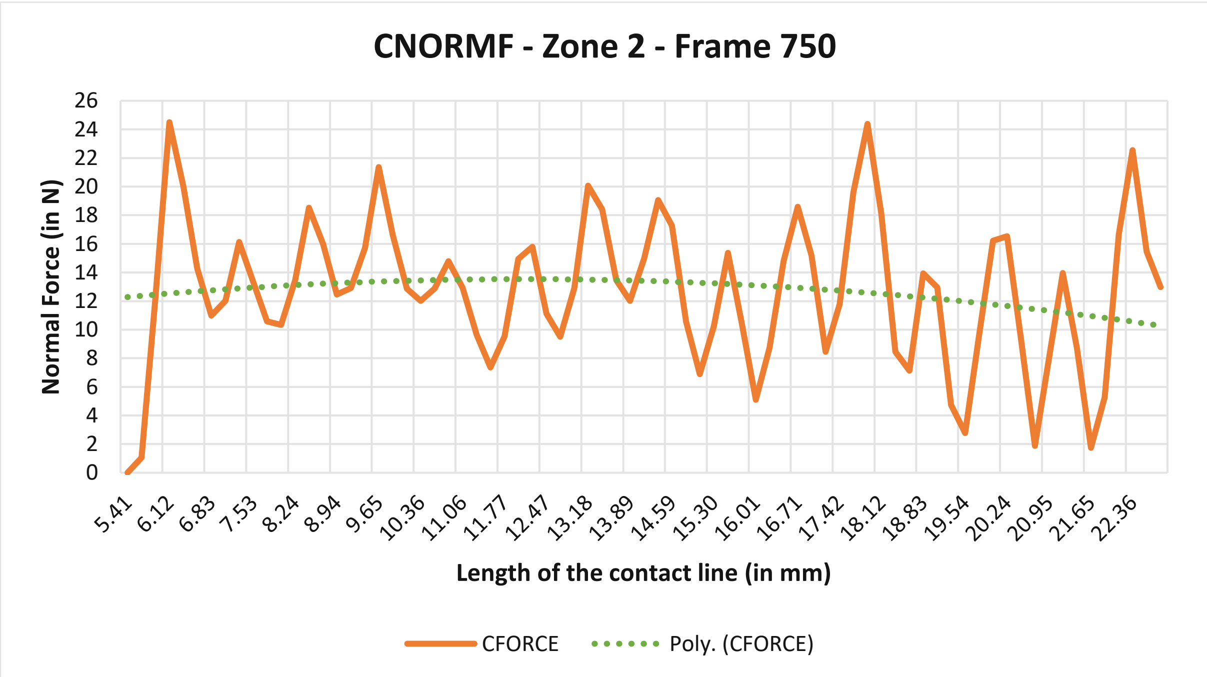

Figure 77: *Normal forces distribution on the contact line in Zone 2 for Job-3 in Frame 750*

Contact Zone 3

The contact line in Zone 3 is located on the third tooth flank and has a length of 12.14 mm. The first 3 and the last 24 path points are excluded. The average force on the contact line is 11.55 N and the maximum force is calculated 22.36 N at 3.16 mm. The parabolic function is defined as $y = -0.0031x^2 + 0.077x + 14.144$.

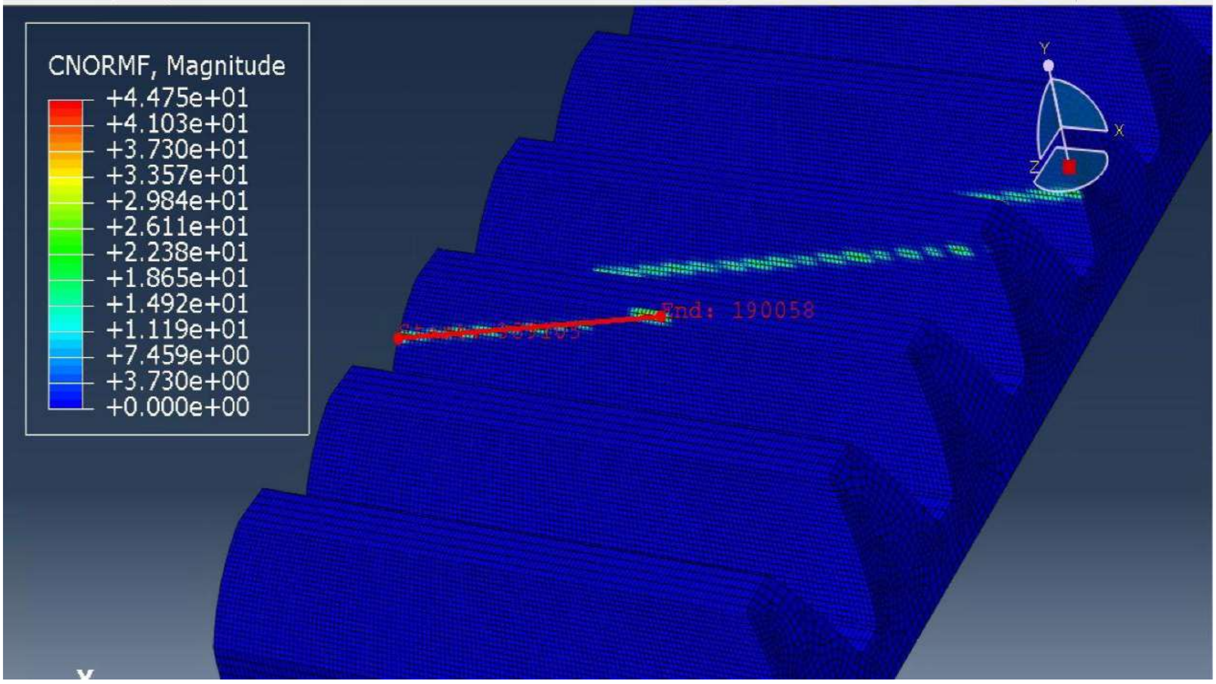

Figure 78: *Contact line in Zone 3 for Job-3 in Frame 750*

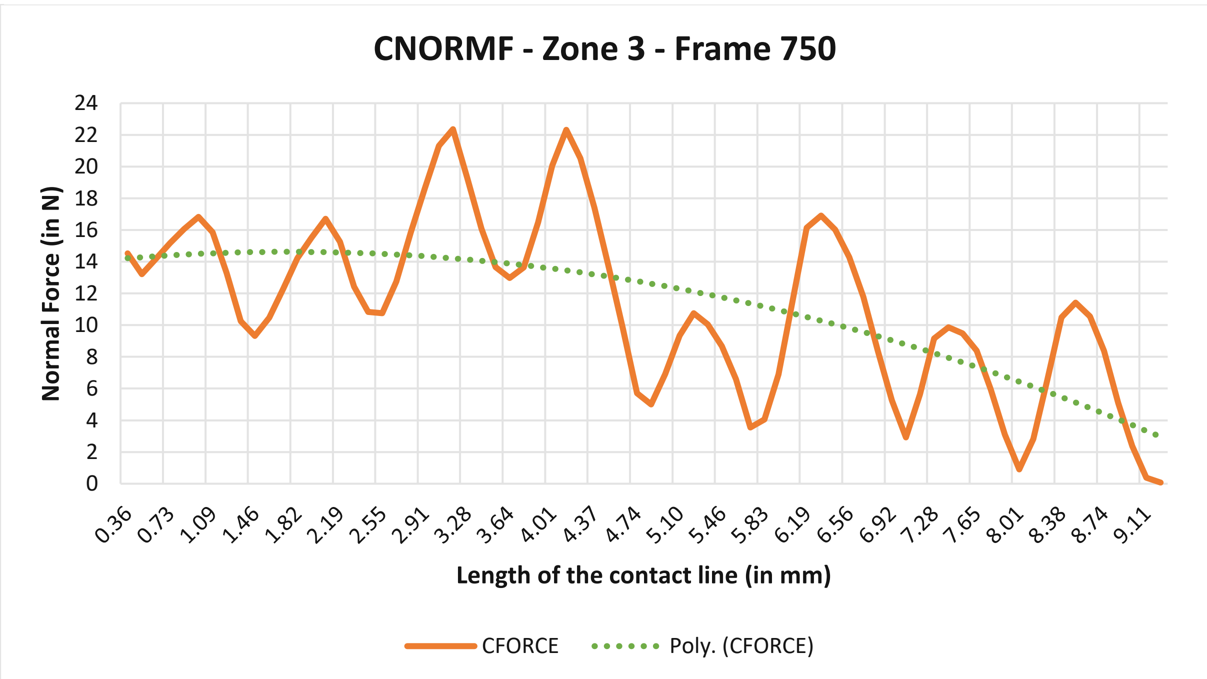

Figure 79: *Normal forces distribution on the contact line in Zone 3 for Job-3 in Frame 750*

6.4 Results Comparison

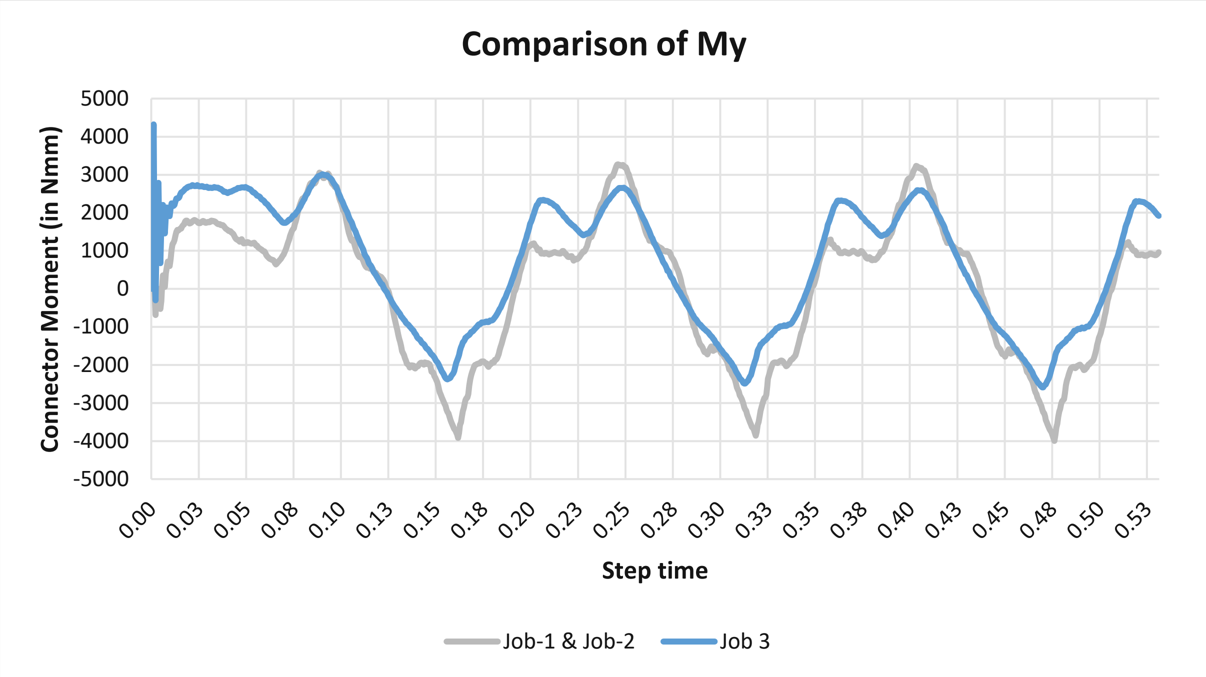

Figure 80: *Comparison of the moments on the y axis*

The simulation results came as expected for all three cases. There are ideally three teeth in contact between the rack and pinion, and dependent on the positioning of the contact lines it was expected to see periodic moments in the radial directions and a constant reaction moment in the pinion axis simulated through a damping coefficient. This periodicity in the radial directions were observed in three simulations but with different properties. **Figure 80** shows a good comparison of the moments in the y_2 axis for the simulations. As seen from the figure, both lines follow a similar pattern and periodicity. The main difference between these two lines is the maximum and minimum moments values which can be explained with different meshes. The moment in Job-3 exhibits a relatively homogenous and uniform distribution compared to the Job-1 & Job-2 and it could be interpreted that even a finer mesh would improve this feature. A better mesh would then reduce convergence or other numerical errors and improve the stress and strain calculations which will eventually result with an improved load distribution and improved stability.

Figure 81 represents the comparison of the reaction moments in the z_2 axis. Similar arguments can be made for this figure as well. An important point for this comparison is that, it shows closer results to each other, which might suggest that improved mesh does not have same effects for all outputs.

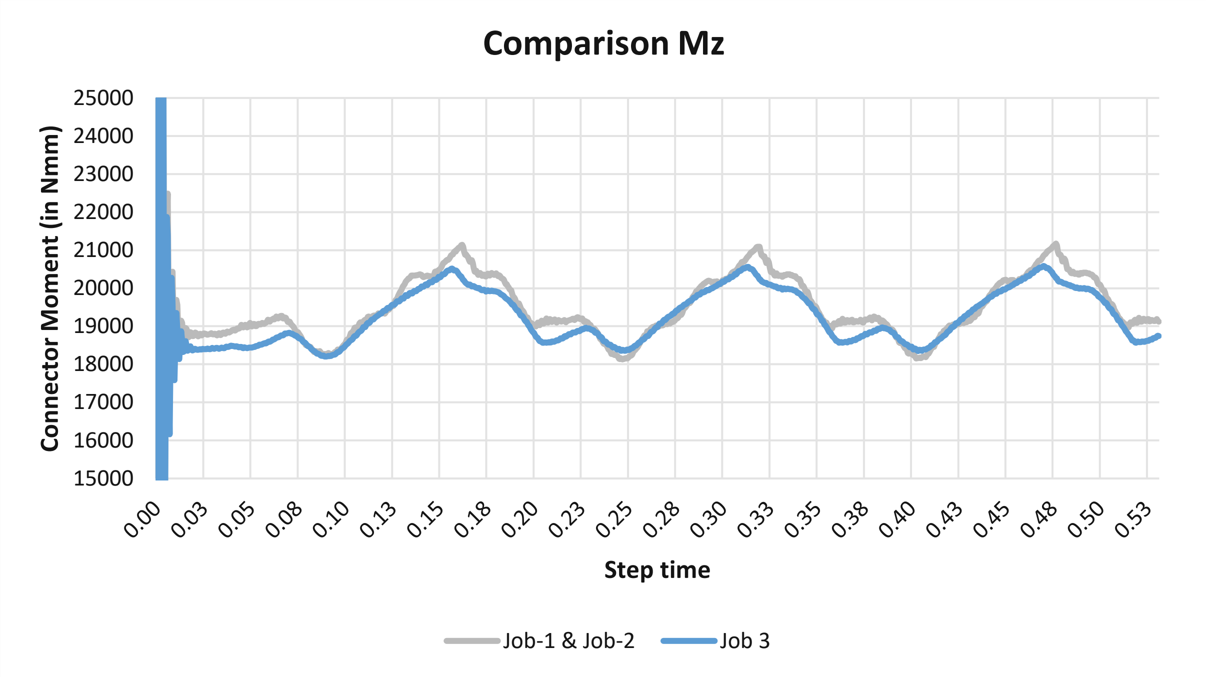

Figure 81: *Comparison of the moments on the z axis*

The damping moments in the pinion rotation axis in **Figure 82** shows again that, the finer the mesh is, the less fluctuations and solver errors there is.

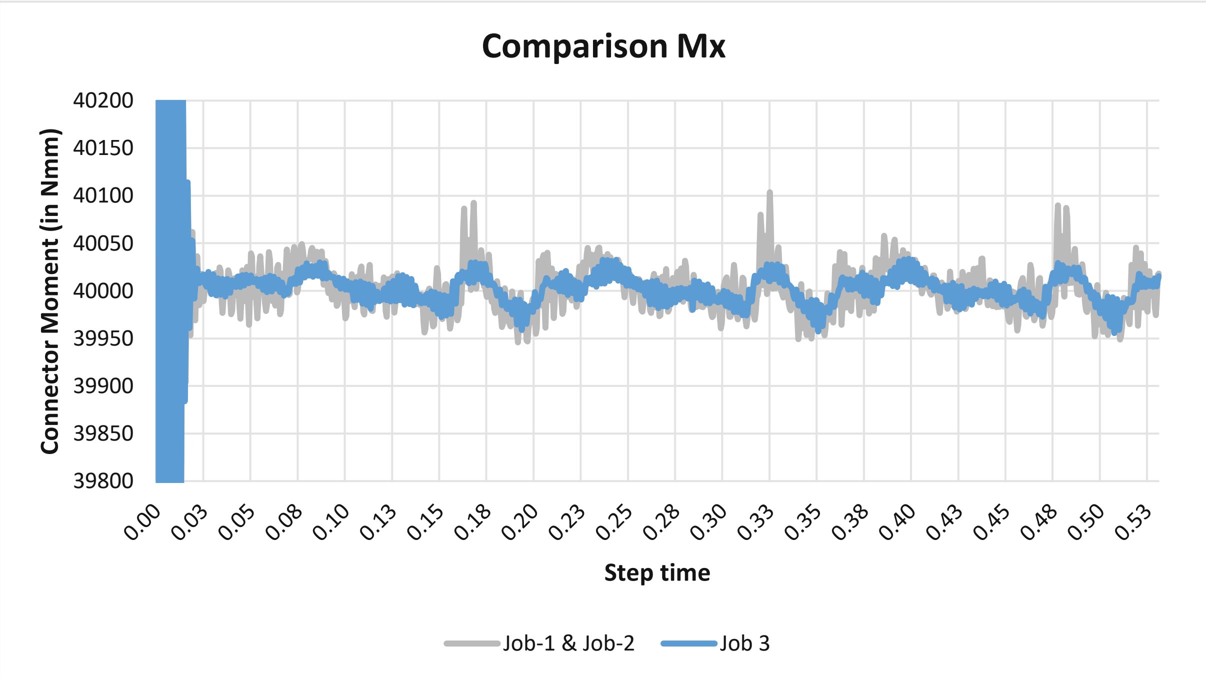

Figure 82: *Comparison of the moments on the x axis*

The values for average and maximum contact forces suggest that Zone 1 experiences the highest average forces considering all investigated frames. This result is logical, as the least amount of path points were investigated in Zone 1 compared to the other zones. This is followed by Zone 2 and Zone 3. Zone 3 shows the least amount of average forces, because most of the stresses were focused on the top of the tooth on the chamfer, and were excluded from the analysis. Moreover, the highest maximum forces were observed in Zone 2, followed by Zone 3 and then Zone 1. As illustrated in **Table 7,** the maximum forces for each zone were calculated in Frame 750, which suggest that, rack tooth surfaces act softer at the beginning of the simulation compared to the dynamic progress of the simulation.

	Zone 1		**Zone 2**		**Zone 3**	
	Average Force	**Max. Force**	**Average Force**	**Max. Force**	**Average Force**	**Max. Force**
Frame 150	13.49 N	20.82 N	11.97 N	21.52 N	10.15 N	21.55 N
Frame 450	13.78 N	21.96 N	12.18 N	20.88 N	11.10 N	22.35 N
Frame 750	12.46 N	22.54 N	12.68 N	24.5 N	11.55 N	22.36 N

Table 7: *Comparison of the contact forces*

6.5 Constraints

There were several constraints that prevented this thesis in terms of design and analysis phases, that prevented to achieve more optimal and realistic results.

In terms of design of the rack and pinion, the parameters were specifically constrained through our industrial partner as they wanted to use their standard racks and pinions that are supplied by their suppliers. Initially, the teeth number of the pinion had to be between 8-10, the pressure angle had to be 20°, both the helix angle of the pinion and shaft angle had to be 26°, and the maximum normal module was decided to be 2 mm. As mentioned in Chapter 3, a high contact ratio is easier to achieve with a higher number of teeth, module and helix angles as the contact are increases accordingly. A theoretical high total contact ratio of 2.3 could have been achieved with more lenient parameters such as 12 teeth, 2 mm module and a helix angle of 50°. Although this high contact ratio is desired, these new parameters also bring numerous other challenges such as size, high axial forces and more stress due to increased forces and therefore we decided to limit these parameters. In that sense, the total contact ratio was more or less only manipulated by the selection of profile shift and through the use of tip altering factors in the design phase.

The analysis phase in ABAQUS has also posed numerous challenges such as the step properties. As default, ABAQUS uses an automatic incrementation for the simulation which calculates the increment size (the minimum increment size and the initial increment size are still decided by the user) based on the solver decision regarding the convergence situation. This means that the increment size and number is heavily dependent on the solver capabilities and increment iterations and does not necessarily produces a homogenous solution. When Job-1 for example was calculated using an automatic incrementation, the solver can finish the job in 1 step time with 38 increments. This results with only 38 calculation points and frames for the whole step which is not sufficient enough to read the moments and forces in the connector. The use of fixed increments with the size of 0.0005 was therefore selected for the step property. On the other hand, 2000 fixed increments for the solver creates its own time and computing constraints. As expected, the solver needs much more time and RAM storage for fixed incrementation which prevents the user to do multiple simulations in the same time and as the simulation time and computing power need increases exponentially with the selection of finer mesh, it becomes not probable to analyses very high-quality mesh for this thesis. Initially, a Job-4 with very fine mesh was also planned but the solver predicted around 200 days for the simulation to be over and therefore, it was decided to not do this last simulation. For the same reason Job-3 was stopped before completion. Furthermore, the implicit analysis also prevents of using a damping feature in a surface-to-surface contact which then results with initial moment, force and velocity fluctuations. As seen in Chapter 4, the results show a high frequency and value amplitude at the start and then slowly becomes steady state. It is assumed that, a contact damping feature would prevent such high amplitudes at the beginning of the contact. Moreover, the general idea was to create a BC that would mimic a bearing in real life in order to calculate pinion bearing moments and forces. In this thesis this was created using a Hinge Connector hat has only 1 DOF, whereas in real life bearings are more flexible and should be modelled with 6 DOF. ABAQUS offers a similar type of connection for this purpose called Bushing Connector. This type of connector can be constrained in all direction elastically, plastically, with damping, etc. or can behave free. An ideal case for this thesis would be to use the Bushing Connector which will have very high elastic stiffness in all directions except its rotation axis and damping in the rotation axis. This option was but unfortunately not viable for us as, ABAQUS creates elastic stiffness property using linear springs bot for translation and rotation. This causes unexpected increases in forces and moments as the step time increases due to increase translation and rotation based on Hooke's Law. Another important constraint in the analysis phase was the analysis of the contact behaviour on the rack for simulations with coarser mesh. Because of the coarse mesh, the forces cannot be calculated uniformly on the rack and makes analysing them obsolete. The results showed high normal force accumulations in certain areas and no force values in between them which does not reflects a real time situation. Although a less intensive interpretation also surfaces in Job-3, an assumption can be made more realistically compared to the first two cases. A path analysis was used to analyse the contact forces on the rack. The paths were constructed using a start and an end point and the line was then divided into 100 equal intersections. Another possible way of analysing the forces was to select each node separately on the rack manually and the create the path from these nodes. A major obstacle regarding this method was the difficulty of maintaining a straight line as ABAQUS only allows users to choose intersection points which might not always be aligned with the contact points (with finer mesh this problem could also be solved).

Chapter 5

7 Conclusion

7.1 Summary

This thesis aims to develop a contact model for the interaction between the pinion and the rack, to analyse a crossed helical rack and pinion system optimized for a high total contact ratio, and to perform a finite element analysis of both the bearing moments acting on the pinion and the contact behaviour on the rack in a rack-driven mechanism. The results of this analysis will later be compared with a MBD model in future works in order to analyse the rack and pinion behaviour under specific conditions. The design and calculations of the rack and pinion were based on the initial parameters provided by our industrial partner and were created using KISSSOFT and SolidWorks. In the calculation phase different types of variable parameters such as the profile shift, tip altering factor and normal module were tried in order to achieve a high total contact ratio. The total contact ration was calculated using three different methods: The ISO 21771, The Method of Werner Krause and KISSSOFT calculation which all gave the same results. The designed assembly was then imported to ABAQUS as a STEP file and prepared for analysis. The ABAQUS analysis is created using an implicit dynamic analysis where the pinion is rotated through a moving rack and the pinion is constrained in Step-1 by a Hinge Connector in order to simulate a bearing behaviour. Three different cases with different contact and meshing properties were made and the results are presented in Chapter 3. The first case and the second case are simulated using the same meshing properties but using different hard contact methods while the thirds case is simulated using a finer mesh than the first and second cases. The reaction moments and forces at the pinion support showed differences between the first two cases and the third one the reason being the quality of the mesh. Generally, less excessive peaks and changes are observed when using a higher quality of mesh. In terms of the contact lines and contact forces the third case was examined in three different contact zones in three different step times. Each zone can be distinguished by their contact force distributions and their polynomial functions which are similar for all step times.

7.2 Outlook

The results of the present FEM analysis are going to be used as a basis for the MBD simulation where the whole electric power steering (EPS) is modelled. The modelled steering system is created according to the used BC's and connectors in the FEM simulation in terms of DOF, and impressed moments and forces. An MBD simulation is necessary to truly analyse the dynamic behaviour of the whole sytstem including the rack, the pinion, the yoke, the tie rods, the steering shaft and other mechanical elements such as springs and dampers. According to the visualisation of the MBD system, the pinion will be constrained only to rotate in one direction (acting as a Hinge Connector), while also being loaded by a damping moment and the rack also has only one DOF along its axis. Using this modelling based on the FEM analysis, the pinion bearing moments and forces and the resulting contact behaviour will be investigated and compared with the FEM model for validation. Whats important in this validation phase is to correctly model the contact behaviour such as damping, backlash and tolerances and create a computationally viable dynamic model to capture the interactions and behaviours accurately.

It is crucial to design the simulation correctly in order to analyse the system stiffness values, damping behaviour, friction behaviour and force transmission which directly influences the real-time use and application. The results of the FEM and MBD simulations will be useful to make assumptions regarding the steering comfort, steering stresses, vibrations, wear and tear, and steering noise which are important aspects regarding driving comfort. Using this research, automobile companies can do improvements to the whole system in order to reduce unwanted vibrations, reduce the unwanted noise, improve the reaction time and in general, extend the whole lifetime of the compoonents. Thus, it can be argued that this thesis presents an important opportunity to improve vehicle handling and safety. . In addition, this thesis provides valuable insights regarding modelling of a crossed helical rack and pinion system in terms of steering gears. Existing literature regarding FEM modelling of this system were unsufficient and often were deficient in system integration between FEM and MBD. This thesis is therefore relevant to bridge the gap between a structural analysis and multi dynamical analysis by providing easily adaptable models and universal comparable results. Moreover, the analysis of different cases enables readers to comprehend which parameters are more deciding and crucial in terms of structural analysis, and allows a faster initial design and simulation environment. In conclusion, the content of this thesis serves as a foundation in terms of desing, contact behaviour and bearing reaction analysis for steering gears and establishes a framework for the future developments in the analysis of steering gears.

Literature

- Abdulaal, M., & Abdulah, M. Q. (2024). Mathematical model and generation analysis for crossed helical gear system. *World Journal of Engineering*, 1-19.
- Akinnuli, B. O., Ogdengbe, T. I., & Oladosu, K. (2019). Computer Aided Design and Drafting of Helical Gears. 959-968.
- Automotive Systems and Accessories. (2018). *Allied Marker Research*. Retrieved January 4, 2025, from https://www.alliedmarketresearch.com/automotive-steering-system-market
- Bhavikatti, S. S. (2005). *Finite Element Analysis.* New Age International Ltd. Publishers.
- Blundell, M., & Harty, D. (2004). *The Multibody Systems Approach to Vehicle Dynamics.* Elsevier.
- Chandler, F. F. (1924). STEERING-GEAR ANALYSES. *SAE Transactions, 19*, 336-355.
- Chaturvedi, E., Acar, P., & Sandu, C. (2022). Multi-objective macrogeometry optimization of gears: Comparison between sequential quadratic programing and genetic algorithm. *Mechanics Based Design of Structures and Machines*, 1-16.
- Dassault Systems. (2025, April 1). *Abaqus*. Retrieved from https://www.kisssoft.com/en/products/product-overview/kisssoftr-elements
- Dassault Systems. (2025, April 1). *Simpack*. Retrieved from https://www.3ds.com/products/simulia/simpack
- Dassault Systems. (2025, April 1). *SolidWorks*. Retrieved from https://www.solidworks.com/
- Ever-Power. (2024). *Helical Gear Standard Sizes*. Retrieved March 5, 2025, from https://www.ever-power.net/helical-gear-standard-sizes/
- Fankem, S., Weiskircher, T., & Müller, S. (2014). Model-based Rack Force Estimation for Electric Power Steering. *Proceedings of the 19th World Congress The International Federation of Automatic Control Cape Town, South Africa, 47*(3), 8469-8474.
- Harrer, M., & Pfeffer, P. (2017). *Steering Handbook* (1st Edition ed.). Munich: Springer.
- Hlaing, T. T., Win, H., & Thein, M. (2017). Design and Analysis of Steering Gear and Intermediate Shaft for Manual Rack and Pinion Steering System. *International Journal of Scientific and Research Publications, 7*(12), 861-882.
- Hnátík, J., & Kroft, L. (2017). Specific Design of Critical Drivetrain Component. *28th Daaam International Symposium on Intelligent Manufacturing and Automation*, 567-574.

- International Standards Organisation. (1998, August 15). Cylindrical gears for general and heavy engineering - Standard basic rack tooth profile.

- International Standards Organisation. (2007). ISO 21771: Gears — Cylindrical involute gears and gear pairs — Concepts and geometry. ISO.

- Khalifa, M. Z. (2021, November). Comparing stress distribution, strain, and total deformation in contact surface for the three types of rack and pinion. *Periodicals of Engineering and Natural Sciences*, pp. 956-968.

- Khondaker, S. A., MD, W. I., & Ibriju, I. (2020). FINITE ELEMENT ANALYSIS OF RACK-PINION SYSTEM OF A JACK-UP RIG. *International Journal of Advances in Mechanical and Civil Engineering, 7*(2), 42-46.

- KISSSOFT. (2019). *Crossed Helical Gear with Rack*. Retrieved Januarry 20, 2025, from https://www.kisssoft.com/en/news-and-events/newsroom/crossed-helical-gear-with-rack

- KISSSOFT. (2025, April 1). *KISSSOFT*. Retrieved from https://www.kisssoft.com/en/products/product-overview/kisssoftr-elements

- Krause, W. (2002). Überdeckung von Schraubenstirnradgetrieben. *Die Antriebstechnik*, 54-56.

- Larsson, T. (2001). Multibody Dynamic Simulation in Product Development. Luleå: Luleå University of Technology.

- Litvin, F. L., Gonzalez-Perez, I., Fuentes, A., Vecchiato, D., & Sep, T. M. (2005). Generalized concept of meshing and contact of involute crossed helical gears and its application. *Computer Methods in Applied Mechanics and Engineering, 194*(34-35), 3710-3745.

- Marano, D., Pellicano, F., Pallara, E., & Piantoni, A. (2018). Modelling and simulation of rack-pinion steering systems with manufacturing errors for performance prediction. *International Journal of Vehicle Systems Modelling and Testing, 13*(2), 178-198.

- Mathcad. (2025, April 1). *PTC Mathcad*. Retrieved from https://www.mathcad.com/en

- Mathworks. (n.d.). *Mathworks*. Retrieved January 7, 2025, from https://it.mathworks.com/discovery/finite-element-analysis.html

- Niemann, G., & Winter, H. (1986). *Maschinenelemente Band 3: Schraubrad-, Kegelrad-, Schnecken-, Ketten-, Riemen-, Reibradgetriebe, Kupplungen, Bremsen, Freiläufe* (2nd Edition ed.). Springer.

- Okerke, M., & Keates, S. (2018). *Finite Element Applications A Practical Guide to the FEM Process.* Springer.

- Peršin, G. (2013). Fault detection and localization of mechanical drives based on data fusion techniques. Ljubljana: University of Ljubljana.

- Princeton Edu. (n.d.). *Princeton Edu*. Retrieved January 13, 2025, from https://www.princeton.edu/~timeteam/gears.html

- Radzevich, S. P., & Storchak, M. (2022). *Advances in Gear Theory and Gear Cutting Tool Design.* Stuttgart: Springer.

- Rahnejat, H. (2000). Multi-body dynamics: historical evolution and application. *Proceedings of the Institution of Mechanical Engineers, Part C: Journal of Mechanical Engineering Science, 214*(1), 149-173.

- SIMULIA. (2016). *Abaqus Analysis User's Guide.* Retrieved March 3, 2025, from http://130.149.89.49:2080/v2016/books/usb/default.htm?startat=pt01ch01s01abo01.html

- SIMULIA. (2016). *Abaqus/CAE User's Guide.* Retrieved March 5, 2025, from http://130.149.89.49:2080/v2016/books/usi/default.html

- Suryanvanshi, O. D., Sathe, P. P., & Takey, M. A. (2017). Designing of the Rack and Pinion Gearbox for All Terrain Vehicle for the Competition BAJA SAE India and Enduro Student India. *IJRET: International Journal of Research in Engineering and Technolog*, 79-84.

- Szabó, B., & Babuška, I. (2011). *Introduction to Finite Element Analysis: Formulation, Verification and Validation.* Wiley.

- Vienna University of Technology. (2023). *Noise and Vibration*. Retrieved January 7, 2025, from https://www.tuwien.at/en/mwbw/mec/e325-01-research-unit-of-technical-dynamics-and-vehicle-system-dynamics/research-projects/noise-and-vibration

- Vullo, V. (2020). *Gears Volume 1: Geometric and Kinematic Design* (10th Edition ed.). Rome: Springer.

- Weigand, M., Kral, P., & Dencsi, D. (2016). *Maschinenelemente.* Vienna: Vienna University of Technology.

- Wittel, H., Muhs, D., Jannasch, D., & Voßiek, J. (2015). *Roloff/Matek Maschinenelemente Normung, Berechnung, Gestaltung* (22nd Edition ed.). Augsburg: Springer.

- Yanjun, X., Lihu, H., Jiayu, Z., & Yanchun, X. (2014). Dynamic Analysis of Gear and Rack Transmission System. *The Open Mechanical Engineering Journal, 8*, 662-667.

- Zhen, C., Ming, Z., & Alfonso, F.-A. (2019). Geometric Design, Meshing Simulation, and Stress Analysis of Pure Rolling Rack and Pinion Mechanisms. *Journal of Mechanical Design, 142*, 1-10.

Appendix A

KISSsoft

Crossed axis helical gear pair (Gear 1, $z \geq 6$)

Untitled

Contents

1 Messages

Calculation is consistent.

Gear 2:
The measurement over pins is smaller than the tip diameter. This might produce an incorrect measurement!

2 Overview

Calculation method:	Only geometry calculation
Drawing or article number:	
Gear 1:	0.000.0
Gear 2:	0.000.0

3 Tooth geometry

Geometry calculation according to	Niemann, ISO 21771:2007	
Running center distance (mm)	[a]	22.226
Rack height (mm)	[Hz]	12.500
Center distance tolerance	ISO 286:2010 Measure js7	
Shaft angle (°)	[Σ]	26.0000
Normal module (mm)	[mn]	2.0000
Transverse module (mm)	[mt]	2.2252
Normal Diametral Pitch (1/in)	[Pnd]	12.70000
Transverse Diametral Pitch (1/in)	[Ptd]	11.41468
Normal module at operating pitch circle (mm)	[msn]	2.0002
Normal pressure angle (°)	[αn]	20.0000
Helix angle (°)	[β]	26.0000

		Pinion	Rack
Number of teeth	[z]	10	
Helix angle at reference circle (°)	[β]	26.0000	0.0033
Facewidth (mm)	[b]	30.00	25.00
Hand of gear	[L/Rβ1]	left	
Hand of gear	[L/Rβ2]		right
β, is used in the calculation (°)	[β]	26.0000	-0.0033
Lead angle at reference diameter (°)	[γ]	64.0000	-89.9967
Helix angle at operating pitch circle (°)	[βs]	26.0033	-0.0033
Accuracy grade	[Q-ISO 1328:2013]	A6	A6

4 Materials

Gear 1

18CrNiMo7-6, Case hardening steel, case-hardened, ISO 6336-5 Figure 9/10 (MQ), Core hardness >=25HRC Jominy J=12mm<HRC28

Gear 2

18CrNiMo7-6, Case hardening steel, case-hardened, ISO 6336-5 Figure 9/10 (MQ), Core hardness >=25HRC Jominy J=12mm<HRC28

	------ Pinion-----------------	Rack------
Surface hardness	HRC 61	HRC 61

5 Geometry

5.1 Reference profiles

Reference profile Gear 1

Reference profile	1.25 / 0.25 / 1.0 ISO 53:1998 Profil C	
Dedendum coefficient	[hfP*]	1.250
Root radius factor	[ρfP*]	0.250
	[ρfPmax*]	0.472
Addendum coefficient	[haP*]	1.000
Tip radius factor	[ρaP*]	0.000
Protuberance height coefficient	[hprP*]	0.000
Protuberance angle	[αprP]	0.000
Tip form height coefficient	[hFaP*]	0.000
Ramp angle	[αKP]	0.000
	not topping	
Smallest radius of curvature, root rounding (mm)	[ρmin.e/i]	0.675 / 0.684

Reference profile Gear 2

Reference profile	1.25 / 0.25 / 1.0 ISO 53:1998 Profil C	
Dedendum coefficient	[hfP*]	1.250
Root radius factor	[ρfP*]	0.250
	[ρfPmax*]	0.472
Addendum coefficient	[haP*]	1.000
Tip radius factor	[ρaP*]	0.000
Protuberance height coefficient	[hprP*]	0.000
Protuberance angle	[αprP]	0.000
Tip form height coefficient	[hFaP*]	0.000
Ramp angle	[αKP]	0.000
	not topping	
Smallest radius of curvature, root rounding (mm)	[ρmin.e/i] ------	----------------- 0.501 / 0.501 ------

5.1.1 Information on final machining

		Pinion	Rack
Dedendum reference profile	[hfP*]	1.250	1.250
Tooth root radius reference profile	[ρfP*]	0.250	0.250
Addendum reference profile	[haP*]	1.000	1.000
Protuberance height coefficient	[hprP*]	0.000	0.000
Protuberance angle (°)	[αprP]	0.000	0.000
Tip form height coefficient	[hFaP*]	0.000	0.000
Ramp angle (°)	[αKP]	0.000	0.000

Type of profile modification:	none (only running-in)		
Tip relief by running in (µm)	[Ca L/R]	0.0 / -0.0	0.0 / -0.0

5.2 Basic data

Sum of profile shift coefficients	[Σxi]	0.3000

Pinion Rack

Transverse module (mm)	[mt]	2.2252	2.0000
Axial module (mm)	[mx]	4.5623	
Normal pressure angle at the operating pitch circle (°)	[αsn]	20.019	20.019
Transverse pressure angle at the operating pitch circle (°)			

	[αst]	22.067	20.019
Axial pressure angle at the operating pitch circle (°)	[αsx]	39.728	-89.990
Transverse pressure angle (°)	[αt]	22.046	20.000
Axial pressure angle (°)	[αx]	39.702	89.991
Base helix angle (°)	[βb]	24.326	0.003
Profile shift coefficient	[x]	0.3000	0.0000
Generating profile shift coefficient	[xE.e/i]	0.2629/ 0.2423	-0.0371/-0.0577
Involute length (mm)	[l_dFa-l_dFf]	4.165	4.402

5.2.1 Tip chamfer or tip rounding

------------------ ------

		Pinion	Rack
Tip chamfer (mm)	[hK]		0.100
Tooth tip chamfer angle (°)	[δhK]		45.000
Tip rounding (mm)	[rK]	0.001	
Section	[/]	2	

Tip rounding: 2-in transverse section, 3-in axial section, 4-In normal section

5.3 Diameters and their allowances

		Pinion	Rack
Reference diameter (mm)	[d]	22.252	10.500
Operating pitch circle diameter (mm)	[ds]	22.255	11.098
Base diameter (mm)	[db]	20.625	
Tip alteration (mm)	[k*mn]	0.140	0.000
Tip diameter (mm)	[da]	27.732	12.500
(mm)	[da.e/i]	27.732 /27.711	12.500 /12.500
Tip diameter allowances (mm)	[Ada.e/i]	0.000 /-0.021	0.000 / 0.000
Tip form diameter (mm)	[dFa]	27.731	12.400
(mm)	[dFa.e/i]	27.731 /27.710	12.400 /12.400
Active tip diameter (mm)	[dNa]	27.731	12.400
(mm)	[dNa.e/i]	27.731 /27.710	12.400 /12.400
Root diameter (mm)	[df]	18.452	8.000
(mm)	[df.e/i]	18.304 /18.221	7.926 / 7.885
Active root diameter (mm)	[dNf]	0.000	-4989.500
(mm)	[dNf.e/i]	0.000 / 0.000	-4989.500 /-4989.500
Root form diameter (mm)	[dFf]	20.625	8.264
(mm)	[dFf.e/i]	20.627 /20.626	8.189 / 8.148

------------------ ------

5.4 Tip clearances and tooth heights

		Pinion	Rack
Addendum, $m_n(h_{aP}*+x+k)$ (mm)	[ha]	2.740	2.000
(mm)	[ha.e/i]	2.740 / 2.729	2.000 / 2.000
Dedendum, $m_n(h_{fP}*-x)$ (mm)	[hf]	1.900	2.500
(mm)	[hf.e/i]	1.974 / 2.015	2.574 / 2.615
Tooth height (mm)	[h]	4.640	4.500

5.5 Roll angle

------ ------------------ ------

		Pinion	Rack
Roll angle at dFa (°)	[ξ_dFa.e/i]	51.496 /51.409	20.922 /20.922
Roll angle to dNa (°)	[ξ_dNa.e/i]	51.496 /51.409	20.922 /20.922
Roll angle at dFf (°)	[ξ_dFf.e/i]	0.860 / 0.568	20.771 /20.770

5.6 Tooth thickness and pitch

		Pinion		Rack
Normal tooth thickness at tip circle (mm)	[san]	0.769		1.686
(mm)	[san.e/i]	0.721 / 0.669		1.632 / 1.602
without consideration of tip chamfer/tip rounding				
Normal space width at root circle (mm)	[efn]	0.000		1.322
(mm)	[efn.e/i]	0.000 / 0.000		1.352 / 1.292
Lead height (mm)	[pz]	143.330		
Axial pitch (mm)	[px]	14.333		107709.311
Normal pitch, base circle (mm)	[pbn, pen]		5.904	
Normal pitch, reference circle (mm)	[pn]		6.283	
Normal pitch, operating pitch circle (mm)	[psn]		6.284	

------ ------------------ ------

5.7 Sliding

		Pinion		Rack
Sliding velocity at operating pitch circle (m/s)	[vgs]		0.00	
Max. sliding velocity at tip (m/s)	[vgg]	0.00		0.00
Mean sliding velocity (m/s)	[vgm]		0.00	

5.8 Contact ratios

------ ------------------ ------

		Pair
Length of path of contact (mm)	[gan]	9.383
Length A-S (mm)	[AS]	5.584
Length S-E (mm)	[SE]	3.799

		Pinion		Rack
Transverse contact ratio	[εα]	1.320		1.589
Overlap ratio	[εβ]	0.270		0.000
Total contact ratio	[εγ]		1.589	
Total contact ratio with allowances	[εγ.e/m/i]		1.594 / 1.588/ 1.581	

------ ------------------ ------

6 Measurements for tooth thickness

6.1 Tooth thickness tolerances

Pinion	Rack

Tooth thickness tolerance		DIN 3967 cd25	DIN 3967 cd25
Tooth thickness allowance (normal section) (mm)	[Asn.e/i]	-0.054 /-0.084	-0.054 /-0.084

6.2 Base tangent lengths

		Pinion	Rack
Number of teeth spanned	[k]	2.000	
Base tangent length (no backlash) (mm)	[Wk]	9.646	
Base tangent length with allowance (mm)	[Wk.e/i]	9.595 / 9.567	

(mm)	[ΔWk.e/i]	-0.051 /-0.079	
Diameter of measuring circle (mm)	[dMWk.m]	22.397	

6.3 Measurement over balls and pins

		Pinion	Rack
Theoretical diameter of ball/pin (mm)	[DM]	3.931	3.417 *
* According to ANSI/AGMA 2002-C16 eq. 95			
Effective diameter of ball/pin (mm)	[DMeff]	4.000	3.500
Radial single-ball measurement, no backlash (mm)	[MrK]	14.739	13.051
Radial single-ball measurement (mm)	[MrK.e/i]	14.692 /14.665	12.977 /12.936
Diameter of measuring circle (mm)	[dMMr.m]	23.425	
Diametral measurement over two balls, no backlash (mm)	[MdK]	29.478	
Diametral measurement over two balls (mm)	[MdK.e/i]	29.383 /29.330	
Diametral measurement over pins, no backlash (mm)	[MdR]	29.478	
Measurement over pins according to DIN 3960 (mm)	[MdR.e/i]	29.383 /29.330	
Measurement over 3 pins, axial, AGMA 2002 (mm)	[dk3A.e/i]	29.383 /29.330	

6.4 Tooth thickness

		Pinion	Rack
Medium tip diameter (mm)	[da.m]	27.722	10004.000
Reference chordal height from da.m (mm)	[hac]	2.851	2.000
Tooth thickness at height hac, chord (mm)	[sc]	3.568	3.142
(mm)	[sc.e/i]	3.516 / 3.487	3.088 / 3.058
Tooth thickness on reference circle, arc (mm)	[sn]	3.578	3.142
(mm)	[sn.e/i]	3.524 / 3.494	3.088 / 3.058

6.5 Backlash

		Pair
Radial backlash (mm)	[jrw.e/i]	0.241 / 0.138
Circumferential backlash (transverse section) (mm)	[jtw.e/i]	0.176 / 0.100
Center distance allowances (mm)	[Aa.e/i]	0.011 /-0.011
Backlash free center distance (mm)	[aControl.e/i]	22.078 /21.995
Backlash free center distance, allowances (mm)	[jta]	-0.148 /-0.231

		Pinion	Rack
Tip clearance (mm)	[c0.i(aControl)]	0.203	0.343

Torsional angle with rack fixed:		
Total torsional angle (°)	[j.tSys]	0.9759/ 0.5576
Backlash with fixed pinion:		
Backlash (mm)	[j.tSys]	0.1756/ 0.1004

7 Toothing tolerances

	Pinion	Rack

According to ISO 1328-1:2013, ISO 1328-2:1997

One or more gear data values (m_n, b or d) lies beyond the limits covered by the standard. Tolerances are calculated using the formulae in the

standard. The values are outside the official range of validity!			
Accuracy grade	[Q]	A6	A6
Single pitch tolerance (µm)	[fpT]	8.00	8.00
Base pitch tolerance (µm)	[fpbT]	7.42	7.52
Sector pitch tolerance (µm)	[Fpz/8T]	0.00	0.00
Profile form tolerance (µm)	[ffαT]	8.50	8.50

Profile slope tolerance (µm)	[fHαT]	7.00	7.00
Profile tolerance, total (µm)	[FαT]	11.00	11.00
Helix form tolerance (µm)	[ffβT]	9.50	9.50
Helix slope tolerance (µm)	[fHβT]	8.50	8.50
Helix tolerance, total (µm)	[FβT]	13.00	13.00
Cumulative pitch tolerance, total (µm)	[FpT]	23.00	23.00
Adjacent pitch difference tolerance (µm)	[fuT]	12.00	12.00
Runout tolerance (µm)	[FrT]	20.00	20.00
Single flank composite tolerance, total (µm)	[FisT]	31.00	31.00
Single flank composite tolerance, tooth-to-tooth (µm)	[fisT]	8.00	8.00
Radial composite tolerance, total (µm)	[FidT]	26.00	26.00
Radial composite tolerance, tooth-to-tooth (µm)	[fidT]	9.50	9.50

FidT (Fi") and fidT (fi") according to ISO 1328:1997 calculated with the geometric mean values for m_n and d.

According to ISO 1328-2:2020

Accuracy grade	[Q]	R38	R46
Radial composite tolerance, total (µm)	[FidT]	23.00	93.00
Radial composite tolerance, tooth-to-tooth (µm)	[fidT]	14.00	55.00

Rack tolerances calculated according to DIN 3961:1978 with number of teeth and pinion reference circle.

8 Supplementary data

8.1 Masses and moment of inertia

		Pinion	Rack
Mass - calculated with da (g)	[m]	97.527	

8.2 Indications for the manufacturing by wire cutting

		Pinion	Rack
Deviation from theoretical tooth trace (µm)	[WireErr]	2319.9	0.0
Permissible deviation (µm)	[Fb/2]	6.5	6.5

9 Modifications and determination of the tooth form

9.1 Profile and flank line modifications

Gear 1

Symmetric (both flanks)

- Flank line crowning

Cb = 1.000 µm

bx=30.000mm, rcrown=112500mm

9.2 Data for the tooth form calculation

Calculation of Pinion

Tooth form, Pinion, Step 1: Final machining (automatic)

haP*= 1.115, hfP*= 1.250, ρfP*= 0.250

Tooth form, Pinion, Step 3: Chamfer/rounding (automatic)

r= 0.001 mm, in transverse section

Calculation of Rack

Tooth form, Rack, Step 1: Final machining (automatic)

haP*= 1.047, hfP*= 1.250, ρfP*= 0.250

Tooth form, Rack, Step 2: Chamfer/rounding (automatic)

10 Remarks

10.1 Conventions

- Specifications with **.e/i** mean: Maximum value **.e** and Minimum value **.i**, taking all tolerances into account.
- Specifications with **.m** mean: Mean value within tolerance.

- The circumferential backlash specification and the backlash-free center distance for the tooth thickness check are not exact and are only guide values.

10.2 Calculations and factors

- The active root diameter and the active tip diameter are calculated as specified by Pech.

End of report (list)